STRUCTURES AND STABILITY OF CLUSTERS AND NANOWIRES OF GOLD AND OTHER TRANSITION METALS

A THESIS

Submitted to the
FACULTY OF SCIENCE
PANJAB UNIVERSITY, CHANDIGARH
For the degree of

DOCTOR OF PHILOSOPHY

2014

PRIYANKA

CENTRE OF ADVANCED STUDY IN PHYSICS
PANJAB UNIVERSITY, CHANDIGARH
INDIA

*Dedicated
To
Gunbir And Seerat*

Contents

Acknowledgements

I would like to express my sincere gratitude and thanks to my esteemed supervisor, Prof. Keya Dharamvir. Her wide knowledge and logical way of thinking have been of great value for me. Her understanding, encouraging and personal guidance has provided a good basis for the present thesis. She is an excellent example of a successful woman physicist and professor.

A special thanks and a grateful acknowledgement goes to Dr. Hitesh Sharma, who has guided during my initial years of my Ph.D. He has encouraged me and suggested new ideas regarding my work.

I am thankful to the Chairman, Department of Physics, Panjab University for providing adequate facilities to work in the department. I would like to thank my lab-mates for their unending support through whole of my research period. A special thanks to Isha who has helped in learning of the code. I am heartily thankful to my seniors Shuchi Di, Narinder Di, Veena Mam, Dr Ali and Shobhna Mam for their constant guidance and support. I'm grateful to Seema, Pooja for their immense help in learning the code. I'm also thankful to Sumali and Seema Gautam for their cooperation and healthy discussions. A special thanks to Kiran, Gagandeep, Vaishali, Vaneetha, Kulwinder, and Anjali for providing with supportive and cooperative environment in lab. I'm also thankful to my friends Neelu, Jaspreet, Reema, Amarjot for their cheerful presence in my life.

I'm grateful to my Mother in law for unconditional support and love she has given me and my children. Without her encouragement and support I wouldn't have been able to complete this whole work efficiently. I'm thankful to her and my Father in law for taking care of my kids in my

absence. Especial thanks to my sister in law Ramandeep, who has always been supportive and encouraging.

I'm lucky to have a loving and supportive life-partner, Sarbjeet Singh. He has always been source of inspiration and strength of my life. He has always encouraged me to chase my dreams and without his persuasion, this work would not have been completed. It brings a smile on my face to mention the names of two little angels Gunbir and Seerat who have changed my life and made me a stronger person. Their innocent faces love and trust on me has always encouraged me during my low times to get up and fight back. Their smile always brings a boost of positive energy in me.

My deepest gratitude goes to my parents for their love and support throughout my life. This dissertation was simply impossible without them. I am indebted to my father and mother for their understanding and unconditional love. They have always supported me in every way and whatever I chose in my life. My father has a never die attitude towards life from which I have learnt a lot and it always helped me to achieve my goals. My mother has always prayed for me more than anyone else. My brother, Vineet in his own way, have always motivated me and supported me throughout this work. Also my cousin sister, Shuchi deserves special thanks for her ways to make me smile. My father has always wanted me to do Ph.D., by submitting this thesis I hope to fulfill his dream.

At the end, I'm thankful to God for providing me the strength to complete this work and fulfill my dream. I dedicate this thesis to my loving and caring family.

Priyanka

Abstract

Gold is known to exhibit a vast range of interesting geometries as its stable ground state. It evolves from planar structures to cage like, to tubular and finally core shell structures as the size of the nanocluster increases. The central theme of this thesis is to discuss the structural and electronic properties of gold nanoclusters, nanotubes and nanowires and study the interaction of gold with other elements. The physical and chemical properties of Au differ from the other noble metals such as Cu and Ag due to relativistic effects. In order to explain the importance of relativistic effects in the structural evolution of gold a combination of a semi empirical and first principle approaches is used. It is well known that with the introduction of different foreign elements as a substitutional or at the endohedral sites of the nanostructures; their structural, electronic and vibrational properties are altered. A systematic density functional study has been conducted on the interaction of gold with transition metals and group 14 elements and studies on the effect of impurity on the structural and electronic properties of gold clusters have been carried out.

In Chapter 1, we present a general introduction to different gold nanostructures and discuss the effects of doping on their structural, physical and chemical properties. The work done in this field till date is reviewed in detail.The Semi empirical approach-The Gupta Potential and the First principle methods based on density functional theory (DFT) , employed for the calculations carried out in this work, are described in Chapter 2. Chapter 3 discusses the effect of different approaches on the low lying geometries of small gold clusters. The two approaches predict different lowest geometries for gold clusters for n ≤ 13 .While the use of Gupta Potential has predicted the early onset of 3D geometries, the DFT predicts planar structures for n upto 13.

Chapter 4 discusses the effect of doping Si and Ge on the ground state structures of pure gold clusters. It is found that on doping silicon and germanium atoms in Au_n clusters, they adopt 3D structures from n=3 onward. The ground state geometries of the Au_nGe clusters show patterns similar to silicon doped gold clusters except for n = 6 , 9 and 10. The binding energy per atom of Au_{n+1} cluster shows an increase with the introduction of Si and Ge atoms. The binding energy per atom of germanium doped clusters is smaller than the corresponding silicon doped gold clusters. The HOMO–

LUMO gap of both Silicon and Germanium doped gold clusters lies in the range of semiconductors; so they can be used as novel materials in nanostructured devices.

In Chapter 5, we have carried out a DFT study of the $M_{12}@Au_{20}$ (M= C, Si and Ge) clusters. The Au_{32} is a highly stable cage with the icosahedral (I_h) symmetry. It is found that the addition of dopant atoms increases the average binding energy. $C_{12}@Au_{20}$ is the most stable with the highest binding energy. Pure Au_{32} cage is found to be chemically inert with HOMO-LUMO gap of 1.59eV. The HOMO–LUMO gap of $M_{12}@Au_{20}$ cluster is much smaller and should be relatively chemically reactive.

In Chapter 6, we have studied the effect of encapsulation of small chain of Cu and Ag atoms within a short segment of hexagonal gold nanotube i.e., Au_{24} tubular cage using DFT. The Cu doped Au_{24} tubular cages were found to have higher energy gap than the Ag doped cages except for $Cu_2Au_{24\text{-}II}$. It implies that Cu doped gold cages are more stable than Ag doped. The Mulliken population analysis, reveals that the d obitals of M (Cu, Ag) atoms in $M@Au_{24}$-I and $M@Au_{24}$-II clusters are dominant core orbital participating in bonding.

Chapter 7 extends the above and describes the results of our systematic study of structural and electronic properties of of the tubular X_MAu_N (X= Si, Al and Au, M=3, 6, 9 and N= 24, 42, 60) clusters. It was found that the encapsulations of Si and Al atoms do not destroy the tubular frameworks of the gold host though they change the energy hierarchy of the pure Au_N isomers, showing a high possibility to form a novel binary cluster with gold providing tubular structures. It was concluded that the Si and Al atoms can form long chains within Au nanotube with a gap after every 4-6 layers of Au atoms to accommodate the size mismatch between Si-Si, Al-Al and Au layers. The Si doping within Au_N tube is more compatible than the Al doping.

In Chapter 8 we present a DFT study of the structures, energy variations, force and modulus of two linear finite chains of gold with five and seven atoms and comparison of the results with similar calculations done through Gupta Potential. The calculated value of breaking force for two monoatomic chains using DFT is more or less in agreement with experimental results.

The Chapter 9 presents the results of prelimilnary work on the phonon study of pure gold hexagonal nanotubes . In the absence of parallel experimental or theoretical work on phonon dispersion relations, we cannot compare the results.

Lastly Chapter 10 gives the brief summary of the work done in this thesis and its scope in future.

List of Figures

List of Tables

Chapter 1

1. Introduction

1.1 A brief note on nanoparticles

"There's Plenty of Room at the Bottom - An Invitation to Enter a New Field of Physics." a visionary talk by Richard Feynman's at Caltech in 1959 gave birth to the idea of nanotechnology. His talk inspired the scientists to develop new devices and machines that could be constructed from the components containing tens or hundreds of atoms. A nanoparticle is the most fundamental component in the fabrication of nanostructured devices. It is far smaller than the everyday objects which are governed by Newton's laws of motion and bigger than an atom or a simple molecule that are governed by quantum mechanics. They are the particles with number of atoms or molecules bonded together with a radius between 1-100nm. At this size, structure built from them exhibit new electronic structure, conductivity, chemical reactivity, mechanical properties etc [1]. Clusters form the building blocks of different nanostructured materials.

The clusters are nanoparticles composed of countable number of atoms, intermediate in size between the individual atom and the bulk. Their property differs from the bulk material in terms of electronic structures [2]. The electronic structure of a cluster consists of discrete molecule like energy levels and exhibits strong size dependence while the bulk material has smoothly varying continuous band structure. Clusters are also different from conventional molecules. The Molecules have fixed compositions and definite structures, whereas clusters can exist in diverse stoichiometries and multiple geometries (or isomers). Clusters can be neutral or charged. They may be homogeneous or heterogeneous. Like molecules they are held together by different kinds of forces, e.g. metallic bonds (as in alkali and coinage metal clusters), ionic forces (as in NaCl clusters), covalent chemical bonds (as in carbon and silicon clusters), or Van der Waals attraction (as in He and Ar clusters) [3,4,5]. Clusters provide an ideal medium for studying different properties such as, geometric and electronic structure, melting temperature, magnetic moment etc, not only by changing the size one atom at a time but also by changing geometry.

It is observed that the change in these properties take place upto a critical size, e.g. the electrical conductivity of a metal strongly depends on the mean free path. If the size

of the particle is less than the characteristics length it is possible to observe new properties [1].

By studying the properties of small clusters and working toward the larger ones, scientists can better understand the origins of known bulk material properties. The different properties of clusters are also strongly characterized by quantum size effects. Study of clusters as a function of size enables one to track the manner in which size dependent properties change from molecular-like to the bulk limit. As an example we can study the Au_{20} cluster, which has a beautiful pyramidal structure in which all the gold atoms are on the four surfaces of a tetrahedron, resembling that of Au (111) surface [6]. Thus clusters provide valuable models for surface chemistry and catalysis. Besides presenting novel properties interesting for fundamental research, clusters also hold promise for several applications.

Nanotubes and nanowires constitute an important class in nanoelectronics with their potential applications as nanodevices or as connectors between them. Recent advances in experimental techniques, such as Scanning Tunneling Microscopy (STM) [7, 8] and electron-beam lithography [9], are giving rise to fabrication of wires at nanometre scale. Properties of nanotubes and nanowires are actively studied both experimentally and theoretically [10-13].

1.2   Why Gold??? - Historical background and applications

Gold nanoparticles (AuNPs) have emerged as an object of great interest in the fields of physics, chemistry, biology, medicine, material science as well as some interdisciplinary field due their attractive electronic, optical, thermal and catalytic properties. Compared with other nanostructures, study of metallic nanoparticles is found to be more flexible owing to synthetic control of their shape, size, composition etc.

Historical importance of gold lies in the role played by it due to its exquisite qualities among metals, making it exceptionally valuable from the earliest civilizations till date. The earlier use of gold nanoparticles appeared in Roman era as an elaborate decorating material. The beautiful "Lycurgus Cup" (owned by the British Museum), which is red in transmission and green in reflection, contains silver-gold bimetallic nanoparticles of around 50-100 nm in diameter [14]. Until the seventeenth century, the gold colloids were used to colour glass and their synthesis was described by the Italian glass makers. Later, in 1857, Michael Faraday carried out his first remarkable

experiments on metal colloids and described various colors of gold particles using different preparations [15]. He observed the optical properties of gold nanoparticles from different preparations and described them scientifically. Today, it is well-known that the various colors of liquid-dispersed gold nanoparticles having different sizes is due to *size effect,* i.e., the properties of nanoparticles may change when their size changes.
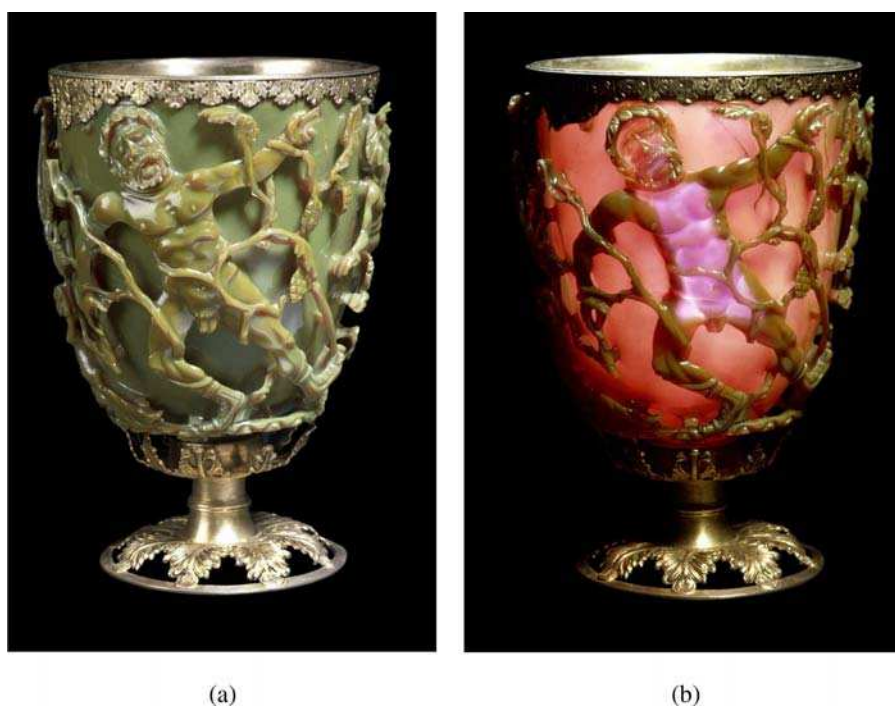
Figure 1.1 Image of the Lycurgus cup, probably made in Rome in fourth century (from the British Museum free image service) (a): light falling from outside. (b): light falling from inside.

Gold is the most anciently administered medicine. Pure metallic gold when ingested in small quantities is found to be non toxic and it does not react with the body. It is believed since medieval times that gold is beneficial for the health. The thousands of years old Indian ayurvedic medicine system involves the use of gold in its medicines. For example, *Swarna Bhasma* comprises of gold nanoparticles with an average size of about 60 nm. With tremendous progress in technology over a recent decade, a large number of nanoscale structures have emerged possessing novel properties suitable for applications in the field of biomedicine. Among the various metallic nanostructures studied, colloidal gold nanospheres are found to be more popular due to fast and simple methods of preparation. Due to ease of preparation of colloidal gold nanoparticles , metallic gold can have a renewed potential in the field of modern medicine such as for imaging, diagnostics, drug delivery or radiotherapy [16 -18].

Gold has become an important nanoscale electronic component because of its resistance to oxidation and its mechanical strength. At nanosize the bulk gold, exhibit different electronic structure which is intermediate between the band structure of the bulk metal and the discrete energy levels of molecules with a characteristic highest occupied molecular orbital (HOMO)–lowest unoccupied molecular orbital (LUMO). Also in comparison to other inorganic nanomaterials, the gold nanoparticles can be synthesized in large variety of shapes and sizes.

To avoid the oxidation or precipitation of gold nanoparticles in the solution phase or controlling size during growth of nanoparticles, stabilizing agents or ligands are used [19]. An example of ligand stabilized AuNPs, is $Au_{55}(PPh_3)_{12}C_{16}$ ('Au_{55}') (Fig. 1.2) , also known as 'Schmid cluster' with a core size of 1.4 nm studied using single-electron tunnelling (SET) is shown to be a promising subunit in nanoelectronic devices [20-23]. A lot of different studies have been performed for the preparation of different types of AuNPs, varying in size, shape and ligand shell composition [24 - 26]. In an experiment, a prototype of a nano-switch was built using a layer of Au nanoparticles, in which the conductivity of the system was altered electrochemically [27]. A composite of polystyrene and 2-naphtolenethiol-capped Au nanoparticles has been found to exhibit electrical transitions when induced by strong electrical fields, suggesting a potential application in memory devices [28]

Gold offers many of the 'topdown' fabrication advantages of silicon. It is also least susceptible of all metals to oxidation. The use of gold has seen significant growth in the areas of electronics, particularly within telecommunications and information technology. For example the battery connections in mobile phones are made up of gold contacts. Gold bonding wires are used extensively in semiconductor packages. In designing nanodevices, the work on nanowires as potential connectors in nanodevices is in progress in various research labs around the world.

Applications of Gold nanoparticles also include nanosized sensors, which could be used to detect species that have specific affinities for nanoparticles or as a filter to select particles of given size [29, 30].
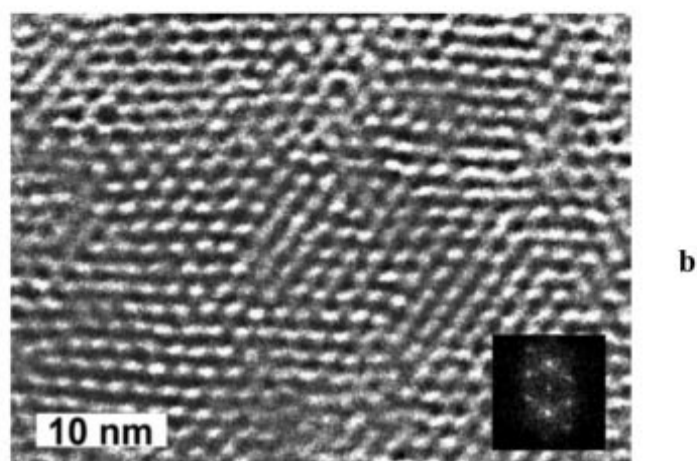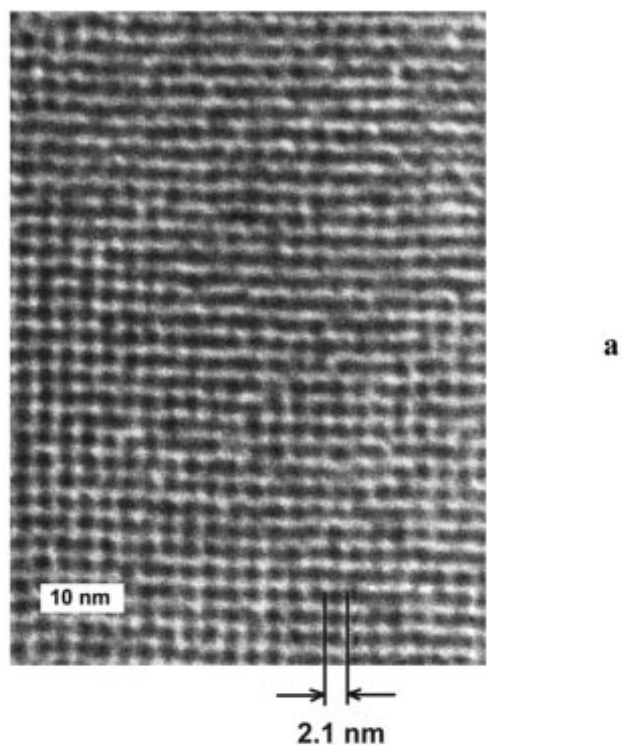
Figure 1.2 TEM images (**a**) square planar and (**b**) hexagonal arrangements of Au$_{55}$ clusters, generated on PEI (poly ethyleneimine) and PPE (poly *p*-phenylene ethynylenes) films respectively

Another interesting use of gold can be as catalyst in fuel cell applications, pollution control and chemical processing. There has been intense interest in using supported nanoclusters as model catalysts. Recent advancement in technology allows the synthesis of gold nanoclusters with excellent size control, allowing for precise measurements of size-dependent catalytic performance [31, 32]. In recent years, researchers have made remarkable advances in solution-phase synthesis of thiolate-protected gold nanoclusters. Such clusters have a precise composition with number of

metal atoms (n) and ligands (m), denoted as $Au_n(SR)_m$, with n ranging up to a few hundred atoms[33].

It can be presumed that the use of gold nanoparticles will increase dramatically in the near future in varied fields. The gold nanowires as conducting contacts in nanoelectronics will contribute to the progress of nanotechnology. The use of gold as catalysis seems to have already started. Gold nanoparticles in combination with biomolecules will have commercial applications in medical diagnostics in near future.

1.3   Relativistic effects in gold

According to the Bohr 's model of the atom states, the electrons in the 1*s* orbital are closest to the nucleus, and moves with a velocity v of 1.6×10^8 metres per second in the orbit to avoid falling into the nucleus. This velocity is more than half the speed of light: $c \approx 3 \times 10^8$ m/s. According to Einstein such high velocity of electrons results in increased electron mass according to equation (1.1),

$$m_r = \frac{m_0}{\sqrt{1 - \frac{v^2}{c^2}}}$$

(1.1)

The orbital radius varies inversely with mass of electron, given by equation (1.2)

$$a_0 = \frac{\hbar}{m_e c \alpha}$$

(1.2)

where a_o is Bohr's radius , $\hbar$ is the reduced Planck's constant and α is the fine-structure constant . Thus the relativistic increase in mass of the electron will cause a contraction of its orbit. It also signifies that the electrons will be near the nucleus most of the time and thereby contract the radius for small principal quantum numbers. This results in the relativistic contraction and stabilization of all s and p orbitals [34].

This effect is significant not only for the innermost electrons, but it also strongly affects electrons in *s* orbitals (and lesser extent p orbitals) in outer shells. The higher angular momentum *d*, *f*, and *g* orbitals are farther from the nucleus and experience stronger screening of the nuclear attraction by s and p shells and hence are less affected by relativistic contraction. Therefore the d and f shells will undergo relativistic expansion and destabilization. These relativistic effects scale roughly with Z^2 and become important for elements heavier than the lanthanides [35].

Gold (Z = 79) is the last stable element present in the periodic table among the other stable elements (mercury, thallium, lead, and bismuth). The electrons of the gold atom experience an intense electrostatic attraction due to the presence of 79 protons in its

nucleus. The yellow appearance of bulk gold is attributed to strong relativistic effects exhibited by it. Due to the relativistic contraction of s orbitals in gold, the energy levels shift closer to d orbitals (which are less affected by relativity). This shifts the light absorption (5d→6s transition) from the ultraviolet down into the lower frequency blue visual range. Therefore gold absorbs blue light more than the other visible wavelengths of light, this makes a piece of gold appear yellow (under white light) to human eyes. A non-relativistic gold would be white.

While in Ag similar transition occurs, but because of the relativistic effects the 4d-5s distance in Ag is much greater than the 5d-6s distance in Au; hence silver appears white. The relativistic effect has raised the 5d orbital and lowered the 6s orbital [36]. Another important impact of a relativistic effect is the initial resistance of gold towards oxidation. Due to the relativistic contraction of 6s orbital toward the nucleus and stronger electrostatic attraction of the 79 protons in the nucleus, the "atomic radius" of gold reduces considerably. Only the strongly reactive substances can tug gold's 6s^1 electron out from where it's place. The importance of relativistic effects in gold has been a topic of theoretical and experimental research for a long time [36-39].

1.4   Structure of Gold

Bulk gold is soft, yellow metal with the face centered cubic crystal structure, its melting point is 1068°C and has excellent electrical conductivity. But at nanoscale some these properties tend to change, these changes are exploited in field of nanotechnology [40]. Due to lack of translational symmetry the structure of nanoparticles is different from the bulk structure of the same materials. This results in a complicated competition in energetic stability of various structural motifs. Thus, it is important to characterize both experimentally and theoretically the structure of nanoparticles. Due to its electronic configuration, bulk gold is a good conductor of electricity, with its conductivity only beaten by copper and silver. But at nanoscale the gold structures, depending on shape and substrate, can actually be semi-conductors [41]. The study of structures of gold nanoclusters of various sizes and their impact on the various properties such as electronic, optical etc is areas of active research in cluster science because of possible applications in the nanoelectronic devices [42-46].

The gold nanoparticles can be amorphous or may have various morphologies, including decahedra, truncated-octahedra, or icosahedra for different sizes [47]. The icosahedral and decahedral structures are non crystalline and have five fold symmetry,

hence can not be packed together to make macroscopic crystal. These structures are only found to exist at nanoscale. Also the surface effect becomes significant at nanoscale; therefore the internal energy must be minimized with respect to electronic configuration, surface energy and elastic strain resulting in the change in the structure of gold. It has been observed that icosahedron yields an efficient compromise between surface energy and packing density [16].

1.4.1 Magic geometric numbers and magic electron numbers

The bulk state adopts a packing arrangement which minimizes its free energy. At nanoscale, the atoms in clusters have a tendency to minimize surface-to-volume ratio to form closely packed, high-symmetry cluster structures. These high-symmetry structures are constructed from specific shells of atoms called as geometric shells.

If a number of atoms that can be packed complete the geometric shells of a high-symmetry structure, it is said to be magic geometric number [48].

For example, icosahedral structures (I_h symmetry) are constructed from one central atom surrounded by geometric shells consisting of 12, 42, 92, 162, etc. atoms. Thus the respective magic atom numbers are 1 + 12 = 13, 13 + 42 = 55, 55 + 92 =147, 147 + 162 = 309, etc.The structures with an octahedral symmetry (O_h) have face-centred cubic (FCC) packing. There geometric shells can be completed in two ways. The first way is the formation of the cuboctahedral geometry having the same magic atom numbers of the icosahedra: 13, 55, 147, 309, etc. In the other way, a basic octahedron is built from 6 atoms, and the larger clusters are constructed by surrounding that central octahedron with the subsequent shells of 38, 102, 198, etc. atoms, resulting in octahedral clusters with the respective magic atom numbers are 6, 44, 146, 344, etc. On removing the corner atoms from the octahedral, we get a truncated-octahedral. The truncated-octahedral species can be either cuboctahedral geometry which has triangular (111) facets or the plain called truncated-octahedral geometry which has hexagonal (111) facets. The magic atom numbers for the truncated octahedral geometry are: 38, 116, 260, etc.
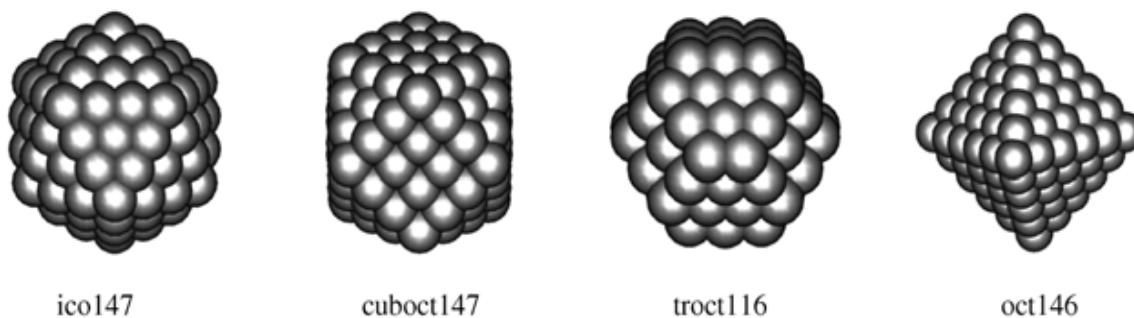
Figure 1.3 Few high-symmetry clusters having the geometric shells completed with the magic numbers: 147-atom icosahedron, 147-atom cuboctahedron, 116-atom truncated octahedron, 146-atom octahedron,

According to quantum mechanics, electrons within clusters occupy different energy levels. These energy levels form electronic shells in clusters. The *jellium model* [49] is used to describe the electronic distribution for a cluster. It assumes a spherical charge distribution and considers the positive charges of the nuclei as a uniform positively charged background.

In the jellium model, each electron moves in a potential field which resembles that of an isotropic harmonic oscillator, allowing the analytic solution for the single-electron Schrödinger equation. The electronic shells are determined as the energetic sequence of eigen functions: (1s), (1p), (1d, 2s), (1f, 2p), (1g, 2d, 3s), etc. The Pauli Exclusion Principle governs the occupations of orbital electrons, yielding the *magic electron numbers:* 2, 8, 20, 40, 70, etc., for the completion of the respective shells [46]. Fig. 1.4 shows the jellium electronic shells and the corresponding magic electron numbers corresponding to the Schrödinger equations for one electron with spherical symmetry, interacting electrons with spherical symmetry, and interacting electrons with octahedral symmetry.

1.4.2 Magic clusters of Gold

According to various studies gold at nanoscale can adopt a wide variety of structures. The structure of gold nanoparticles plays an important role in determining their physical and chemical properties. The gold clusters containing fewer than 15 atoms prefer to form flat planar structures [50]. The spherical structures become favorable when the total number of valence electrons in the cluster is equal to or near the value of 2, 8, 18, 20, 32, 50, 72,..., $2(L+1)^2$ electrons, where L is an integer.
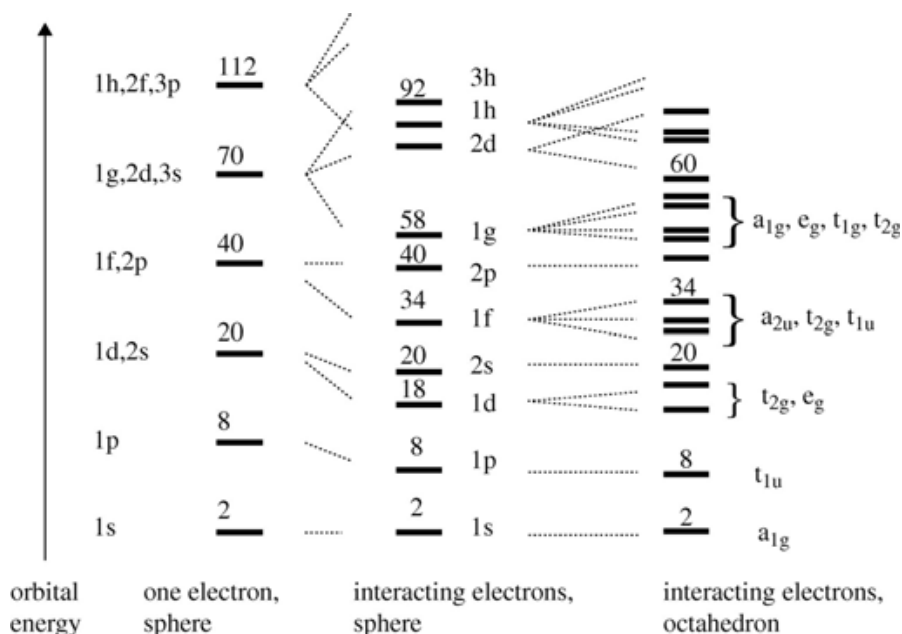
Figure 1.4 Energy levels in the jellium model [46].

Yadav et al. have reported a magic magnetic cage cluster of gold, Gd@Au_{15}, using first principle approach. They have called it a magic cluster as Gd atom being trivalent, when doped into Au_{15} cluster it imparts extra stability within the 18 valence electron rule [51]. Another gold cluster exhibiting closed shell magic structure is Au_{20}. It has a highly symmetric and unique tetrahedral structure whose every atom lies on the surface [52]. Even if one atom is removed to form Au_{19}, its tetrahedral symmetry is still retained. It is proposed to be found in chemically synthesized $Au_{20}(PPh_3)_8$ clusters [53,54].
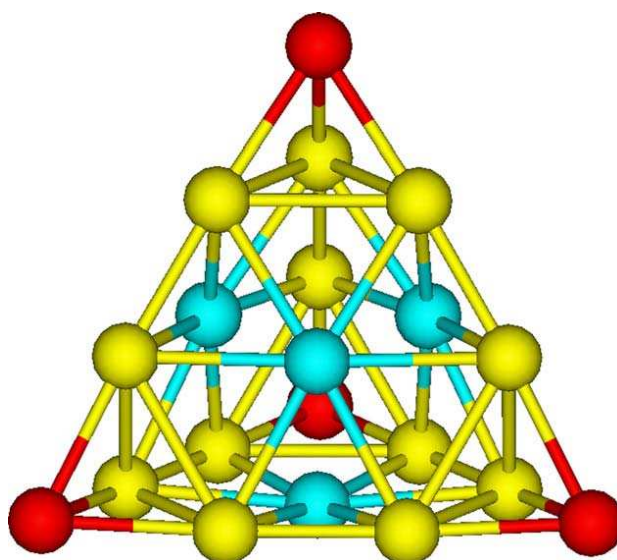
Figure 1.5 The tetrahedron (T_d) ground-state of gold Au_{20} cluster.

1.5 Pure Gold clusters

The properties of nanoparticles are known to change with its size and shape. The structures of gold nanoparticles are found to be very different from those of other noble metals. Gold is known to have unique properties due to inclusion of the strong relativistic effects and aurophilic attraction (stronger tendency of gold to form close metal-metal interactions) [55]. Intensive experimental [56-61] and theoretical [62-70] efforts have been made to study their chemical and physical properties.

The synthesis of colloidal solutions of passivated Au nanoparticles using thiolate ligands has encouraged further studies [71, 72]. These clusters are relatively stable and can be easily manipulated for experimental observations.

To understand the different structures and other unique properties of gold clusters, different techniques have been used to probe their structures. Theoretically, different approaches such as an ab-initio density functional theory (DFT), empirical and semi empirical-based molecular dynamics (MD) calculations are used to investigate the structural, energetic and electronic properties of gold clusters.

The semiempirical potential calculations makes the use of Gupta potential (GP), Murrell- Mottram (MM) potential, embedded-atom-method (EAM) interatomic potential, and Sutton-Chen (SC) potential to describe the interactions in Au clusters. The MM potential predicts that geometries of Au_{2-40} clusters to be distributed on octahedron, decahedron, icosahedron and hexagonal prism [73]. The SC potential predicts compact structures for Au_{2-80} clusters [74].

The two-body interactions like the Lennard Jones (LJ) or Morse potential also favor compact cluster structures [75]. The two body potential such as LJ may not sufficient to adequately model the metallic clusters with increasing cluster size. It requires including all n-body forces in an effective many-body potential such as in the Sutton-Chen or Gupta potential. However the n- body potentials are found to be computationally expensive because of their many body character.

A comparative study of gold clusters up to 200 atoms was performed using GP and SC [78]. The potential parameters were obtained by fitting the properties of bulk Au to experimental-fitted (exp-fitted) parameters of Wu et al. [76, 77]. Furthermore, for SC potential, parameters fitted by DFT were also used to determine the lowest energy structures. It was observed that for Au clusters with n = 3–11, 13–19, 26, 30, 33, 35, 37, and 38, both SC and GP predicts same motifs however; there exists energy

difference for the two potentials. Results also showed that in Au100–200 clusters, the dominant motif for both potentials is decahedral. In another study the magic clusters Au_{38}, Au_{55} and Au_{75} were studied using Gupta potential and were found to have amorphous-like, face-centered-cubic (fcc), and decahedral structures, respectively [79,80].

The Jahn-Teller and spin-orbit effects are found to play an important role in predicting the lowest energy structures of gold clusters, e.g., the lowest energy structure of the gold trimer (Au_3) [81] or the anion 20-gold cluster (Au_{20}^{-1}) [82]. The use of any potential will give an ideal triangle as the lowest energy geometry for the interaction between three atoms and an ideal tetrahedron for the interaction between four atoms. But in the case of metal clusters it is different. The bonding in homonuclear coinage metals ground state is due to single s electron on each atom and their d orbitals are involved in electron correlation and spin–orbit effects. The heavier trimer such as Au_3 cluster retains its D_{3h} symmetry due to large spin–orbit stabilization and does not undergo a Jahn–Teller distortion which would have reduced the symmetry to C_{2v} [83]. It was suggested by Bersuker, that spin-orbit coupling could dominate the Jahn Teller distortions [84]. Thus it suggests that the gold clusters do not follow the pattern predicted by Lennard-Jones, Morse or Gupta potential, all favoring a maximum number of close atom–atom contacts.

Another aspect which is not explained by semi empirical potentials is the onset of 2D geometries in small Au_n clusters. It is observed that the transition from two-dimensional to three-dimensional structures occurs at n >13 in Au_n clusters [50, 64]. The preference for planarity in gold clusters cannot be explained by the many-body potentials, such as the Gupta or Sutton- Chen potential [85]. The preference for planarity of small gold cluster compounds has been attributed to the relativistic effects [86]. The GP or other similar potential cannot account correctly for many-body effects and the relativistic effects which are important to obtain the correct shape and structures of small to medium sized gold. To include the many-body effects in gold clusters, their preference for planarity and to study their electronic properties we use DFT.

There is a vast literature available on theoretical investigations of electronic and structural properties of small, homonuclear, neutral, and ionic gold clusters using density functional theory (DFT) or *ab initio* methods. Structures and energetics of

neutral and ionic gold clusters $Au_n^{\pm}$ up to the decamer are discussed in Refs. 87 - 91.

A two dimensional to three dimensional transitions in small gold clusters is widely discussed and studied. Wang et al. [68] using DFT calculations have found planar structures (2D) for gold clusters up to n= 6 and more compact spherical structures (3D) starting n= 16, and flat cage-like structures in-between, while Fernandez et al. [92] found 2D structures up to Au_{11} using DFT/GGA with the transition from 2D to 3D occurring at Au_{12}. In contrast, the 2D/3D structural transition for Cu and Ag occur at n=6. Landman et al. have observed that Cu_7^- and Ag_7^- have compact 3D structures, while Au_7^- is planar. It was found that this is due to relativistic effects as non relativistic Au_7 would behave similar to copper and silver [86]. Koskinen et al. studied the dynamics of Au_n^- (n= 11–14) and showed the co-existence of 2D and 3D structures at finite temperatures [93]. In general, different studies including the systematic searches for the global minimum structures of larger cluster sizes, predicts the two- to three dimensional 2D→3D transition to occur at $n \geq 13$ [50, 94, 95]. However, the results are ambiguous and sensitive to the method chosen. Hence the 2D →3D transition in neutral Au_n is predicted to occur somewhere between n=13 and 15. Similar trends are found for the cationic and anionic gold species [89, 96]. The strong relativistic and spin-orbit (SO) coupling effects in gold make it theoretically very challenging to determine the true global minimum structures of even relatively small gold clusters. Therefore, state-of-the-art experimental data, in conjunction with extensive theoretical studies, are needed in order to obtain unequivocal structural information of gold clusters.

Experimentally, the first molecular-beam experiment was conducted on gold clusters using a liquid metal ion source to generate small singly and doubly charged cluster cations. The ion-intensity distributions showed structure dependence on size [97, 98]. The experimental photoelectron spectra (PES) of Au_n have been reported by Taylor et al. [99]. Nowadays a number of modern experimental techniques have been used to study size-selected gold clusters, such as ion mobility [64], photoelectron spectroscopy (PES) [56, 100], infrared multiphoton dissociation spectroscopy [53, 102], and trapped ion electron diffraction (TIED)[103, 104]. Recently, using Ar-tagging, the coexistence of both the 2D and 3D isomers in the cluster beam of Au_{12}^- has been shown and also obtained isomer-specific photoelectron spectra for this critical cluster [105].

The next important gold cluster is Au_{20} (Fig. 1.4). It was found by PES and DFT study that Au_{20} adopts tetrahedral structure with a large HOMO-LUMO gap. It was identified by Wang et al.and has been recently confirmed by Apra et al. [106-108]. It is a very ordered structure with no internal atoms and can be understood as a small section of fcc-bulk gold cut along four intersecting close packed (1 1 1) planes. It gives a deep minimum on the potential energy surface isolated from its isomers and has a well-defined melting point with a melting temperature comparable to bulk gold [109]. In contrast, the other isoelectronic metals such as Cu_{20} and Ag_{20} have amorphous-like 3D structures. The difference is attributed to strong relativistic effects, which enhances s-d hybridization in gold [92]. The tetrahedral motif can be found in other metal clusters also. Johansson and Pyykko [110] have shown its presence in cadmium for the first five clusters containing 4, 10, 20, 35, and 56 atoms using first principle method. The image showing 20 atoms of gold bound together to make a tetrahedron have been developed by Scientists at the University of Birmingham by using a special probe beam to image is shown in Fig. 1.6 [108].
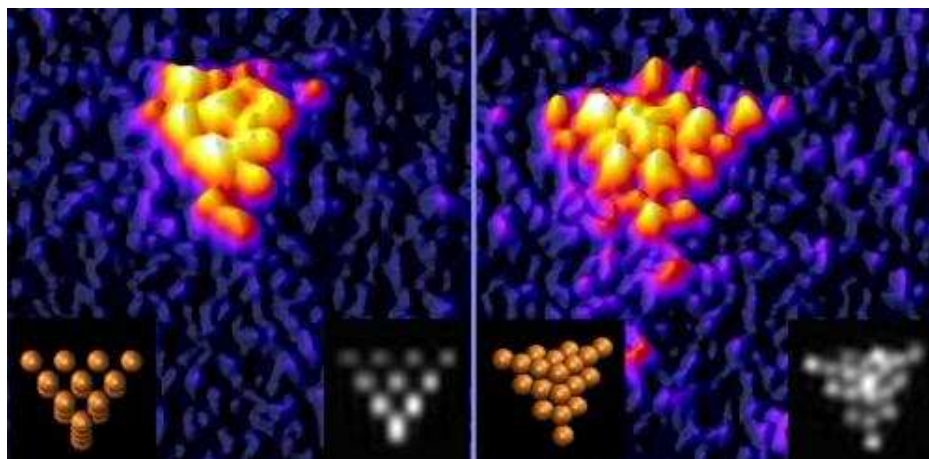
Figure 1.6 The tetrahedron of 20 gold atoms. Image credit: University of Birmingham

There have been increasing research efforts directed toward the exploration of structural evolution of gold clusters in the size range of $20 < n < 55$. Previous theoretical studies have suggested the existence of highly symmetric hollow-cage structures Au_{32}, Au_{42}, and Au_{50} as well as hollow-tubular structure Au_{26} [111-116]. Bulusu et al. [117] have conducted a joint theoretical and experimental study of low-lying structures of gold cluster anions Au_n^- in the size range of $n = 21-25$. For $n = 21-24$, they have found that the pyramid-based structures are competitive for $n = 21-23$ and the hollow-tubular structures dominate at n = 24. They found that at n= 25 a structural transition from hollow tubular to core/shell compact structure takes place.

14

The tubular structure of Au_{24} has been verified by Xing et al. and Zeng's group with different experimental techniques [117, 118]. The tubular Au_{24} structure can be used to accommodate a guest atom to form a new kind of endohedral tubular gold cluster.

A joint experimental PES and theoretical study predicts a core/shell compact structure for the anion Au_{32}^- [119]. The Au_{32} known as first gold fullerene, has an icosahedral symmetry with a large energy gap of 1.56 eV. It has high stability and was predicted theoretically by Gu et al. [112]. Another important gold clusters which has been studied both experimentally and theoretically is Au_{55}, so-called 'magic number' cluster. It contains the right number of atoms for very stable geometries, making it ideally suited to catalysis [120]. A catalyst consisting of 55 atoms a gold cluster was developed by Lambert et al. is shown in Fig. 1.7 [120]. In PES study of Cu_n^-, Ag_n^- and Au_n^- clusters with n =53-58, Hakkinen et al. have found that structure of Cu_{55}^- and Ag_{55}^- exhibit icosahedral symmetry while Au_{55}^- structures found to have lower symmetry. This behavior is related to strong relativistic bonding effects in gold [121].
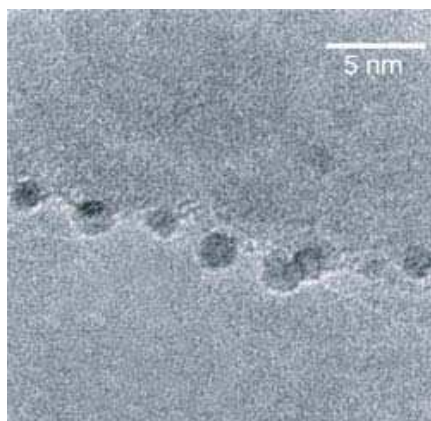
Figure 1.7 Showing catalytically active Au_{55} nano clusters

The Au_{72} using DFT and MP2 calculations, is shown to exist as a hollow nanosphere having an Icosahedral symmetry. A recent study has shown that could [122]. As the size increases, the gold cluster shows a more metallic behavior. As confirmed in a recent study with the increase in size, the cage like structures is not favored in energy owing to the low coordination [123].

In an experimental study of structure of 38, 75, 101, 146, 200, 225, and 459 Au nanoclusters were found to consist of ordered core structures. For 38, 225, and 459 atom gold clusters were found to have fcc truncated octahedral motif while the rest had the truncated decahedral motif [72, 124]. Currently there are no experimental techniques that can determine the structure of a cluster directly and unambiguously.

This can be achieved using various theoretical methods. The current theoretical approaches come with limitations which do not make it easy to predict the ground state geometry with absolute certainty because clusters can have numerous low lying isomers protected by energy barriers. As cluster size increases, the number of structural isomers on the potential energy surface increases exponentially and search for the ground state geometry becomes a very difficult task.

1.6 Doped Gold Clusters

Doping clusters with a foreign atom offers an additional dimensionality to fine tune their structures and properties. The introduction of a dopant atom in a coinage metal cluster can change its structural and electronic as well as magnetic properties and improve their stability significantly [125-128]. To enhance the stability of gold clusters and tailor their physical and chemical properties a large number of theoretical and experimental studies have been carried out on Au clusters doped with various dopants. These bimetallic clusters can have potential utility in new nanomaterials as building blocks. There have been many studies of $M@Au_n$ clusters, especially for 3d Transition metal impurity.

It all started with the prediction of a highly stable icosahedral cluster, constructed by 12 gold atoms with an encapsulated impurity atom at centre, $M@Au_{12}$ (M = W, Ta$^-$, Re$^+$) which was predicted by Pyykko and Runeberg and was later confirmed experimentally [129, 130]. The stability of these gold-covered clusters has been attributed to relativistic effects and aurophilic attractions [55]. Since then there have been lot of theoretical studies on doping of gold clusters with different elements. The electronic structure and magnetic properties of transition metal- doped Au clusters $M@Au_6^-$ (M = Ti, V, Cr) was investigated by Li et al. using PES and DFT calculations [131].

A systematic investigation was carried out by Meng et al. [132] on the geometries and electronic properties of 3d, 4d, and 5d impurity doped Au_6 clusters by using relativistic all electron DFT calculation. It was found that the ground state for all the $M@Au_6$ clusters is with transition metal atom placed at the centre of an Au_6 ring.

As discussed earlier that Gold clusters with n up to 15 atoms have planar structures and thereafter three-dimensional (3D) structures become favorable. It has been found by introducing a suitable impurity in gold clusters we can have an early onset of 3D structures. A magic magnetic cage cluster of gold, $Gd@Au_{15}$ is found to be potential candidate for cancer therapy and possessing a large magnetic moment of 7 μ_B could

be beneficial for magnetic resonance imaging [51]. With Gd doping, we find that the GdAu$_n$ clusters favor 3D structures beyond n=9 as their lowest in energy structure.

The magic number cluster containing 20 gold atoms (Au$_{20}$) with tetrahedral pyramidal structure is a highly stable and chemically inert cluster. A natural question to ask would be how the high stability and chemical inertness associated with Au$_{20}$ are altered when it is doped with a metallic atom. Pal et al. [133] have studied the effect of substitution by Ag and Cu atoms on the structural and electronic properties of gold clusters using a combination of PES and DFT. They have found that overall effect of the isoelectronic substitution is minor on the structures except that the dopant atoms lower the symmetries of the doped clusters. The structural and electronic properties of Au$_{19}$X clusters doped with Li, Na, K, Rb, Cs, Cu, and Ag have been studied by Ghanty et al. [134] using relativistic density functional theory. They found that endohedrally doped Au$_{19}$X clusters (X = Li, Na, and Cu) have binding energies comparable to those of the corresponding exohedrally doped clusters while the endohedrally doped cage-like structures of larger atoms (X = K, Rb, Cs, and Ag) are found to be less stable than the corresponding exohedral structures.

Another group of interesting elements which would be doped in gold are the group 14 elements C, Si, Ge and Sn. Theoretical and experimental studies had already shown that the Si and Ge as well as Sn atom doped into the sixteen-atom golden cage cannot form a stable geometry. The dopant atom is found to be either exohedral (Ge and Sn) or it becomes a part of the gold cage (Si) [135,136]. A detailed theoretical study of the structural and electronic properties of CAu$^q_{16}$ (q = −1, 0) was conducted by Fa et al. [137]. They have found that the endohedral structures of both neutral and anionic C-doped gold clusters are not the most stable configurations but they rather are distorted closed flat cages. In another theoretical study by Walter it is suggested that the endohedral doping of the Au$_{16}$ cage by Al or Si yields a geometrically robust, tuneable oxidation and reduction agent [138]. While doping the hollow golden cage Au$_{16}^-$ with Si, Ge etc prefers an exohedral geometry, the Cu atom (or a Ag atom) results in the endohedral cluster Cu@Au$_{16}^-$ (or Ag@Au$_{16}^-$) causing little structural deformation to the original golden cage [139]. Thus the doping of group 14 elements may have different effect on the structural and other physical as well as chemical properties of gold clusters in comparison with transition metal.

In this thesis effect of doping of different elements i.e, both transition elements and

group 14 elements on gold clusters will be investigated.

1.7 Gold Nanotube and Nanowires

To exploit the different size dependent properties of gold, efforts have focused on creating nanostructures of various geometries such as nanorods [140,141], nanorings [142], nanowires [143] where the controlled variation of dimensions has been shown to permit the changes in different properties. Nanotubes have one of the highest aspect ratios of any objects in nature. Their length can exceed several millimeters for diameters down to less than a nanometer. Similar to CNT, the gold nanotube can be made by rolling up a sheet of gold triangular lattice. The notation n, m denotes the chiral vector $C=na_1+ma_2$ where a_1 and a_2 are the basis vectors of a two-dimensional gold triangular lattice (Fig. 1.8). The (5, 5) gold nanotube has enough hollow space to accommodate a monoatomic chain (MAC) inside and has been predicted to be the most stable tube theoretically [144].

An experimental study using UHV-TEM has confirmed the formation of Pt and Au single-wall nanotubes (SWNT). The Pt tubes were found to consist of 5 or 6 atomic rows helically coiled around the axis of the tube [146] while gold's SWNT was observed to be composed of 5 helical strands [147]. Sen et al. have conducted a DFT based study on the nanowires of different types of elements, such as alkali, simple, transition and noble metals and inert gas atoms, having a stable structure made from staggered pentagons with a linear chain passing through their centers.
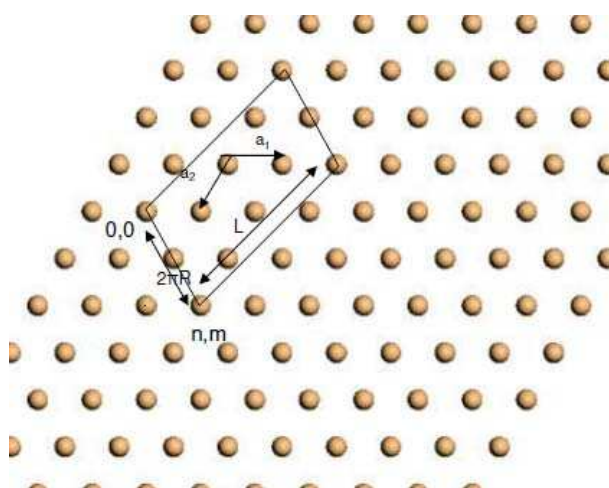
Figure 1.8 The gold SWNTs obtained by cylindrical folding of the 2D triangular lattice. The tube circumference is |**C**|, and radius $R = (n^2 + m^2 -nm)^{1/2} / |a_1{}^2|$, where n of tube are the helical strands and m defines the chirality.

They have found all nanowires of different elements except Xe, are metallic in the pentagonal structure [148]. In another first principle study by Senger it was shown that free-standing gold chiral (*n, m*) tubes with $3 \leq n \leq 5$ are stable and exhibit novel electronic and transport properties [149].
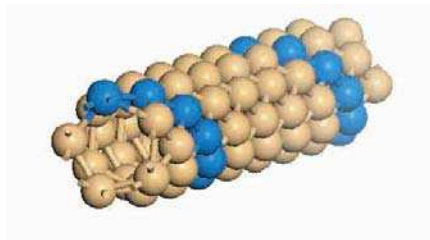
Figure 1.9 Tubular structures of gold [149]

One-dimensional nanowires or monoatomic chains (MAC's) have also attracted much attention in recent years because of their broad applications in different areas, such as in nano-mechanical and nano electronic devices. Metallic nanowires with well-defined structures several nanometres in size have been fabricated by using various methods [150-153]. The formation of monoatomic chains of metal was observed and studied by both experiments and MD simulations [154 - [156].

The freestanding MACs are metastable and hard to be used directly in application [157]. So the application of MACs would require stabilizing them without significantly changing their unique properties. One of the solutions could be to encapsulate them into a stable tubular structure [158-161]. The strong tube-TM interaction is expected to modulate the electronic structures of the guest atoms to enhance their magnetic properties In an interesting DFT study by Zhu et al. of the magnetic properties of gold nanotubes encapsulating transition metal (TM=Co and Mn) and monoatomic chains TM@Au , it is found that the TM chains can be significantly stabilized with a gold nanotube coating [162].This work has motivated us to study the encapsulation of MAC's within a gold nanotube and study the changes it brings in the different properties.

1.8 Work done and its scope

The present study gives an insight to the interesting world of gold nanostructure and the effect of doping on it. The work involves the DFT study of structural and electronic properties of pure gold clusters and gold clusters doped with different impurities such as Cu, Ag, C, Si and Ge. We have also studied the tubular gold

structures, monoatomic chains of gold and finally presented a brief review on the phonon dispersion of gold nanotube. A combination of semi empirical and first principle approach is used to study the optimization of structures of gold clusters upto 14 atoms and study the relativistic effects on their geometry.

A detailed DFT study has been conducted on the changes in the structural and electronic properties of gold nanostructure on doping them with transition elements such as Cu and Ag and with group 14 elements such as C, Si and Ge. The size of gold nanostructures studied lies over range of small clusters upto intermediate size i.e., $3 \leq n \leq 60$. It is well known the properties of nanoclusters changes with size and with the introduction of impurity atoms. It will be interesting to explore the changes in structures and other related properties of gold nanoclusters for their application as novel material.

1.9 Broad outline of the Thesis

A systematic study of gold nanoclusters, nanotubes and nanowires and the effect of impurity on their structural and electronic properties have been conducted. The computational methodology is a combination of a semi empirical approach and density functional theory, which is used to study optimization of the geometrical structure of pure gold clusters. Effect of doping of different foreign elements on the structural, electronic and vibrational properties of gold clusters is studied using DFT. In this thesis, we discuss some of the properties of doped nanostructures in detail.

In Chapter 1, gives the general introduction to different gold nanostructures and discuss the effects of doping on the structural, physical and chemical properties of these nanostructures. The work done in this field till date is also reviewed here in details. The computational methodology used in our thesis is discussed in Chapter 2. The Semi empirical approach- The Gupta potential and the first principle methods based on density functional theory (DFT) have been employed for the calculations carried out in this work The Chapter 3 addresses the issue of relativistic effects on the low lying geometries of small gold clusters. The two approaches predict different lowest geometries for gold clusters for $n \leq 13$ .The GP predicts the early onset of 3D geometries while the DFT predicts planar structures for n upto 13.

Chapter 4 gives a systematic DFT study of endohedral doping of Si and Ge atoms in gold clusters. It is found that the doping of silicon and germanium atoms in Au_n clusters, results in early onset of 3D geometries. The binding energy per atom Au_{n+1}

cluster shows an increase with the introduction of Si and Ge atoms. The binding energy per atom of germanium doped clusters was found to be smaller than the corresponding silicon doped gold clusters.

In Chapter 5 we have carried out a DFT study of $M_{12}@Au_{20}$ (M= C, Si and Ge) clusters. Pure Au_{32} cage is found to be chemically inert with HOMO-LUMO gap of 1.59eV. It is seen on doping of Au_{32} cage the HOMO–LUMO gap reduces, making it chemically reactive.

In Chapter 6, we have explored the effect of encapsulation of small chain of Cu and Ag atoms within Au_{24} tubular cage. In general, the Cu doped Au_{24} tubular cages are more stable than the Ag doped cages.

The Chapter 7 describes the results of our systematic study of structural and electronic properties of of the tubular $X_M Au_N$ (X= Si, Al and Au, M=3, 6, 9 and N= 24, 42, 60) clusters. It was found that the encapsulations of Si and Al atoms do not destroy the tubular frameworks of the gold host .

The Chapter 8 describes the DFT study of the stretching of small monoatomic chains of gold and calculates their breaking force and modulus.The results were compared with similar calculations done using GP.

In Chapter 9, we have presented an algebra based on calulation of force constants to study the phonon dispersion relation for gold nanotube. Chapter 10 gives the summary of the work done in this thesis and its future scope.

Bibliography

[1]   P. Jr.Owens, Introduction to Nanotechnology, Wiley publications (2003).

[2]   D. J. Wales, J. P. K. Doye, J. Phys. Chem. A 101, 5111 (1997).

[3]   J. A. Alonso, Structure and Properties of Atomic Nanoclusters (Imperial College Press), London (2005).

[4]   O. Echt et al., J. Chem. Soc. Faraday Trans. 86, 2411(1990).

[5]   T. P. Martin, Physics Reports 273, 199(1996).

[6]   J. Li, X. Li , H. J. Zhai, L. S. Wang, *Science* 7 , 299 , 5608 , 864-867 (2003).

[7]   H. Ohnishi, Y. Kondo, K. Takayanagi, Nature 395, 780 (1998).

[8]   A. I. Yanson, G. Rubio Bollinger, H. E. van den Brom, N. Agrait, J. M. van Ruitenbeek, Nature 395, 783 (1998).

[9]   H. Hegger, K. Hecker, G. Reckziegel, A. Freimuth, B. Huckestein, M. Janssen, and R.Tuzinski, Phys. Rev. Lett. 77,3885 (1996).

[10]   J. W. Kang, H. J. Hwang, J. Kor.Phys. Soc., 42, S708-S712 (2003).

[11]   J.C. González, V. Rodrigues, J. Bettini, L. G. C. Rego, A. R. Rocha, P. Z. Coura, S. O. Dantas, F. Sato, D .S. Galvão, D. Ugarte , Phys. Rev. Lett.93, 126103 (2004).

[12]   Y. J. Lee, M. Brandbyge, M. J. Puska, J. Taylor, K. Stokbro, and R. M. Nieminen, Phy. Rev. B 69, 125409 (2004).

[13]   D. K. Avasthi , A. Kumar , R. Singhal, A. Tripathi, D. S. Misra, J Nanosci Nanotechnol. 10, 6, 3767-79 (2010).

[14]   BritishMuseum,http://www.britishmuseum.org/explore/online_tours/museum and exhibition/theartofglass/thelycurguscup.aspx. (2012)

[15]   M. Faraday, Philos. Trans. R. Soc. London 147, 145 (1857).

[16]   G. Frens , Nat. Phys.Sci 241,20-22,(1973).

[17]   Materials World, 11, 2, p.12-14 (2003).

[18]   P .Mukherjee , R. Bhattacharya , N. Bone, Y. K. Lee , C. R. Patra, S. Wang, L. Lu, C. Secreto, P. C.   Banerjee, M. J. Yaszemski , N. E. Kay,   D. Mukhopadhyay , J. Nanobiotechnology 5, 4 (2007).

[19]   C.W. C. Warren (Ed), Bio-Applications of Nanoparticles, Advances in Experimental Medicine and Biology 620, 207 (2007).

[20]   G. Schmid, Y. P. Liu, M. Schumann , T. Raschke, C. Radehaus, Nano Lett. 1, 405 (2001.)

[21]   G. Schmid, M. Bäumle, N. Beyer, Angew. Chem. 112, 187-189(2000); Angew. Chem. Int. Ed. 39, 181(2000).

[22]   G. Schmid, N. Beyer, Eur. J. Inorg. Chem. 835 (2000).

[23]   Th. Sawitowski, St. Franzka, N. Beyer, M. Levering, G. Schmid, Adv. Funct. Mater. 11, 169(2001).

[24] C. Burda, X. Chen, R. Narayanan, M. A. El-Sayed ,Chem. Rev. 105, 1025–1102 (2005).

[25] M. Grzelczak, J. Pérez-Juste, P. Mulvaney, L. M. Liz-Marzán, Chem. Soc. Rev. 37, 1783–1791 (2008).

[26] G. Periyasamy and F. Remacle, Nano Lett. 9, 3007–3011 (2009).

[27] D. I. Gittins, D. Bethell, D.J. Schiffrin, R.J. Nichols, Nature 408, 67(2000).

[28] J. Y. Ouyang, C. W. Chu, D. Sieves, Y. Yang, Appl. Phys. Lett. 86, 123507 (2005).

[29] C. Wang , C. Yu, Reviews in Analytical Chemistry 32, 1, 1–14 (2012).

[30] K. Saha, S. S. Agasti, C. Kim, X. Li, V. M. Rotello, Chem.Rev. 112, 2739−2779 (2012).

[31] H. Qian, M. Zhu, Z. Wu, R. Jin, Acc. Chem. Res. 45, 1470–1479 (2012).

[32] T. Tsukuda, Bull. Chem. Soc. Jpn. 85, 151–168 (2012).

[33] G. Li, R. Jin, Acc Chem Res. 46, 8, 1749-58 (2013).

[34] K. S. Pitzer, Acc. Chem. Res. 12 , 8 (1979).

[35] P. Pyykkö, Chem. Rev. 88, 563 (1988).

[36] P. Pyykko, J. P. Desclaux, Acc. Chem. Res. 12, 8, 276(1979).

[37] K. Pitzer, Accnts. Chem. Res. 12, 271(1979).

[38] N. Kaltsoyannis, J. Chem. Soc., Dalton Trans. 1 (1997).

[39] M. Jansen , Solid State Sciences 7 , 1464–1474(2005).

[40] R.P. Andres et al., Science 272, 1323 (1996).

[41] M. Valden, X. Lai and D.W. Goodman, Science 281, 5583, 1647(1998).

[42] S. Bulusu, X. C. Zeng, J. Chem. Phys. 125, 154303 (2006).

[43] J. Wang, G. Wang, and J. Zhao, Phys. Rev. B 66, 035418 (2002).

[44] M.J. Ford , B. Soul´e de Bas, M.B. Cortie, Materials Science and Engineering B 140, 177–181(2007).

[45] A. K. Murthy, R. J. Stover, A. U. Borwankar, G. D. Nie, S. Gourisankar, T. M. Truskett, K. V. Sokolov, K. P. Johnston, A.C. S. Nano 7,1(2013).

[46] Z. Li ,C. V . Ciobanu , J. Hu ,J. P. Palomares-Báez, J. L. Rodríguez-López, R. Richards , Phys. Chem. Chem. Phys. 13, 7 (2013).

[47] Z. Y. Li, N. P. Young, M. Di Vece, S. Palomba, R. E. Palmer, A. L. Bleloch, B. C. Curley, R. L. Johnston, J. Jiang, J. Yuan, Nature (Lett.) 451, 46 (2008).

[48] F. Weigend and R. Ahlrichs, Phil. Trans. R. Soc. A 368, 1245 (2010).

[49] K. Clemenger, Phys. Rev. B 32, 1359 (1985).

[50] B. Yoon, P. Koskinen, B. Huber, O. Kostko, B. von Issendorff, H. Häkkinen, M. Moseler, U. Landman,Chem Phys Chem 8, 157 (2007).

[51] B. D. Yadav, V. Kumar, Phys. Lett. 97, 133701 (2010).

[52] D. M. P. Mingos, Y. Slee, Z. Lin, Chem Rev 90, 383(1990).

[53] P. Gruene, D. M. Rayner, B. Redlich, A. F. G. Van der Meer, J. T. Lyon, G. Meijer, A. Fielicke, Science 321, 674 (2008).

[54] H.F. Zhang, M. Stender, R. Zhang, C. Wang, J. Li, L. S. Wang, J. Phys. Chem. B 108, 12259 (2004).

[55] P. Pyykko, Angew. Chem. Int. Ed. 43, 4412–4456 (2004).

[56] H. Hakkinen, B. Yoon, U. Landman, X. Li, H. J. Zhai, L.S. Wang, J. Phys. Chem. A 107, 6168 (2003).

[57] Y. Gao, W. Huang, J. Woodford, L.S. Wang, X.C. Zeng, J. Am. Chem. Soc. 131, 9484 (2009).

[58] T.G. Schaaff, W.G. Cullen, P.N. First, I. Vezmar, R.L. Whetten, W.G. Cullen, P.N. First, C. Gutieerez-Wing, J.Ascensio, M.J. Jose-Yacama, J. Phys. Chem. 101, 7885 (1997).

[59] K. Koga, H. Takeo, T. Ikeda, K.I. Ohshima, Phys. Rev. B 57, 4053 (1998).

[60] C.L. Cleveland, U. Landman, T.G. Schaaff, M.N. Shafigullin, P.W. Stephens, R.L. Whetten, Phys. Rev. Lett. 79, 1873 (1997).

[61] B. Palpant, B. Prevel, J. Lerme, E. Cottancin, M. Pellarin, M. Treilleux, A. Perez, J.L. Vialle, M. Broyer, Phys. Rev. B 57, 1963 (1998).

[62] B.H. Hess, U. Kaldor, J. Phys. Chem. 112, 1809 (2000).

[63] M.A. Omary, M.A. Rawashdeh-Omary, C.C. Chusuei, J.P. Fackler, P.S. Bagus, J. Chem. Phys. 114, 10695(2001).

[64] F. Furche, R. Ahlrichs, P. Weiss, C. Jacob, S. Gib, T. Bierweiler, M. Kappes, J. Chem. Phys. 117, 6982 (2002).

[65] Z. Zhang, A. Berg, H. Levanon, R. Fessenden, W.D. Meisel, J. Am. Chem. Soc. 125, 7959 (2003).

[66] J. Zheng, J.T. Petty, R.M. Dickson, J. Am. Chem. Soc. 125, 7780 (2003).

[67] J. Li, X. Li, H.J. Zhai, L.S.Wang, Science 299, 864 (2003).

[68] J. Wang, G. Wan, J. Zhao, Phys. Rev. B 66, 035418-1–035418-6. (2002).

[69] J. Zhao, J. Yang, J.G. Hou, Phys. Rev. B 67, 085404 (2003).

[70] K. Sugawara, F. Sobott, A.B. Vakhtin, J. Chem. Phys. 118, 7808 (2003).

[71] R.L. Whetten, J.T. Khoury, M.M. Alvarez, S. Murthy, I. Vezmar, Z.L. Wang, P.W. Stephens, C.L. Cleveland, W.D. Luedtke, U. Landman, Adv. Mater. 8, 428 (1996).

[72] M.M. Alvarez, J.T. Khoury, T.G. Schaa, W. Shagullin, I. Vezmar, R.L. Whetten, Chem. Phys. Lett. 266, 91(1997).

[73] N.T. Wilson and R.L. Johnston, Eur. Phys. J. D 12, 161-169 (2000).

[74] J.P.K. Doye, D.J. Wales, New J. Chem. 22 ,733–744(1998).

[75] P. M. Morse, Phys. Rev. 34, 57 (1929).

[76] A.W. Jasper, N.E. Schultz, D.G. Truhlar, J. Phys. Chem. B 109, 3915–3920 (2005).

[77] X. Wu, S. Chen, Y. Sun, Y. Chen, Computational and Theoretical Chemistry 1002, 43–48 (2012).

[78] T. Pawluk, L. Xiao, J. Yukna, L.C. Wang, J. Chem. Theory Comput. 3, 328–335(2007).

[79] I. L. Garzon, K. Michaelian, M.R. Belran, A. Posada-Amarillas, P. Ordejon, E. Artacho, D. Sanchez-Portal, J.M. Soler, Phys. Rev. Lett. 81, 1600–1603(1998).

[80] I. L. Garzon, Alvaro Posada-Amarillas, Phys Rev B 54,16 (1996).

[81] Y.S. Shen, J.J. BelBruno, J. Phys. Chem. A 109, 512 (2005).

[82] J. Li, X. Li, H.-J. Zhai, L. S. Wang, Science 299, 864 (2003).

[83] G. Bravo-Pérez, I. L. Garzón, O. Novaro, J. Mol. Struct. THEOCHEM 493, 225 (1999).

[84] I.B. Bersuker, The Jahn-Teller Effect, *Cambridge* University Press (2006).

[85] A. Hermann, R.P. Krawczyk, M. Lein, P. Schwerdtfeger, I. P. Hamilton, J.J.P. Stewart, Phys. Rev. A 76, 013202(2007).

[86] H. Hakkinen, M. Moseler, and U. Landman, Physical Review Letters 89, 033401-1–033401-4 (2002).

[87] A. V. Walker, J. Chem. Phys. 122, 094310 (2005).

[88] H. Häkkinen , U. Landman, Phys. Rev. B 62, R2287 (2000).

[89] F. Remacle, E. S. Kryachko, J. Chem. Phys. 122, 044304 (2005).

[90] V. Bonačić-Koutecký, J. Burda, R. Mitrić, M. Ge, G. Zampella, P. Fantucci, J. Chem. Phys. 117, 3120 (2002).

[91] A. Castro, M. A. L. Marques, A. H. Romero, M. J. T. Oliveira, A. Rubio, J. Chem. Phys. 129, 144110 (2008).

[92] E. M. Fernandez, J. M. Soler, I. L. Garzón, L .C. Balbas, Phys. Rev. B – Condensed Matter, 70, 165403-1–165403-14 (2004).

[93] P. Koskinen, H. Hakkinen, B. Huber, B. von Issendorff, M. Moseler , Phys. Rev. Lett. 98, 015701-1–015701(2007).

[94] M. P. Johansson, A. Lechtken, D. Schooss, M. M. Kappes, F. Furche, Phys. Rev. A 77, 053202 (2008)

[95] L. Xiao, B. Tollberg, X. Hu, L. Wang, J. Chem. Phys. 124, 114309 (2006)

[96] S. Gilb, P. Weis, F. Furche, R. Ahlrichs , M. M. Kappes , J. Chem. Phys. 116, 4094–4101(2002).

[97] P. Sudraud, C. Colliex, J. Vandewalle, J. Phys. Lett. 40, L207–L211*(1979).*

[98] W. D. Knight, K. Clemenger, W. A. de Heer, W. A. Saunders, M. Y. Chou, M .L. Cohen, Phys. Rev. Lett. 52, 2141–2143 (1984).

[99] K. J. Taylor, C. L. Pettiette-Hall, O. Cheshnovsky, R. E. Smalley, J. Chem. Phys. 96, 3319 – 3329(1992).

[100] C. Jackschath, I. Rabin, W. Schulze, B. Bunsen-Ges. 96, 1200 –1204(1992).

[101] H. Häkkinen, M. Moseler, O. Kostko, N. Morgner, M. A. Hoffmann, B. von Issendorff, Phys. Rev. Lett. 93 , 093401 (2004).

[102] L. Lin, P. Claes, P. Gruene, G. Meijer, A. Fielicke, M. T. Nguyen, P. Lievens, Chem Phys Chem . 11 , 1932 (2010).

[103] A. Lechtken, C. Neiss, M. M. Kappes, D. Schooss, Phys. Chem. Chem.Phys. 11, 4344 (2009).

[104] L. M. Wang, J. Bai, A. Lechtken, W. Huang, D. Schooss, M. M. Kappes, X. C. Zeng, L. S. Wang, Phys. Rev.B, 79 , 033413 (2009).

[105] W. Huang , L. S. Wang, Phys. Rev. Lett.102, 153401 (2009).

[106] J. Li, X. Li, H. J. Zhai, L. S. Wang, Science, 299, 864–867 (2003).

[107] E. S. Kryachko, F. Remacle, Int. J. Quant. Chem. 107, 2922–2934 (2007).

[108] (a) E. Apra, R. Ferrando, A. Fortunelli, Phys. Rev. B - Condensed Matter, 73, 205414-1–205414-5 (2006) ; (b) Z. W. Wang , R. E. Palmer, Nanoscale 4, 4947-4949 (2012).

[109] B. Soul´e de Bas, M.J. Ford, M.B. Cortie, J. Phys.: Condens. Matter 18, 55–74 (2006).

[110] M.P. Johansson, P. Pyykko, Phys. Chem. Chem. Phys. 6, 2907–2909(2004).

[111] M. P Johansson, D. Sundholm, J. Vaara, Angew. Chem. Int. Ed. 43, 2678 (2004).

[112] X. Gu, M. Ji, S. H. Wei, X. G. Gong, Phys. Rev. B. 70, 205401(2004).

[113] Y. Gao, X. C. Zeng, J. Am. Chem. Soc. 127, 3698 (2005).

[114] J. Wang, J. Jellinek, J. Zhao, Z. Chen, R. B. King, P.V.R. Schleyer, J. Phys. Chem A, 109, 9265 (2005).

[115] E. M. Fernandez, J. M Soler, L. C Balbas, Phys. ReV. B. 73, 235433(2006).

[116] W. Fa, J. Dong, J. Chem. Phys. 124, 114310(2006) .

[117] S. Bulusu, X. Li, L. S. Wang, X. C. Zeng, J. Phys. Chem. C, 111, 4190-4198 (2007).

[118] X. P Xing, B Yoon, U. Landman, J. H. Parks, Phys. ReV. B, 74, 165423 (2006).

[119] M. Ji, X. Gu, X. Li, X. Gong, J. Li, L. S. Wang, Angew. Chem. Int. Ed 44, 7119 (2005).

[120] (a) M. Turner , V B Golovko, O P Vaughan , P Abdulkin , A. Berenguer-Murcia M S Tikhov , B F Johnson , R M Lambert , Nature. 454, 7207, 981-3 (2008); (b) M. Turner, V. B. Golovko, O. P. H. Vaughan, P. Abdulkin, A. Berenguer-Murcia, M. S. Tikhov, B. F. G. Johnson, R. M. Lambert, doi:10.1038/nature07194 (2008).

[121] H.Hakkinen, M.Moseler, O.Kostko, N. Morgner, M.Astruc Hoffmann, B.V. Issendorff, arXiv:cond-mat/0404184 [cond-mat.other]

[122] A. J. Karttunen, M. Linnolahti, T A Pakkanen, P. Pyykko, Chem. Comm. 4, 465–467(2008).

[123] M. P. Johansson, J. Vaara, D. Sundholm, J. Phys. Chem. C 112, 19311 (2008).

[124] C. L. Cleveland, U. Landman, M. N. Shafigullin, P. W. Stephens, and R. L. Whetten, Z. Phys. D 40, 503 (1997).

[125] D .W Yuan, Y Wang, Z. Zeng, J. Chem. Phys. 122, 114310 (2005).

[126] Q. Sun, Q Wang, J Z .Yu, Z Q Li, J T Wang, J.Phys. 7 1233 (1997).

[127] M B Torres, E M Fernandez, L C Balbas, Phys. Rev. B 71 155412 (2005).

[128] S Y Wang, J Z Yu, H Mizuseki, Q Sun, C Y Wang, Y Kawazoe, Phys. Rev. B 70 ,165413 (2004).

[129] P.Pyykko,N. Runeberg, Angew. Chem. 114, 2278 (2002); P.Pyykko, N Runeberg,. Angew. Chem., Int. Ed. 41, 2174(2002).

[130] X. Li, B. Kiran, J. Li, H. J. Zhai, L. S. Wang, Angew. Chem. Int. Ed. 41, 4786 (2002).

[131] X . Li, B. Kiran, L. F Cui, L. S. Wang, Phys. ReV. Lett, 95, 253401(2005).

[132] Z. Meng , F. X. Juan , Z. L. Xia, H. L. Ming, L. Y. Hua, Chin. Phys. B 19, 4 043103 (2010).

[133] R. Pal, L. M. Wang, Wei Huang, Lai-Sheng Wang, Xiao Cheng Zeng, J. Chem. Phys. 134, 054306 (2011).

[134] T K Ghanty, A. Banerjee, A. Chakrabarti, J .Phy. Chem. C 114, 20-27 (2010).

[135] L. Wang, S. Bulusu, W. Huang, R. Pal, L.S. Wang, X.C. Zeng, J. Am. Chem. Soc. 129, 15136(2007).

[136] Q. Sun, Q. Wang, G. Chen, P. Jena, J. Chem. Phys. 127, 214706(2007).

[137] F. Wei , Y.Aping , Phys. Lett. A 372, 6392–6395(2008).

[138] M. Walter, H. Ha kkinen, Phys. Chem. Chem. Phys. 8, 5407–5411(2006).

[139] L. M Wang, S Bulusu, H. J Zhai, X. C Zeng, L. S. Wang, Angew. Chem., Int. Ed., 46, 2915(2007) .

[140] S. Link, M. A. El-SayedJ. Phys. Chem. B 103, 8410 (1999).

[141] H. W. Wang, C. F Shieh, H. Y Chen, W. C Shiu, B Russo, G. Cao, Nanotechnology 17, 2689–94 (2006).

[142] J. Aizpurua, P. Hanarp, D. S. Sutherland, M. Kall, G .W. Bryant, F. J. G. de Abajo Phys. Rev. Lett. 90, 057401 (2003).

[143] K. Takayangi, Y. Kondo, H. Ohnishi, Japan Soc. Appl.Phys. Int. 3, 3–8 (2001); Y Kondo and K Takayangi, Phys. Rev. Lett. 79, 3455(1997).

[144] R. T. Senger, S. Dag, S. Ciraci, Phys. Rev. Lett. 93, 196807 (2004).

[145] H. W. Wang, C. F.Shieh, H. Y. Chen, W. C. Shiu, B. Russo and G. Cao, Nanotechnology 17, 2689–2694(2006).

[146] Y. Oshima, H. Koizumi, K. Mouri, H. Hirayama, K. Takayanagi, and Y. Kondo, Phys. Rev. B 65, 121401(2002).

[147] Y. Oshima, A. Onga, K. Takayanagi, Phys. Rev. Lett. 91, 205503 (2003).

[148] P. Sen, O. Gulseren, T. Yildirim, I. P. Batra, and S. Ciraci, arXiv:cond-mat/0205313v1 [cond-mat.mtrl-sci] (2002).

[149] R. T. Senger, S. Dag, S. Ciraci, Turk J Phys 29, 269 – 276 (2005).

[150] T T Albrecht, J Schotter, G A Kastle, N Emley , Science 290 , 2126(2000).

[151] S Michotte, S M Tempfli, L Piraux, Appl. Phys. Lett. 82, 4119(2003).

[152] R Sordan, M Burghard, K Kern, Appl. Phys. Lett. 79, 2073(2001).

[153] Z Tang, N A Kotov, M Giersig, Science 297, 237(2002).

[154] P Z Coura, S B Legoas, A S Moreira, F Sato, V Rodrigues, S O Dantas, D Ugarte and D S Galvao , Nano lett. 4, 1187 (2004).

[155] E Z da Silva, A J R da Silva, A Fazzio, Phys. Rev. Lett. 87 256102(2001).

[156] J. I. Pascual, J. Mendez, J. Herrero-Gomez, A. M. Baro,N. Garcia, U. Landman, W. D. Luedtke, E. N. Bogachek,H. P. Cheng, Science 267, 1793 (1995).

[157] J. C. Tung, G. Y. Guo, Phys. Rev. B 76, 094413 (2007).

[158] M. Weissmann, G. García, M. Kiwi, R. Ramírez, C. C. Fu, Phys.Rev. B 73, 125435 (2006).

[159] H. Shiroishi, T. O. da, H. Sakashita, N. Fujima, Eur. Phys. J. D 43,129 (2007).

[160] L. Liu, S. Mu, S. Xie, W. Zhou, L. Song, D. Liu, S. Luo, Y. Xiang, Z.Zhang, X. Zhao, W. Mal, J. Shen, C. Wang, G. Wang, J. Phys. D 39, 3939 (2006).

[161] L. Guan, K. Suenaga, S. Okubo, T. Okazaki, S. Iijima, J. Am. Chem. Soc. 130, 2162 (2008).

[162] L. Zhu, J. Wang, F. Ding, J. Chem. Phys. 130, 064706 (2009).

Chapter 2

2. Computatoional Methodology

2.1 Introduction

A study of cluster structures can be termed as the study of stable structures as only later can be used for practical applications of nanoparticles. Moreover, the structure influences the different physical and electronic properties of the nanoparticles. .

The optimization of geometry is one of the central problems of cluster studies. A cluster at a given finite temperature, with a given size and composition, can have different structural states (isomers), that is, meta-stable states and the most stable state (thermodynamic equilibrium structure) which can be described as local minima (LM) and the global minimum (GM), respectively, on the potential energy surface. Solving an optimization problem means finding the GM – the structural state having the lowest potential energy, as well as low-lying LM. As the cluster size increases the optimization becomes more difficult due to an exponential increase in the number of minima with cluster size [1].

Two different approaches are used for the optimization problems: ab initio and non-ab initio. The first principle or ab initio methods apply many-body quantum theories such as Density Functional Theory (DFT) to calculate the properties of a system from first principles with no parameterization. Despite their high accuracy, ab initio calculations for large clusters (consisting of hundred of atoms or more) are computationally expensive [2]. The non-ab initio approach (i.e., the empirical or semi- empirical approach) involves the use of empirical atomistic potentials which have parameters fitted to experimental data.

There are two different models of atomistic potentials which are often used in cluster studies: pair-wise potentials, such as the Morse potential and the Lennard-Jones, and many-body potentials, such as the Gupta and Sutton-Chen potentials. The main difference between the many-body potentials and pair wise potentials is that the interaction between two atoms is not only dependent on two atoms, but also upon their local environment. [1, 3, 4].

As discussed in the Chapter 1, we will be mainly studying gold clusters, nanotubes and nanowires. We have used a combined empirical and ab initio approach to study structural and energetic configurations of pure gold clusters.

Gupta potential (GP) have been widely employed to determine the different configurations of gold nanoclusters of various size ranges [5, 6]. The empirical approach is preferred in order to overcome the computational limitations imposed by more computationally expensive first principles approaches The GP is suitable and versatile for modeling noble and quasi-noble metals. However, in order to study electronic effects on the structure, it is important to verify the predictions of the GP using first principles calculations i.e., Density Functional Theory (DFT) [7].

DFT methods are the most widely used ab initio methods in computational material science and solid state physics due to their high accuracy and computational efficiency (among the first-principle methods).Since we have used both GP and DFT methods in our research, we will discuss both methods in details in the following sections.

2.2. Gupta Potential- The Semi Empirical approach

The potential energy of an N body system can be expanded in terms of interactions involving up to N particles.

$$V = V^{(0)} + \sum_{i}^{N} V_i^{(1)} + \sum_{i}^{N-1} \sum_{j \rangle i}^{N} V_{ij}^{(2)} + \sum_{i}^{N-2} \sum_{j \rangle i}^{N-1} \sum_{k \rangle j}^{N} V_{ijk}^{(3)} + \underline{\quad\quad} + V_{123\ldots N}^{(N)} \quad\quad (2.1)$$

$V^{(0)}$ denotes the background energy of the system, taken to be zero if there is no external field acting on the system.

$V_i^{(1)}$ is the energy of isolated atom i and is taken to be zero if the atom is in ground state

$V_{ij}^{(2)}$ is the two body interaction between atom i and j there are higher order terms

$V_{123\ldots N}^{(N)}$ involving all the particles of the system.

In pair potential only the interactions between pairs of particles are calculated and the summation becomes [8]

$$V = \sum_{i=1}^{N-1} \sum_{j \rangle i}^{N} V_{ij}\left(r_{ij}\right) \quad\quad (2.2)$$

where $V_{ij}\left(r_{ij}\right)$ denotes that the functional form of the potential is dependent on the interparticle separation, r_{ij}. The effect of the changes in the electron density which causes the binding between the two atoms has been averaged into a functional form, V_{ij}, which approximates the interactions within the system.

The above potential describes the interaction between particles and ignores the relation with other particles of the system. But in metallic system the bonding electrons are delocalized over large number of atoms and the bonding between two atoms depends on the local environment. Hence pair potentials do not give accurate description of metallic system leading to the development of many body potentials to give better description of interatomic interactions.

In order to include the many body character in the bonding scheme one can either include the higher terms in potential energy e.g. Murrell-Mottram Potential or through dependency on the local electronic density e.g Gupta potential. The many-body component into the bonding comes from the local electron density dependence on the configuration of the whole system [8]. The potentials those include the many body effect are the Embedded Atom Model (EAM), the Finnis-Sinclair potential, the Sutton-Chen potential and the Gupta potential .

2.2.1 Gupta Potential

We have used many body potential to study the structural stability of small gold clusters. This potential has already been used in studying of structural and related properties of variety of clusters e.g. Pb, Ni& Ag, Au, Zn, Cd [9-12].

The many body Gupta potential is derived from Gupta's expression for the cohesive energy of bulk material. It is based on the tight-binding second-moment approximation [13, 14]. It includes a repulsive pair term V_{ij}^{r} and many body attractive term V_{ij}^{m}

$$V = \sum_{i-1}^{N} \left[\sum_{\substack{j=1 \\ j \neq i}}^{N} V_{ij}^{r}\left(r_{ij}\right) - \sqrt{\sum_{\substack{j=1 \\ j \neq i}}^{N} V_{ij}^{m}\left(r_{ij}\right)} \right] \qquad (2.3)$$

$$V_{ij}^{r} = A \exp\left(-p\left[\frac{r_{ij}}{r_o} - 1\right]\right) \qquad (2.4)$$

$$V_{ij}^{m} = \xi^{2} \exp\left(-2q_{ij}\left[\frac{r_{ij}}{r_o} - 1\right]\right) \qquad (2.5)$$

where r_{ij} is the distance between two atoms, A, r_o, ζ, p and q are the parameters fitted to experimental values of the cohesive energy, lattice parameters and independent elastic constants for the reference crystal at 0K.

31

The Gupta potential has been parameterized by Cleri and Rosato for a wide variety of metals [14].

2.3. First Principle or Ab-initio methods

The semi empirical method discussed above relies on the experimental data rather than theoretical information whereas the quantum mechanical methods (ab initio, or first-principle method) do not use any empirically or experimentally derived quantities. One of the limitations of the empirical-potential approach is that they cannot tell us the electronic properties of a given material.

Various quantum chemistry techniques are used in materials science for performing the electronic structure calculations and can simulate systems composed of small molecules to one thousand atoms up. We can have different quantum mechanical methods such as Hartree Fock method, DFT. The methods involve solving of many electron Schrödinger equation.

The time-independent, non-relativistic Schrödinger equation for a system of N interacting electrons, (in atomic units):

$$\hat{H}\,\Psi\!\left(\left\{\vec{R}_I\right\},\left\{\vec{r}_i\right\}\right)= E\Psi\!\left(\left\{\vec{R}_I\right\},\left\{\vec{r}_i\right\}\right) \tag{2.6}$$

where ψ is a true many-body wave function of the system which depends on each of the spatial coordinates of each of the N electrons; E is the eigen ground state energy of the electrons; r_i, R_I are the sets of electronic and ionic coordinates with indices i and I representing all electrons and ions respectively.

The Hamiltonian for interacting electrons in a many-body system is given by,

$$\hat{H} = -\sum_i \frac{\hbar^2}{2m}\nabla_i^2 - \sum_I \frac{\hbar^2}{2M_I}\nabla_I^2 + \frac{1}{2}\sum_{i,j}\frac{e^2}{\left|r_i - r_j\right|} - \sum_{I,i}\frac{Z_I e^2}{\left|R_I - r_i\right|} + \frac{1}{2}\sum_{I,J}\frac{Z_I Z_J e^2}{\left|R_I - R_J\right|} \tag{2.7}$$

where Z_I and M_I are ionic charges and ionic masses, m is the mass of electron.

1st term represents the kinetic energy of each electron,

2nd term represents the kinetic energy of ions or nuclei

3rd term is the interaction energy between different electrons or Hartree term V_H,

4th term is the potential acting on each electron due to the atomic nuclei,

and 5th term is the interaction energy between ions.

It is very difficult to solve the many-body Schrödinger equation (2.6) and the respective Hamiltonian (2.7), because of the large difference between the masses of

electrons and the nuclei. Therefore the electrons respond much more rapidly to the changes in their surroundings compared to nuclei. In order to simplify the many body wave functions the "Born-Oppenheimer Approximation" is used, which treats the nuclei adiabatically leading to a separation of electronic and nuclear coordinates in it. This decoupling of electronic and nuclear coordinates is then applied to equation (2.7) .The stationary electronic state is then described by a wave function ψ (r_1, r_2,……,r_n) fulfilling the many-electron Schrödinger equation,

$$\hat{H}\,\Psi\; =\; \left[\sum_{i}^{N} -\frac{\hbar^2}{2m}\nabla_i^{\,2} + \sum_{i}^{N} V^{ext}\left(\vec{r}_i\right) + \sum_{i\langle j} U\left(\vec{r}_i,\vec{r}_j\right) \right]\Psi\; =\; E\,\Psi \qquad (2.8)$$

where $\hat{H}$ is the electronic molecular Hamiltonian, N is the number of electrons and U is the electron-electron interaction, E is electronic energy of the system. The term 4th and 5th of equation (2.7) combines to form a fixed external potential acting on $V^{ext}\left(\vec{r}_i\right)$ electrons due to nuclei.

Even with this simplification, the many body problem remains difficult to solve. The accuracy of these quantum mechanical techniques depends on the effectiveness of the methods to deal with many electron system. The many electron system can be described using Hartree-Fock (HF) and density functional methods.

2.3.1 Hartree Fock Method

The Hartree-Fock method is a variational, wavefunction-based approach where the full many-body wave function is replaced by a single Slater determinant. Then the wave function Ψ can be written as a single Slater determinant:

$$\Psi\; =\; \frac{1}{\sqrt{N!}}\left|\left(\Psi_1\left(r_1\right)\Psi_2\left(r_2\right)\cdots\cdots \; \Psi_N\left(r_N\right)\right)\right| \qquad (2.9)$$

Although it is a many-body technique, the approach followed is that of a single-particle picture. The electrons are assumed to occupy single-particle orbitals making up the wavefunction. Each electron feels the presence of the other electrons indirectly through an effective potential. Thus each orbital is affected by the presence of electrons in other orbitals.The limitation of HF approximation is in order to get vanishingly small error; one needs a large number of different Slater determinants. To improve up the results one may employ post-Hartree-Fock methods i.e., DFT

2.3.2 Density Functional Theory (DFT)

Density functional theory is among the most popular and successful quantum mechanical approaches applied to the matter. It determines the properties of a system solely as a function of the electron density. It is widely used for the simulation of the electronic structure of clusters, molecules and nanowires [15-17]. It can predict the properties of the ground state of any system of electrons.

Density functional theory (DFT) allows the replacement of complicated N electron wave function ψ (r_1, r_2, ..., r_n) and associated Schrödinger equation by simpler electron density $n(\vec{r})$.

$$n(\vec{r}) = N \int d^3 r_1 \int d^3 r_2 ..... \int d^3 r_N \Psi^*(r_1, r_2 .... r_N) \Psi \ (r_1, r_2 .... r_N) \quad (2.10)$$

The DFT formulism is based on two fundamental mathematical theorems proposed by Kohn and Hohenberg in 1964 [18].

Theorem **I**: For any system of interacting particles in an external potential V^{ext} (**r**), the potential V^{ext}(**r**) is uniquely determined, except for a constant, by the ground state particle density n_o(**r**).

Theorem **II**: A universal functional for the energy $E[n]$ in terms of the density n(**r**) can be defined, which is valid for any external potential V^{ext}(**r**). For any particular V^{ext}(**r**), the exact ground state of the system is the global minimum value of this functional, and the density n(**r**) which minimizes the functional is the exact ground state density n_o(**r**).Thus, one writes the total energy E of the system as a functional of the charge density.

$$E[n] = T[n] + \int V^{ext}(n) n(r) dr + V_H[n] + E_{xc}[n] \quad (2.11)$$

where T is kinetic energy, V^{ext} is external potential acting on system including the electron-nuclei interaction, **V_H** is Hartree energy describing electron- electron coulomb repulsion

$$\mathbf{V_H} = \frac{e^2}{2} \int \frac{n(r) n(r')}{|r - r'|} dr dr' \quad (2.12)$$

and E_{xc} is exchange-correlation energy because it contains contributions from the Hartree-Fock (HF)-like exchange of electrons of same spin, and the correlation of the individual electrons, due to Pauli repulsion. It was difficult to evaluate the kinetic energy of electrons directly from charge density. The potential V^{ext} and the total energy E are universal but unknown functionals of the density.

Kohn and Sham (KS) [19] showed that there exists a mapping between the full interacting problem and a one-particle problem, in which the one-particle wavefunctions give the exact density. They suggested using single electron orbitals wavefunctions ψ_i to define density as

$$n(r) = \sum_i^N \sum_s \left| \Psi_i(r,s) \right|^2 \tag{2.13}$$

where N is the number of electrons and kinetic energy of a system of non interacting electrons with electron charge density as

$$T[n(r)] = -\frac{\hbar^2}{2m} \sum_i^N \left\langle \Psi_i \left| \nabla^2 \right| \Psi_i \right\rangle \tag{2.14}$$

Kohn and Sham solved the variational problem of minimizing the energy functional by applying the Lagrangian method of undetermined multipliers to equation (2.8). The Schrödinger equation for N non interacting electrons moving in an effective potential can now be written as

$$-\frac{\hbar^2}{2m} \nabla^2 \Psi_i(r,s) + V_{eff}(r) \Psi_i(r,s) = \varepsilon_i \Psi_i(r,s) \tag{2.15}$$

where V_{eff} is

$$V_{eff}(r) = V_{ext}(r) + e^2 \int \frac{n(r')}{|r - r'|} dr' + \frac{\delta E_{xc}[n]}{\delta n} \tag{2.16}$$

These equations form the Kohn-Sham orbital equations. This system is then solved iteratively, until self-consistency is reached. It starts with an initial guess for n(r), then calculates the corresponding V_{eff} and solves the Kohn-Sham equations for $\Psi_i(r,s)$. From these one calculates a new density and starts again. This procedure is then repeated until convergence is reached. The steps to achieve self consistency are presented in form of a flowchart (see Fig. 2.1).

The main problem arises in solving equation (2.15), is how to approximate the exchange correlation functional $E_{xc}[n]$. One of the first approaches is the local density approximation (LDA) [20]. It states that an inhomogeneous system is treated as locally-homogeneous, and the functional is approximated as an integral of the local functional $\varepsilon_{xc}(n)$ multiplied with the electron density, over the system volume and is given by

$$E_{xc}[n] = \int \varepsilon_{xc}(n) n(r) d^3 r \tag{2.17}$$

where $\varepsilon_{xc}(n)$ is exchange correlation energy. The local density approximation gives exact solutions for a homogeneous electron gas, so it works well for systems in which the electron density does not vary too rapidly.

Self-Consistent Kohn-Sham Equations
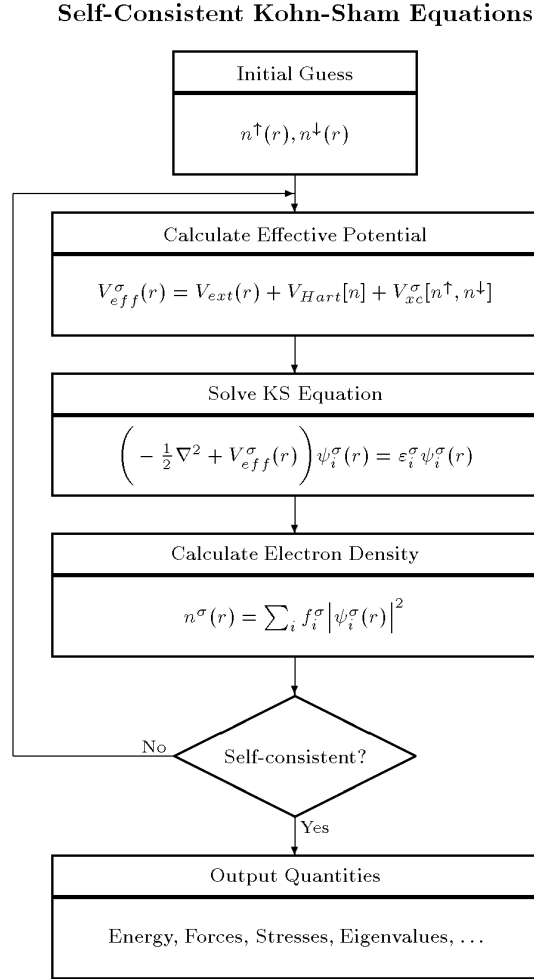
Figure 2.1 Flow chart describing a self-consistent cycle for electron density.

The next step beyond the local-density approximation is to include the gradients of the density at the point where we want to calculate $\varepsilon_{xc}(n)$. In a non homogeneous system, the exchange correlation potential at the point r depends not only on the value of the density at r but also on its variation close to r. This type of system requires another approximation known as *Generalized Gradient Approximation (GGA)* which includes the information from the gradient of the electron density [21, 22].

$$E_{xc}[n] = \int \varepsilon_{xc}(n, \nabla n(r))n(r)d^3r \qquad (2.18)$$

In our work, we have used a generalized gradient approximation to the exchange-correlation energy. There exist quite a number of different parameterizations of LDA

and GGA. The local density approximation (LDA) with the Perdew - Zunger parametrization of the correlation energy of a homogeneous electron gas was calculated by Ceperley and Alder [23]. For GGA, two of the most widely used functionals are the Perdew Wang functional (PW91) [24] and the Perdew- Burke-Ernzerhof functional (PBE) [25].

Adding additional constraints to functionals of n, ∇ n, or the kinetic energy density, one gets so-called meta- GGA [26, 27] approximations. For our research, we have used both GGA-PBE and GGA- PW 91 for the parameterizations of the exchange-correlation energy. It has been reported in a theoretical study that for the structures and energies of gold clusters the GGA functionals provide overall better performance than the LDA and hybrid GGA functionals [28].

2.4 Basis Function

Solving the Kohn-Sham equation (2.15) requires information about the molecular orbitals which is represented by some sets of functions called the basis set. These functions are usually atomic orbitals. There are different methods which propose different basis functions and each method has its advantages and shortcomings at the same time. Few of them are discussed here.

2.4.1   Linearized augmented plane wave (LAPW) basis

The linearized augmented planewave (LAPW) method [29] is used for solving the equations of DFT. It is a variational expansion approach which approximates the solutions as a finite linear combination of basis functions. Its methodology includes the dividing the unit cell into two parts: spheres around each atom in which the wave functions varies rapidly and are atomic-like; and the remaining interstitial region, where the wave functions are not atomic-like and are much smoother. Each basis function is defined as a plane wave in the interstitial region connected smoothly to a linear combination of atomic-like functions in the spheres. The LAPW basis is accurate and efficient for the solution of the all-electron ab initio electronic-structure problem. However, it is computationally very expensive and is difficult to implement.

2.4.2   Plane wave (PW) method

The plane wave (PW) basis set is extensively used as it is easy to implement, uses simple basis functions and allows systematic convergence. PW basis sets are often

used in combination with an 'effective core potential (ECP) ' or pseudo potential, hence are only used to describe the valence charge density.

In PW basis set, the representation of Kohn Sham orbital would require a continuous, and infinite, basis set. Applying the periodic boundary conditions, the orbital ψ_i may be written as

$$\Psi_{i,k}(r) = \sum_{G} c_{i,k}(G) e^{i(k+G).r} \qquad (2.19)$$

where the sum is over reciprocal lattice vectors **G** and k is a symmetry label which lies within the first Brillouin zone.

The core electrons are concentrated very close to the atomic nuclei, therefore the density gradients near the nuclei are not easily described by a plane-wave basis set, it requires the use of very high energy cutoff

$$\frac{\hbar^2 |k+G|^2}{2m_e} \leq E_{cut} \qquad (2.20)$$

Thus, the convergence of the calculation with respect to basis set may be ensured by variation of a single parameter, E_{cut}. Thus PW offers a major advantage over many other basis set choices, as the calculated properties often show extreme sensitivity to small changes in basis set.The main disadvantage of the use of a PW basis set is it requires a large number of basis functions to accurately represent the Kohn-Sham orbitals.

2.4.3 Localized basis sets

The plane wave basis functions because of their extended nature over the whole system cannot be used in linear-scaling calculations; hence a different choice has to be made, in which the basis functions are localized in real-space. The different representations of atomic orbitals are Gaussian type [30, 31], Slater type [32] and numerical atomic orbitals [19, 33]. Numerical atomic orbital (NAO) are discussed in detail in the following section:

Numerical atomic orbitals

Numerical atomic orbitals (NAO's) are best suited to linear scaling methods as they are very flexible, strictly localized, and only few of them are required for accurate

results. The basis orbitals are products of spherical harmonics times numerical radial functions centered on atoms:

$$\Phi_{Ilmn}(r) = R_{Ilm}\left(\left|\vec{r}_I\right|\right)Y_{lm}\left(\hat{r}_I\right) \qquad (2.21)$$

where, I is the index of the atom, m is the angular momentum quantum number, n is the number of degenerate orbitals with same l and m, R_{Ilm} is the radial part describing the degrees of freedom and Y_{lm} denotes the spherical harmonics. The main features of a basis set of atomic orbitals are:

Size: From the nomenclature of Quantum Chemistry, a hierarchy of basis sets is given as first-ξ, second- ξ orbital, etc. A single- ξ (also called minimal) basis set has one radial function per angular momenta channel. Radial flexibility is obtained by adding a second function per channel called as double- ξ (DZ). The split valence scheme [34, 35, 36] is widely used to explain the basis sets and is applied to localized NAOs.

Range: Cutoff radii of orbitals or the strictly localized orbitals (zero beyond a cutoff radius) are used in order to obtain sparse Hamiltonian and overlap matrices for linear scaling. The accuracy and computational efficiency of the calculations depend upon defining all the different cutoff radii for strictly localized orbitals by a single parameter called "*Energy Shift*". It is the energy raise suffered by the orbital when confined defines all the cutoff radii [37].

Shape: The shape of the orbitals at larger radii depends on the cutoff radius and on the localization of the orbitals. The first proposal was an infinite square-well potential which has been widely used for minimal bases within the ab initio tight-binding scheme of Sankey and collaborators [38]. A new soft confinement potential was later proposed [18]. It is flat in the core region, starts of at some internal radius r_i with all derivatives continuous, and diverges at r_c ensuring a strict localization .

For a given system and basis size, the range and shape of the orbitals are defined as described above, depending on parameters: the energy is minimized with respect to all of them.

2.5 Pseudopotential

Most of the physical properties of solids are dependent on the valence electrons and the core electrons (though to much smaller extent). Since the core electrons are relatively unaffected by the chemical environment of an atom, their contribution to the total binding energy does not change when isolated atoms are brought together to

form a molecule or crystal. Therefore the actual energy differences of interest are the changes in valence electron energies, and if the binding energy of the core electrons can be subtracted out, the valence electron energy change will be a much larger fraction of the total binding energy, and hence can be calculated accurately.

The pseudo potential approximation removes the core electrons and replaces them and the strong ionic potential by a weaker pseudopotential. This pseudopotential will act as a set of pseudo wave functions rather than the true valence wave functions. Another reason for the use of pseudopotential approximation is a very large number of plane waves are required to expand the tightly bound core orbitals. Therefore a vast amount of computational time would be required to calculate the electronic wave functions and perform an all-electron calculation. The pseudopotential approximation allows the expansion of electronic wave functions using a much smaller number of plane wave basis states. An ionic and valence potential wavefunction and the corresponding pseudopotential and pseudo wave function are illustrated schematically in Fig. 2.2
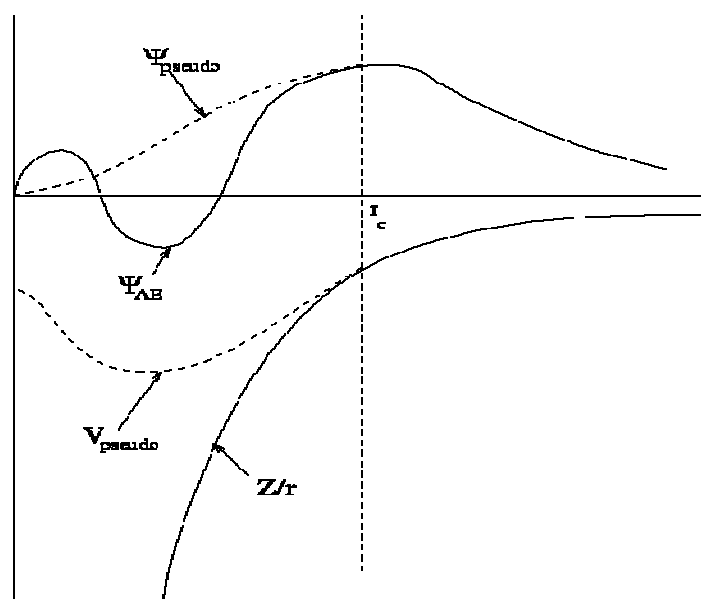
Figure 2.2 An illustration of all-electron (solid lines) and pseudoelectron (dashed lines) potentials and their corresponding wave functions. The radius r_c, is the cut off distance after which all-electron and pseudoelectron values match.

Since the core states are localized in the vicinity of the nucleus, the valence states must oscillate rapidly in this core region in order to maintain this orthogonality with the core electrons. This rapid oscillation results in a large kinetic energy for the valence electrons in the core region, which roughly cancels the large potential energy due to the strong Coulomb potential. Thus the valence electrons are much more

weakly bound than the core electrons. The pseudopotential is constructed in such a way to replace the valence electron wave-functions, which oscillate rapidly in the core region, by *pseudo-wave-functions*, which vary smoothly in the core region [39, 40]. It can be from the graph that outside the core region the two potentials are identical, and the scattering from the two potentials is indistinguishable.

The general form for pseudopotential is:

$$V_{\ln} = \sum_{lm} |lm\rangle V_l \langle lm|$$ (2.22)

where, $|lm\rangle$ are the spherical harmonics and V_l is the pseudopotential for angular momentum *l*. A pseudopotential that uses the same potential for all the angular momentum components of the wave function is called a *local pseudopotential* [44]. A nonlocal pseudopotential uses a different potential for each angular momentum component of the wave function. Local pseudopotentials are computationally much more efficient than nonlocal ones.

A good pseudopotential must ensure that the integrals of the squared amplitudes of the real and the pseudo wave functions inside the core regions are identical and are equal outside the core region. This is achieved by using a non-local pseudopotential. Pseudopotentials of this type are known as non-local norm-conserving pseudopotentials and are the most transferable as they are capable of describing the scattering properties of an ion in a variety of atomic environments.

The pseudopotential is not unique, therefore several methods of generation exists. One of the methods was proposed by Troullier and Martin [41] which is further transformed from a semi-local form into the fully non-local form by Kleinman and Bylander (KB) [42]. Another approach was suggested by Vanderbilt [43], involves relaxing the norm conservation requirement in order to generate much softer pseudopotentials Ultrasoft pseudopotentials attain much smoother (softer) pseudo-wave functions which use fewer plane-waves for calculations of the same accuracy. This is achieved by relaxing the norm-conservation constraint, which offers greater flexibility in the construction of the pseudo-wave functions. Other common pseudopotentials commonly used in DFT calculations are Effective core potentials (ECPs). The ECPs replaces the core electrons in a calculation with an effective potential, thus eliminating the need for the core basis functions. In addition to replacing the core, they are used to represent relativistic effects, which are largely confined to the core.

Following points are to be kept in mind for constructing a pseudopotential

  i.   Choice of exchange-correlation potential (LDA or GGA), relativistic or non relativistic.

  ii. Flavor for the pseudopotential construction (Troullier-Martins etc.).

  iii. The valence shell electronic configuration of a free-atom.

  iv. The choice of cut off radii, r_c. If the value of r_c is too large, its radial behavior inside r_c may be too different from that of the all-electron function. On the contrary, setting r_c too short may result in large fluctuations. So it is appropriate to choose r_c just beyond the last maximum of the all-electron function.

  v.   Use of core correction is important if a non-negligible overlap occurs between core and valence functions.

Pseudopotential must be tested before using since it is generated with just one specific atomic configuration. A good pseudopotential should be transferable. In our calculations, all the pseudopotentials were generated by the Troullier and Martins method [41].

2.6 Computational Details

A large number of DFT based codes are available today. These include WEIN2k, CRYSTAL, GAUSSIAN-09, VASP, ABINIT, PWSCF, SIESTA and many others. The choice of a computational code will depend on the system under consideration as some codes are better suited for particular type of problems and materials than others. These computational codes can be broadly classified as - all-electron and pseudopotential methods. WIEN2k, CRYSTAL, are all-electron methods, which take into account, the wave functions of all electrons in each atom, from 1s upwards. On the contrary, SIESTA, ABINIT, PWSCF, and VASP are pseudopotential methods. In such methods, only valence electrons (some may include so-called semi- core states) are explicitly included in the equations, whereas deep core states are excluded from the treatment. This is usually accurate enough for describing chemical bonding, equilibrium geometry, phonons etc. However, the properties like e.g. hyper fine field at atom cores, isomer shift, electric field gradient which depends up on core electrons, are not well explained.

Another important distinction is the choice of basis functions for expanding the solutions of the Kohn-Sham equation. There are three different methods in this regard: *(i)* those which use atom centered bases, and *(ii)* atom-independent ones such as plane waves, and, *(iii)* hybrid methods, which combine numerical accuracy in intra atomic regions with reasonable flexibility in the interatomic region. The codes like CRYSTAL, SIESTA use atom-centered bases, commonly called tight-binding group of methods; ABINIT, VASP use plane waves, and the basis in WIEN2k is a hybrid one. Among the various methods discussed, we have used SIESTA code [45] and VASP code for calculating all the structural, electronic and vibrational properties of pure and doped gold clusters and nanotube structures.

2.6.1. SIESTA Code

SIESTA (Spanish Initiative for Electronic Simulation with thousands of atoms) is a computational code based on DFT which calculates ground state properties of the systems. This code does not perform many-electron wave calculations and deals with electron density which is in many aspects good and reasonable bit is a single determinant density. The computational cost for various ab initio quantum mechanical codes scales as N^3, with the number of atoms N, whereas SIESTA is one of the few codes that scales only linearly with number of atoms i.e. "order-N method" [O(N)] scaling.

SIESTA uses the standard Kohn-Sham self-consistent density functional method in the local density (LDA-LSD) or generalized gradient (GGA) approximations. It employs norm-conserving pseudopotentials in their fully non local (Kleinman-Bylander) form. It uses atomic orbitals with finite support as a basis set, allowing unlimited multiple-zeta and angular momenta, polarization and off-site orbitals. It has some problems in describing Vander-Waals which has been overcome in the recent versions interactions and hydrogen bonds. The ATOM program is provided with the SIESTA code for pseudopotential generation. The various parameters such as cut off radii used for generation pseudopotentials are provided in each respective Chapter.

The vibrational frequency analysis of the lowest enrgy geometries was done using the VIBRA utility provided with SIESTA. It computes the force constants and corresponding vibrational frequencies of a given geometry. A geometry is truly optimized if the computed vibrational frequencies,

- have three acoustic modes with $\omega < 0.1 \text{cm}^{-1}$ and all other modes have positive frequencies.

- if some are negative ones, this indicates bad initial lattice relaxation

2.6.2 VASP Code

VASP is a plane-wave all-electron code using the projector-augmented wave method to describe the electron-core interaction. It was developed by Georg Kresse and his coworkers [46-49]. The code uses fast iterative techniques for the diagonalization of the DFT Hamiltonian and allows performing total-energy calculations and structural optimizations for systems with thousands of atoms and ab initio molecular dynamics simulations for ensembles with a few hundred atoms extending upto many thousands. A comparative investigation of the performance of plane-wave (VASP) and local-basis set methods (using the GAUSSIAN and SIESTA package) in structural studies of small gold clusters was performed by Gruber et al.[50].They have concluded that relatively lower binding energy of planar clusters provided by SIESTA and GAUSSIAN03 which could be a consequence of a lower "effective quality" of the basis set for systems .We have used VASP for the optimization of gold nanotubes.

2.7. Geometric Optimization

A geometry optimization procedure consists of sampling points on the potential energy surface, searching for minima. The technique used to search for the minimum is called the optimization algorithm. In principle, the cluster total energy E_{tot} corresponding to a certain structure gives the forces (using Hellmann –Fenyman Theorem) [51]

$$\vec{F} = -\frac{\partial E}{\partial R} \tag{2.23}$$

and the energy is minimized by allowing the structure to relax to new equilibrium position.

If the total energy does not reach an extremum, the forces will be non-zero and make atoms move to a new structure. At an extremum, the forces vanish and a stationary point is found. The structure will be accepted as a new optimized one if the extremum is a minimum (local minimum). Different methods are provided within the computational codes for geometrical optimization such as Monte Carlo, Conjugate gradient method, Steepest descent method etc. We will explain the conjugate-gradient technique.

2.7.1. Conjugate-gradients (CG) technique

The conjugate-gradients provide a simple and effective procedure for implementation of minimization approach. The initial direction is taken to be the negative of the gradient at the starting point. A subsequent conjugate direction is then constructed from a linear combination of the new gradient and the previous direction that minimized the function. This technique, the search direction is generated using information about the function obtained from all the sampling points along the conjugate gradients path. It is important, however, to implement the conjugate gradients technique in such a way as to maximize the computational speed and to minimize the memory requirement so that calculations are not limited by the available memory.

2.8. Discussion and Conclusions

In this chapter, we have described the methodology applied in semi-empirical and first principle methods to calculate the properties of nanomaterials. We have discussed many body Gupta potential and density functional theory in detail as it forms the basis of our work done in this thesis. By minimizing the total energy of the system under consideration, the optimized geometries and related properties of various structures have been calculated. It has been observed that the choice of approach used effect the structural and electronic properties of nanoparticles.

Bibliography

[1]   D. J. Wales, H. A. Scheraga, Science 285, 1368 (1999).

[2]   R. L. Johnston, Dalton Trans. 4193 (2003).

[3]   D. J. Wales, J. P. K. Doye, J. Phys. Chem. A 101, 5111 (1997).

[4]   J. P. K. Doye, D. J. Wales, J. Chem. Soc., Faraday Trans. 93, 4233(1997).

[5]   A. Bruma, R. Ismail, L. O. PazBorbon, H. Arslan, G. Barcaro, A. Fortunelli , Z. Y. Li , R. L. Johnston , Nanoscale 5, 646 (2013).

[6]   D. T. Tran, R. L. Johnston, Proc. R. Soc. A   467, 2131, 2004-2019 (2011).

[7]   R. Ferrando, A. Fortunelli, G. Rossi, Phys. Rev. B: Condens. Matter Mater. Phys. 72, 085449(2005).

[8]   N. T. Wilson Thesis 'The Structure and Dynamics of Noble Metal Clusters' School of Chemistry, University of Birmingham (2000).

[9]   J. P. K. Doye, Comp. Mater. Sci. 35, 227-231 (2006).

[10]   K. Michaelian, N. Rendon, I. L. Garzon, Phys Rev B 60, 3 (1999).

[11]   K. Michaelian, M. R. Beltran, I. L. Garzon, Phys Rev B 65, 041403(2002).

[12]   I. L. Garzón , A. Posada-Amarillas, Phys. Rev. B 54, 11 796 (1996).

[13]   R. P. Gupta, Phys. Rev. B 23, 6265 (1981).

[14]   F. Cleri, V. Rosato, Phys. Rev. B 48, 22(1993).

[15]   A. I. Mares, A. F. Otte, L. G. Soukiassian, R. H. M. Smit, and J. M. van Ruitenbeek, Phys. Rev. B 70, 073401 (2004).

[16]   P. Sen, O. Gulseren, T. Yildirim, I. P. Batra, S. Ciraci, Phys. Rev. B 65, 235433 (2002).

[17]   P. K. Jain, Structural Chemistry 16, 4 (2005).

[18]   P. Hohenburg and W. Kohn, Phys. Rev. B 136, 864 (1964).

[19]   W. Kohn, L.J. Sham, Phys. Rev. 140, A 1133 - A 1138(1965).

[20]   W. Kohn, Rev. Mod. Phys. 71, 1253 (1999).

[21]   J. P. Perdew, Phys. Rev. Lett. 55, 1665(1985).

[22]   J. P. Perdew, Phys. Rev. Lett. 55, 2370 (1985).

[23]   D. M. Ceperley, B. J. Alder, Phys. Rev. Lett. 45, 566 (1980).

[24]   J. P. Perdew, Y. Wang, Phys. Rev. B 45, 23 (1992).

[25]   J. P. Perdew, K. Burke, M. Ernzerhof, Phys. Rev. Lett. 77, 38 (1996).

[26]   M. Filatov and W. Thiel., Phys. Rev. A 57, 189- 199(1998).

[27]   J.P. Perdew, S. Kurth, A. Zupan, and P. Blaha. , Phys. Rev. Lett. 82, 2544-2547(1999).

[28]   S. Ryu, H. W. Lee , Y. K. Han, Bull. Korean Chem. Soc. 32,8 (2011).

[29]   D. Singh, Plane waves, pseudopotentials and the LAPW method, Kluwer

Academic (1994).

[30] M. C. Pyne, M. P. Teter, D.C. Arias, J. D. Joannopoulos, Rev. Mod. Phys. 64, 1045 (1992).

[31] K. N. Kudin, G. E. Scuseria, Phys. Rev. B 61, 16440 (2000).

[32] D. Sholl, J. A. Steckel, Density Functional Theory: A Practical Introduction Wiley-Interscience (2009).

[33] J. Junquera, Ó. Paz, D. Sánchez-Portal, E. Artacho, Phys. Rev. B 64, 235111 (2001) .

[34] S. Huzinaga, Computer Physics Reports 2, 279 (1985); S.Huzinaga et al. Elsevier Sci. Publ. Co., Amsterdam (1984).

[35] A. Szabo and N. Ostlund, Modern Quantum Chemistry, MacMillan, New York, (1982).

[36] E. Artacho, D. S anchez-Portal, P. Ordej on, A. Garćıa, J. M. Soler, Phys. Stat. Sol. (b) 215, 809 (1999).

[37] A. D. Becke, J. Chem. Phys. 98, 5648 (1993).

[38] O. F. Sankey, D. J. Niklewski, Phys. Rev. B. 40, 3979 (1989).

[39] J. C. Phillips, Phys. Rev. 112, 3, 685 (1958).

[40] J. C. Phillips, L. Kleinman., Phys. Rev. 116, 2, 287 (1959).

[41] N. Troullier, Jose Luıs Martins, Phys. Rev. B 43, 3 (1991).

[42] L. Kleinman, D. M. Bylander, Phys. Rev. Lett. 48, 20, 1425 (1982).

[43] D. Vanderbilt, Phys. Rev. B 41, 7892-7895 (1990).

[44] J. Harris, R.O. Jones. Phys. Rev. Lett. 41, 191(1978).

[45] http://departments.icmab.es/leem/siesta/About/overview.html

[46] G Kresse, J. Hafner, Phys. Rev. B 47, 558 (1993).

[47] G. Kresse, J. Furthmler Computat Mater Sci. 6, 15(1996).

[48] G. Kresse, J. Furthmler, Phys. Rev. B 54, 11 169(1996).

[49]   G. Kresse, D. Joubert, Phys. Rev. B 59, 1758 (1999).

[50] M. Gruber, G. Heimel, L. Romaner, J. L. Bras, E. Zojer, Phys. Rev. B 77, 165411(2008).

[51] H.Hellmann,Einfuhrung in die Quntumchemie,Deuticke,Leipzig(1937).

Chapter 3

3. Small Gold Clusters (Au$_n$, n= 1- 14)

3.1 Introduction

The gold clusters and their structural, electronic, and other physical and chemical properties as well as their size dependence, have been extensively studied both theoretically and experimentally [1–8]. The research on gold clusters in the various size ranges is motivated by their applications in catalysis, nanomaterials, and nanotechnology [9-11]. Various measurements using variety of experimental techniques have been performed on Au$_n$ nanoclusters for structural characterization, corresponding to aggregates with n = 20 -200 atoms [12, 13]. Theoretically, the study on Au$_n$ clusters can be performed using methods ranging from molecular dynamics (MD) simulations based on semiempirical n-body potentials [6,14] to first-principles calculations using density functional theory (DFT) [15].

Despite the existence of sophisticated experimental and theoretical tools to study gold nanoclusters, there are still lots of unanswered questions regarding the structural properties such as most stable cluster configuration, lowest-lying isomers, thermal stability, size evolution, etc. [8, 9, 11]. From a theoretical point of view, gold clusters offer an additional challenge due to the importance of relativistic effects and strong spin-orbit couplings. For an understanding of all the properties of small gold clusters it is important to have detailed information on the structural and electronic properties of these systems. Despite the progress achieved, there are still many open questions for gold clusters.

Two different approaches can be employed theoretically to study the structure of gold clusters-the first principle method and semi empirical methods. The parameter-free or first principle study of electronic -structure, uses special, relativistic potentials which predict the smallest gold clusters to be planar [16-22]. The exclusion of relativistic potential leads to three-dimensional structures [23].

Though there are a large number of different studies on neutral/charged gold clusters, an important question which is still unclear is at what size these clusters change from 2D planar structures to 3D structures. Häkkinen et al. [16] suggest that planar structures are energetically competitive with 3D structures up to Au$_{14.}$ Walker [21] has predicted by correlating the 2D-to-3D transition with a linear extrapolation of the energy differences that the transition occurs at Au$_{11}$ while Xiao and Wang [24] have

found that the 2D-to-3D structural transition occurs at Au_{15}. Koskinen et al. [25] have observed experimentally , 3D clusters in the size range n= 12-14 and suggested that GGA calculations predict the correct ground states within this size range of gold clusters . The 2D to 3D transition of gold clusters is important to understand the energetic competition between open and compact isomers, a problem of considerable interest to contemporary electronic structure theory [26].

Jain [27] has predicted a metastable planar zigzag arrangement of Au atoms for every cluster size n ≥ 5 after studying gold clusters Au_n of size n=2–12 atoms with density-functional theory . The influence of ligands on electronic structure of small gold clusters (Au_2, Au_4) has been investigated by Goel et al.using density functional theory (DFT) [28]

The Semi empirical approaches such as the use of Gupta potential (GP) provide a useful alternative to the parameter-free methods. They are computationally less demanding and allow detailed search in structure space. The many body GP has been applied by many theoreticians in unbiased search of structures of gold clusters well above 100 atoms. Michaelian et al. have predicted the existence of disordered global minima for gold clusters of 19, 38, and 55 atoms in size. They have compared the structure factors of the disordered and ordered isomers of gold with experimental x-ray powder diffraction data suggesting that the disordered structures are real [29].The stable structures of Au clusters up to 200 atoms were studied by Wu et al.using GP with experimental-fitted parameters and Sutton-Chen (SC) potential, with both experimental-fitted and density functional theory (DFT)-fitted parameters [30].

In the present study, we have investigated small gold clusters up to 14 atoms using both GP and DFT. The GP describes the interatomic interactions in gold clusters, and the potential parameters were obtained by fitting the properties of bulk Au, such as the cohesive energy, lattice parameters, and independent elastic constants for the reference bulk crystal structure at absolute zero, i.e., experimental-fitted (exp-fitted) parameters [31]. The structural and energetic differences for both approaches were investigated.

3.2 Methodology

3.2.1 Gupta Potential (GP)

Gupta potential (GP) is adopted for the interactions between Au atoms in Au clusters, respectively. This potential is decomposable into a repulsive pair part $V_{ij}{}^r$ and an

attractive glue/many body term V_{ij}^m terms. The interaction potential of all (N) atoms V can be depicted in the following form,

$$V = \sum_{i-1}^{N}\left[\sum_{\substack{j=1 \\ j\neq i}}^{N} V_{ij}^r (r_{ij}) - \sqrt{\sum_{\substack{j=1 \\ j\neq i}}^{N} V_{ij}^m (r_{ij})} \right]$$ (3.1)

$$V_{ij}^r = A \exp\left(-p\left[\frac{r_{ij}}{r_o} - 1 \right] \right)$$ (3.2)

$$V_{ij}^m = \xi^2 \exp\left(-2q_{ij}\left[\frac{r_{ij}}{r_o} - 1 \right] \right)$$ (3.3)

where r_{ij} is the distance between two atoms with index i and j. The parameters A, r_o, ζ, p and q are fitted to experimental values of the cohesive energy, lattice parameters and independent elastic constants for the reference crystal at 0K. The values of the parameters are provided in Table 3.1. The GP has been parameterized by Cleri and Rosato [31] for a wide variety of metals.

Table 3.1 Parameters used in Gupta potential

A(eV)	ζ (eV)	P	q	$r_o(A^o)$
0.2061	1.790	10.229	4.036	2.884

3.2.2 Density Functional Theory (DFT)

We have used the well known Spanish Initiative for Electronic Simulation with Thousands of Atoms computational (SIESTA) code, based on Density Functional theory [32-35]. The electron density functional is treated by the generalized gradient approximation (GGA) with exchange correlation functional parameterized by Perdew, Zunger and Ernzerhof (PBE) scheme [36]. The core electrons are replaced by a non-local norm conserving relativistic pseudopotential factorized by Kleimann-Bylander form [37]. Relativistic pseudo potential for gold is generated with atomic valence electron configurations $5d^{10} 6s^{1.}$ The core radii (in units of Å) for gold are as follows: s (2.55), p (2.98), d (2.22), f (2.00). The valence states were described using DZP (double-zeta + polarization) basis sets. The reciprocal space integrations are carried out at the gamma point. The clusters are optimized inside a simulation cell of 20 Å and energy cutoff of 200 Ry. Geometry optimizations were performed with the conjugate gradient algorithm and the geometries were considered to be optimized when the forces were reduced upto 0.01 eV/Å.

We have verified the computational procedure by calculating the ionization potential (IP) for a gold atom and performing test calculations on Au_2. The IP of the gold atom is found to be 8.90 eV which is in fair agreement with the experimental value of 9.22eV [38].

In Table 3.2, we summarize the computed results using GP and DFT, along with the experimental values which clearly show that the computed values of bond lengths and binding energies (BE) are in fair agreement with experimental values. It can be seen from the Table 3.2 that the values computed for Binding Energy and Bond Length from DFT are closer to the experimental value.

Table 3.2 Computed and experimental Binding Energy per atom (BE) and Bond Length of the dimer Au_2

	Exp	DFT	GP
Bondlength (A⁰)	2.47 [39]	2.55	2.30
B E per atom (eV/atom)	1.15 [39]	1.43	2.41

The ground state geometries of Au_n along with their isomers were manually generated and structures reported in the literature were also considered. Each structure is relaxed to a desired convergence limit. The harmonic vibrational frequency analysis was carried out on the ground state structure to verify the structure.

3.3 Results and Discussion

3.3.1 Structures of Au₃-₁₄ clusters

The local minimum structures of Au_n (n = 3–14) clusters using Gupta potential with exp-fitted parameters and DFT are optimized, which are presented in Fig. 3.1(a) and 3.1(b), respectively.

Au_3	Au_4	Au_5	Au_6

Au_7	Au_8	Au_9	Au_{10}

| Au$_{11}$ | Au$_{12}$ | Au$_{13}$ |
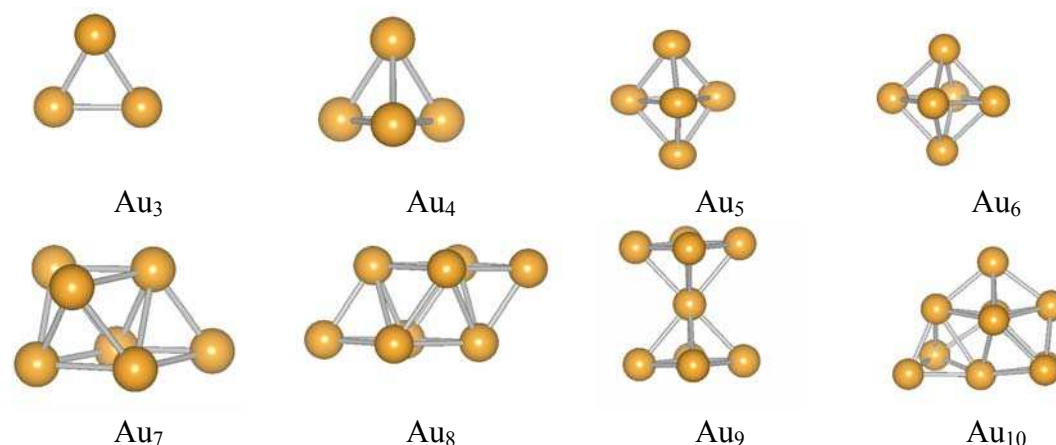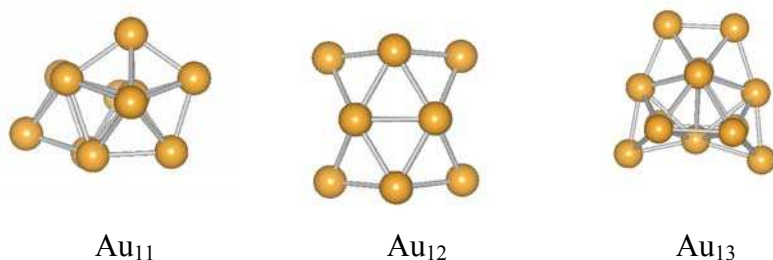
Figure 3.1(a) The optimized geometries of Au$_n$ cluster (n=3 -13) obtained from GP

It is found that the optimized geometries of Au$_n$ clusters using Gupta Potential are three dimensional structures for n ≥ 4. It is seen that though different geometries were given as an input for each Au$_n$ cluster, all the geometries were optimized to one single lowest energy geometry. The minimum energy structure of Au$_3$ cluster is triangle and the Au-Au bond distance is 2.47 Å. The optimized geometry of Au$_4$ cluster has a tetrahedral structure. The configuration of Au$_5$ is triangular bipyramid (hexahedron) and Au$_6$ is an octahedron. These results are in agreement in another recent study of gold clusters using GP [30]. Contrary to Wu et al. [30] the lowest energy geometry of Au$_7$ and Au$_8$ is found to be capped octahedron and a bicapped octahedron respectively .The Au$_9$ has tetrahedron motif while Au$_{10}$ and Au$_{11}$ have distorted pentagonal bipyramidal motif in their lowest energy configuration.

To obtain the lowest energy isomer of Au$_{12}$ and Au$_{13}$, we begin with initial geometries such as icosahedron or cuboctahedron. It is found that while the lowest energy structure of Au$_{12}$ is tubular structure with square cross-section, Au$_{13}$ is neither icosahedron nor cuboctahedron but has an amorphous configuration.

In order to verify the predictions given by the *n*-body Gupta potential and gain insight into the bonding mechanisms and electronic properties of Au$_n$ clusters DFT –GGA was chosen. The calculations were performed to solve the standard Kohn-Sham self-consistent equations in the GGA approximation, using a linear combination of numerical atomic orbitals as the basis set. The ground state (GS) configurations of pure Au$_n$ (n=3 -13) clusters using DFT-GGA are found to adopt planar geometries. The occurrence of planar metal clusters of this size is attributed to strong relativistic bonding effects in gold that reduces the s-d energy gap, thus inducing hybridization of the atomic 5d-6s levels and causing overlap of the 5d shells of neighboring atoms in the cluster [40, 41].

In addition to relativistic effects, the planarity of gold clusters can be explained by using GGA level of theory. The lowest energy structure and its close lying isomer are

presented in Fig.3.1 (b). The results presented are in agreement with previously reported studies [41-44].

For Au_3 trimer, a triangle with C_{2v} symmetry is found to be more stable than the linear chain. The Au_4 has a planar rhombus structure with D_{2h} symmetry about 0.22eV lower in energy than the planar ''Y-shaped'' structure. For Au_5, the trapezoidal ''W-shape'' structure with C_{2v} symmetry is more stable than the 3D trigonal bipyramid by 0.784 eV. The global minima structure of Au_6 is a planar triangular structure with D_{3h} symmetry. It can also be understood in terms of ''W-shaped'' Au_5 capping by an extra atom. The 3D configurations such as pentagonal pyramid and octahedron are found as local minima for Au_6. The experimental photoelectron spectra (PES) study of Au_6 by Taylor et al. predicts low electron affinity (EA) and large HOMO-LUMO gap, which are consistent with the properties of hexagonal structure [45].

Thus planar equilibrium structures have been obtained for Au_{4-6} from ab initio calculations but were not obtained from GP. It is worthy of note that the other small metal clusters, such as Ag_n and Cu_n also adopt similar planar configurations [46].

A planar capped triangle with C_s symmetry is the minimum energy structure of Au_7 and is obtained by adding a gold atom to the planar triangular structure of Au_6. A similar result is reported in other studies [16, 44, and 47]. However, contrary to GGA result, a 3D pentagonal bipyramid structure is preferred in DFT-LDA calculations by Wang et al. [41].

The lowest energy structure for Au_8 cluster is a planar tetra-edge-capped rhombus with D_{2h} symmetry. Both the isomers of Au_8 are found to be 2D planar structures. Our calculated minimum energy structure is in agreement with those reported in the literature [16, 21].

The lowest energy structure of Au_9 is a 'bi-edge-capped hexagon structure with C_{2v} symmetry as in agreement with others [47, 48] and the lowest energy structure of Au_{10} is a tricapped hexagon having D_{2h} symmetry which is in agreement with the result obtained by Walker [21].

Our calculations predict Au_n with n =11-12 to have two dimensional geometries as well. We have a planar tetra capped hexagon with Cs symmetry as the minimum energy structure for Au_{11} similar to Fernández [48]. The next higher energy structure is 3D and is separated by an energy difference of only 0.005 eV from the lowest energy configuration. It is also very similar (though not identical) to the one obtained from GP (see Fig. 3.1a). Both the low energy structures for Au_{12} are planar and can be

understood as penta capped hexagon. The lowest energy structure of Au_{12} is separated from its next higher energy isomer by 0.272 eV.

The Au_{13} cluster is found to have a planar condensed hexagon structure with D_{2h} as lowest structure. Hou and coworkers [49] have also obtained similar structure as the most stable structure. Interestingly the next isomer has precisely the same structure as obtained from GP (see Fig. 3.1a).

The lowest energy structure for Au_{14} is found 3D flat cage like structure. Thus our calculations predict that the transition to 2D -3D for neutral gold clusters takes place at n=14. In contrast, Häkkinen *et al.*[16] suggest that planar structures are energetically competitive with 3D structures up to Au_{14} while Xiao and Wang [24] suggested that the 2D to 3D structural transition occurs at Au_{15}. In general, from our calculations we can say that the turn over from 2D to 3D occurs at n=4 in case of Gupta Potential whereas in DFT it occurs at n=14.

GP does not give the correct lowest energy structures for the small gold clusters. It yields only 3D geometries. However for n > 10, the structures predicted by GP turn out to be similar to the lowest out of 3D isomers obtained from DFT. Thus, GP is seen to be good for gold clusters with larger n, and yields correct 3D structures.

Au₃

Au₄

Au₅

Au₆

Au₇

Au₈

Au₉

Au₁₀

Au₁₁

Au₁₂

Au₁₃

Au₁₄
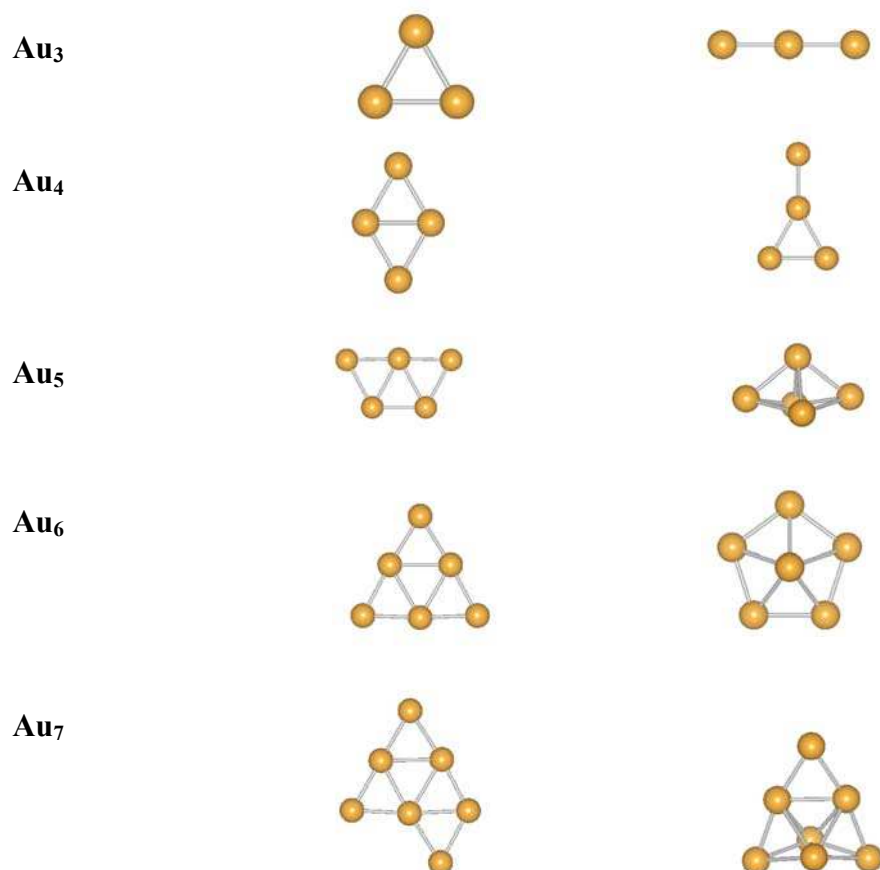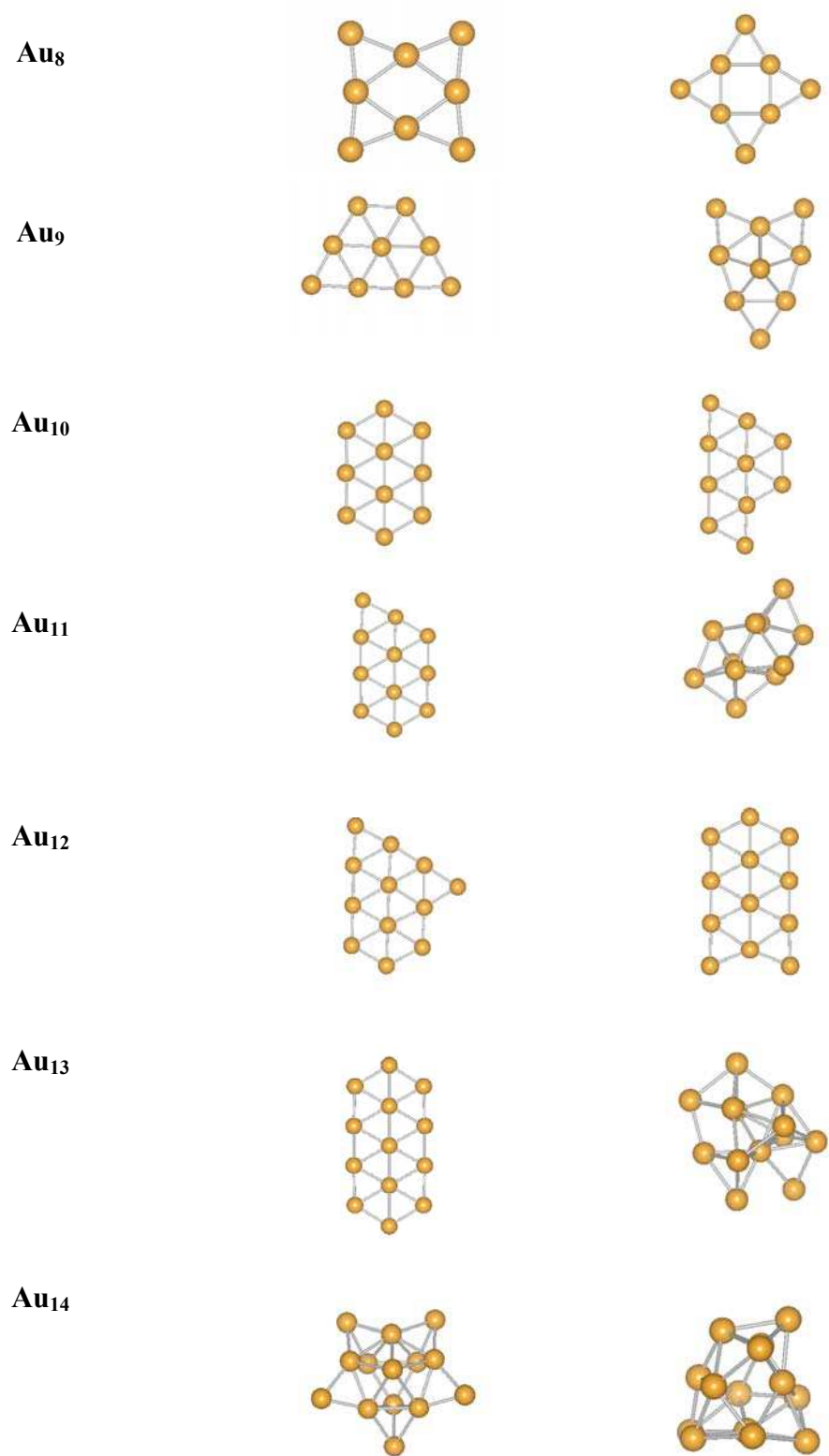
Figure 3.1(b) The optimized geometries of Au_n (n=3 -14) and their close lying isomer obtained from DFT

3.3.2 Energetics

The binding energy per atom is a measure of stability. The average atomic binding energy for Au_n clusters can be defined as

$$E_b(n) = [nE_T(Au) - E_T(Au_n)]/n \qquad (3.4)$$

where $E_T(Au)$ denotes total energy of Au atom and $E_T(Au_n)$ denotes the energy of the Au_n cluster in its lowest energy configuration. The comparison between the binding energy per atom of optimized neutral Au_n clusters computed with GP and DFT are presented in Table 3.3 and plotted in Fig. 3.2. The energies of the next isomers computed from DFT are also given in Table 3.3.

Table 3.3 Binding Energy per atom of neutral optimized gold clusters Au_n calculated DFT and GP. All values are in electron volts per atom (eV /atom).

Cluster Size ,n	3	4	5	6	7	8	9	10	11	12	13	14
DFT (lowest)	1.57	1.99	2.16	2.45	2.41	2.54	2.54	2.65	2.65	2.70	2.70	2.78
DFT (next isomer)	1.52	1.94	2.00	2.31	2.38	2.54	2.52	2.58	2.64	2.68	2.68	2.76
GP	2.72	2.92	3.01	3.09	3.12	3.14	3.00	3.17	3.19	3.21	3.24	--

The binding energy of the neutral optimized gold clusters Au_n (n= 3- 14) seems to increases with increasing cluster size in both GP and DFT case. In general, the binding energy per atom computed for Au_n cluster from GP is higher than the DFT values. It is found that the DFT values are closer to the experimental and other theoretical studies. The binding energy computed in our calculations using DFT-GGA is still higher than the other similar studies [48].

This can be due to the unavailability of the Effective core pseudopotential (ECP) for gold   in SIESTA or the pseudopotential generated by us may not be good enough. Though the binding energies computed are higher but we are able to produce good agreements between the various lowest energy geometries of Gold clusters predicted by us and other similar studies. Although, structurally the 3D structures from DFT are close to those obtained from GP, the stabilization energy values from GP are considerably higher.

It can be seen from the plot, the binding energy per atom increases with cluster size and has a maximum value at Au_6 in agreement with the results of Hakkinen and Landman [19], Xiao and Wang [24].

It indicates that triangular Au_6 is more stable than its neighbours. The peaks in the DFT graph indicates that even numbered gold clusters are more stable than the odd numbered gold clusters.
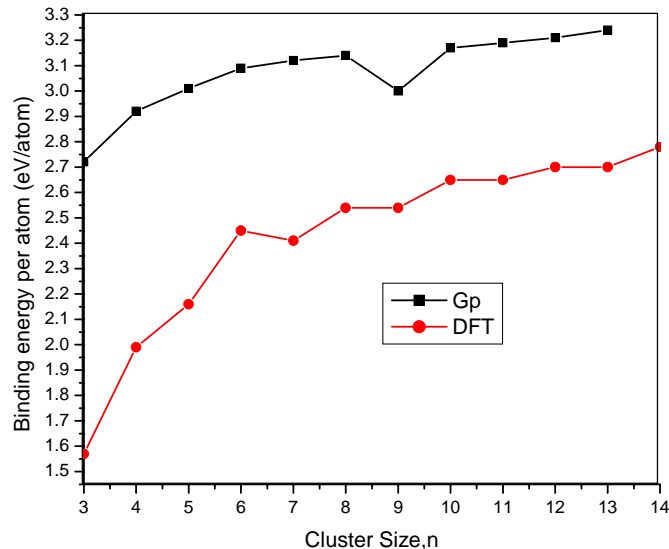
Figure 3.2 The binding energy per atom curve of Au_n clusters for n=3-14 using GP and DFT.

The second-order difference (Δ_2E) of the total energy is a sensitive quantity that characterizes relative stability of atomic clusters as a function of cluster size for different sized Au_n clusters. It is defined as

$$\Delta_2 E(n) = E_T(Au_{n+1}) + E_T(Au_{n-1}) - 2E_T(Au_n) \tag{3.5}$$

Δ_2E as a function of cluster size is plotted in Fig. 3.3 and its shows a comparion of DFT calculations with GP. The results from DFT calculations shows odd-even staggering with peaks at n = 4, 6, 8, 10 and 12, indicating that these clusters are more stable than their neighboring clusters. The exceptionally high stability of Au_6 which is evident in Fig. 3.2 can be observed from this graph also. Our results are in agreement with a relatively recent study on gold clusters [50]. In contrast to the results of DFT, the GP calculations gives peaks at n = 3,5,7,9 and 11. This may be attributed to the difference in the lowest energy geometeries of gold clusters obtained from DFT and GP. While DFT predicts planar structures, the GP gives 3D geometries as lowest energy structures for Au_n clusters (n < 13). The many body potentials like GP do not take into account the directionality of the structure and ignore the electronic structure of a given element.
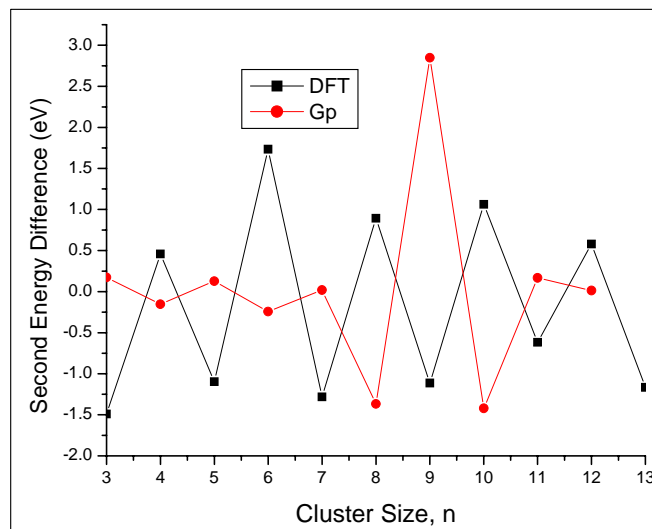
Figure 3.3 The second difference of energy ($\Delta_2 E$) of Au$_n$ clusters (n=3- 13) with DFT and GP calculations

3.4 Electronic Properties

The size dependent electronic properties of Au$_n$ (n= 2 to 14) are investigated using DFT. We have calculated the HOMO-LUMO gap, adiabatic ionization potentials, chemical hardness, electron affinities and chemical potential.

3.4.1 HOMO-LUMO gap

The HOMO-LUMO gap reflects the ability of clusters to undergo activated chemical reactions with small molecules. A large HOMO−LUMO gap is considered important for the chemical stability.
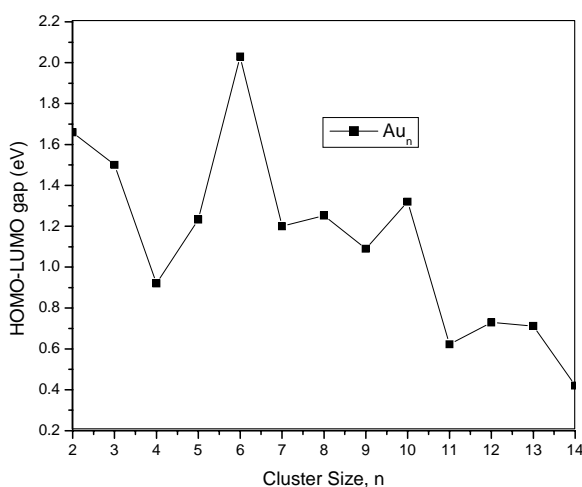
Figure 3.4 The HOMO-LUMO gaps of the lowest energy Au$_n$ (n=2 -14) clusters.

Fig.3.4 illustrates the HOMO-LUMO gaps of the stable structures of Au_n (n=2 -14) clusters. The calculated values are presented in Table 3.4. As seen from the plot, the HOMO–LUMO energy gap shows an odd–even oscillation for n > 4. The even-numbered clusters have larger HOMO–LUMO gap and are relatively more chemically stable than the odd-numbered neighbors. The HOMO–LUMO gap for Au_2, Au_6 and Au_{10} is particularly large with an exception for Au_3 which also has large HOMO-LUMO gap.

The even-odd oscillations of HOMO–LUMO gap can be understood as the effect of electron pairing in orbital. Even sized clusters have an even number of s valence electrons and a doubly occupied HOMO, while it is singly occupied for odd-sized clusters. The electron in a doubly occupied HOMO feels a stronger effective core potential due to the fact that the electron screening is weaker for electrons in the same orbital than for inner-shell electrons.

Though the values of HOMO– LUMO gap computed by us differ but the pattern is similar to the earlier calculations for small Au_n clusters [16, 50, 51].

Table 3.4 HOMO-LUMO gap (E_g), Adiabatic Electron Affinity (AEA), Adiabatic Ionisation Potential (AIP), Chemical Hardness (η) of neutral Gold clusters Au_n calculated at DFT-GGA level through siesta code (SC). All values are in electron volts (eV).

Cluster Size, n	E_g (eV)	AEA	AIP	η
Au_2	1.66	0.52	6.940	3.21
Au_3	1.5	0.88	4.543	1.83
Au_4	0.921	3.08	5.5	1.21
Au_5	1.233	3.94	5.08	1.14
Au_6	2.03	0.97	7.638	6.67
Au_7	1.20	2.31	6.549	2.12
Au_8	1.25	1.75	7.035	2.64
Au_9	1.09	4.11	5.518	0.704
Au_{10}	1.32	1.83	6.88	2.525
Au_{11}	0.622	2.57	6.108	3.538
Au_{12}	0.729	2.46	6.72	2.06
Au_{13}	0.712	2.94	6.326	1.693
Au_{14}	0.42	1.75	5.95	2.1

3.4.2   Ionization Potential and Electron affinity

The Ionization potential (IP) and electron affinity (EA) are defined as follows

$$IP\left(Au_n\right) = E_T\left(Au^+\right) - E_T\left(Au\right) \qquad (3.6)$$

$$EA\left(Au\right) = E_T\left(Au\right) - E_T\left(Au^-\right) \qquad (3.7)$$

The variation in adiabatic ionization potential and electron affinity of Au_n clusters are plotted in Fig. 3.5 as a function of cluster size. An ionization potential is used as an important property to study the change in electronic structure of the cluster with size. An additional step has been taken to match experimental data more accurately by doing the geometry optimization of the cation and anion to calculate the adiabatic IP (AIP) and EA (AEA) respectively. The plot in Fig 3.5 shows even–odd alternative behavior for both IP and EA. It is found that the even-sized clusters with an even number of s valence electrons have larger values of ionization potential compared to their immediate neighbours while the vertical electron affinity values also show an odd–even alterative behavior but in this case, the odd-sized clusters have higher value of electron affinity compared to the even sized ones.
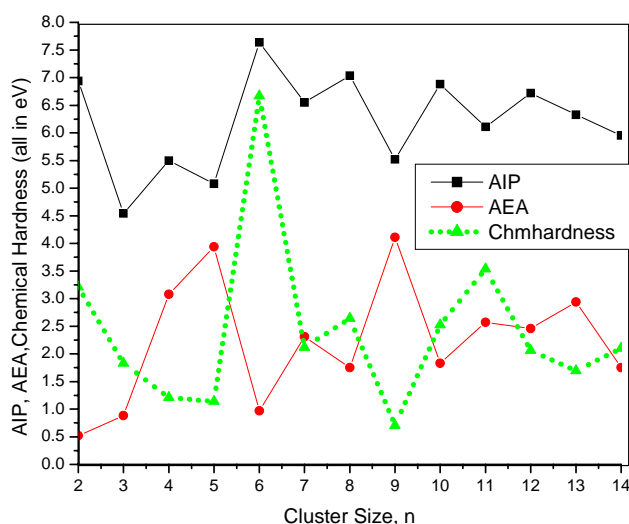
Figure 3.5 The electron affinities (EAs) , ionization potentials (IPs) and Chemical Hardness (η) of lowest energy Au_n clusters for   n=2-14

It is seen that our computed values of IP and EA are less than the experimental values but the pattern obtained in graph is similar to other previous studies [16, 19]. The reason can be non availability of good quality of pseudopotential and basis set for gold in our computational code SIESTA.

3.4.3 Chemical Hardness

The Chemical hardness η is interpreted as the resistance towards change in number of electrons and it is directly related to the stability of clusters. The chemical hardness (η) is defined as $\eta = (VIP-EA)/2$, displayed in Fig. 3.5. It is an electronic property which also signifies the relative stability of molecules. The graph shows peaks for even number of gold atoms, n= 2, 6, 8 (except at n=11) indicating again the high stability of even numbered Au_n clusters.

3.5 Conclusion

We have investigated low-energy geometries and binding energy of gold clusters Au_n, n varying from 2 to 14 using both Gupta Potential and DFT-GGA theory. Different initial guess geometries were considered for all the clusters which lead to a number of structural isomers for each cluster size. Further the electronic properties such as HOMO–LUMO gap, ionization potential, electron affinity and chemical hardness were investigated systematically using DFT .The results can be summarized as follows.

- The Gupta potential favors 3D geometries as the low energy structures of Au_n clusters while DFT favors 2D planar geometries as ground structures for Au_n. Our calculation from DFT predicts that the 2D to 3D transition takes place at n=14.

- The binding energy per atom of Au_n clusters increases with increase in size of cluster for both GP and DFT. It is observed the graph exhibit odd-even oscillations with peaks at even number clusters i.e., n = 2,4,6,8 etc. The binding energy curve indicates exceptionally high stability of Au_6 cluster.

- The variation of HOMO–LUMO gaps, chemical hardness, second energy difference of binding energy, AIP and AEA with cluster size shows odd even alterations. The even-numbered clusters are found to be relatively more stable compared to the odd-numbered ones indicating that electron spin-pairing stabilizes these cluster. Our results are in agreement with other similar studies on gold clusters.

- GP is particularly good for larger clusters (n>10) and for 3D geometries of gold.

Bibliography

1   R. L. Whetten, J. T. Khoury, M. M. Alvarez et al., Adv. Mater. 5, 8 (1996).

2   R. P. Andres, T. Bein, M. Dorogi et al. Science 272, 1323 (1996).

3   C. A. Mirkin, *R. L.* Letsinger, R. C. Mucic, J. J. Storhoff, Nature (London) 382, 607 (1996).

4   A.P Alivisatos, K.P Johnsson, X. Peng, T.E Wilson, C.J Loweth, M. P. Bruchez, P.G. Schultz, Nature (London) 382, 609 (1996).

5   R. P. Andres , J. D. Bielefeld, J. I. Henderson, et al. Science 273, 1690 (1996).

6   W. D. Luedtke, U. Landman, J. Phys. Chem. 100, 13, 323 (1996).

7   D. Bethell, D. J. Schiffrin, Nature (London) 382, 581 (1996).

8   C. L. Cleveland, U. Landman, M.N. Shafigullin, P.W. Stephens, R.L. Whetten, Z. Phys. D 40, 503 (1997).

9   D.W. Goodman, Nature 454, 948–949 (2008).

10   G.J. Hutchings, M. Brust, H. Schmidbaur, Chem. Soc. Rev. 37, 1759–1765(2008).

11   E. Roduner, Chem. Soc. Rev. 35, 583–592 (2006).

12   H. Hovel, I. Barke, Progress in Surface Science 81, 53–111(2006).

13   T. G. Schaaff, M. N. Shafigullin, J. T. Khoury, I. Vezmar, R. L. Whetten et al., J. Phys. Chem. 101, 7885 (1997).

14   I. L. Garzón, A. Posada-Amarillas, Phys. Rev. B 54, 11 796 (1996).

15   Y. Donga, M. Springborg, Eur. Phys. J. D 43, 15–18 (2007).

16   H. Hakkinen, B. Yoon, U. Landman, X. Li, H.-J. Zhai, L.-S. Wang, J. Phys. Chem. A 107, 6168(2003).

17   G. Bravo-Perez, I. L. Garzon, O. Novaro, J. Mol. Str. (Theochem) 493, 225 (1999).

18   H. Gronbeck and W. Andreoni, Chem. Phys. 262, 1 (2000).

19   H. Hakkinen and U. Landman, Phys. Rev. B 62, R2287 (2000).

20   J. Wang, G. Wang, and J. Zhao, Phys. Rev. B 66, 035418 (2002).

21   A. V. Walker, J. Chem. Phys. 122, 094310 (2005).

22   F. Remacle and E. S. Kryachko, J. Chem. Phys. 122, 044304 (2005).

23   N. T. Wilson and R. L. Johnston, Eur. Phys. J. D 12, 161 (2000).

24   L. Wang, L. Xiao, Chem. Phys. Lett. 392, 452-455 (2004).

25   P. Koskinen, H. Häkkinen, B. Huber, B. von Issendorff, and M.Moseler, Phys. Rev. Lett. 98, 015701 (2007).

26   S. Grimme, Angew. Chem., Int. Ed. 45, 4460 (2006).

27   P. K. Jain, Structural Chemistry, 16, 4 (2005).

28 S. Goel, K. A.Velizhanin,A. Piryatinski,S. Tretiak, and S. A. Ivanov, J. Phys. Chem. Lett 1, 927–931 (2010).

29 K. Michaelian, N. Rendon, and I. L.Garzon, Phys. Rev. B 60, 3 (1999).

30 X. Wu, S. Chen, Y. Sun, Y. Chen, Computational and Theoretical Chemistry 1002 43–48 (2012).

31 F. Cleri and V. Rosato, Phys. Rev. B 48, 22, 20 (1993); V. Rosato, M. Guillope, B. Legrand, Philos. Mag. A 50, 321 (1989).

32 P.Ordejon, E. Artacho and J. M. Soler, Phys. Rev. B, 53, R10441 (1996).

33 D. Sanchez-Portal, P. Ordejon, E. Artacho and J. M. Soler, Int. J.Quantum Chem, 65, 453(1997).

34 J. M. Soler, E. Artacho, J. D. Gale, A. Garcia,J. Junquera, P. Ordejon and D. Sanchez-Portal, J. Phys. Condens. Matter 14, 2745 (2002).

35 G. P Robert and Y. Weitao, Density-Functional Theory of atoms and Molecules, Oxford University Press NewYork (1989).

36 Perdew, Burke, Ernzerhof, Phys. Rev. Lett. 77, 3865 (1996).

37 L. Kleinman and D. M. Bylander, Phys. Rev. Lett. 48, 1425(1982).

38 C. Kittle, Introduction to Solid State Physics, 7th ed. Wiley, New York (1996).

39 R. C. Weast, CRC Handbook of Chemistry and Physics, 55th ed. CRC Press,. Cleveland, OH *(*1974).

40 H. Hakkinen, M. Moseler,U. Landman, Phys. Rev. Lett. 89, 033401(2002).

41 P. Pyykko, Chem. Rev. 88, 563 (1988).

42 G Bravo-Perez, I. L Garzon, O. Novaro, Journal of Mol. Struct. (Theochem), 493, 225-231 (1999).

43 H. Hakkinen and U. Landman, Phys. Rev. B. 61,287 (2000).

44 H.M Lee, M. Ge, B. R. Sahu, P. Tarakeshwar and K. S. Kim, J. Phys. Chem. 107, 9994(2003).

45 K.J. Taylor, C. Jin, J. Conceicao, O. Cheshnovsky, B.R. Johnson, P.J. Nordlander, R. E. Smalley, J. Chem. Phys. 93, 7515 (1991).

46 H. Nakashima, H. Mori, M. S. Mon, E. Miyoshi, Int. Conf. on Computational Chemsitry, Egypt (2007).

47 V. Bonacic-Koutecky, J. Burda, R. Mitric, M. Ge, G. Zampella and P. Fantucci, J. Chem. Phys. 117, 3120 (2002).

48 E. M. Fernández, J. M. Soler, I. L. Garzón, L. C. Balbás, Phys. Rev. B 70, 165403 (2004).

49 J. Zhao, J. Yang, J.G. Hou, Phys. Rev. B 67, 085404(2003).

50 A. Deka, R.C. Deka, J. Mol.Struct. : THEOCHEM 870, 83 -93 (2008).

51 J. Wang, G. Wang, J. Zhou, Phys. Rev. B 64 205411(2003).

Chapter 4

4. Doping of gold clusters with Si and Ge atoms

4.1 Introduction

In the previous chapter, we have discussed different geometries of the small pure gold clusters using both Gupta potential and Density Functional Theory. It will be interesting to see how different properties, structural as well as electronic, of gold clusters will change with the introduction of a dopant atom. Doped clusters have received increasing attention because of their distinctive structure and tunable catalytic properties which change with dopant size.

There have been a large number of experimental and theoretical studies on doping of gold clusters of different size ranges with various elements. A highly stable doped gold cluster, icosahedral W@ Au_{12}, was predicted by Pyykko and Runeberg [1] using DFT calculations. In another DFT study, the geometric and electronic properties of 3d, 4d, and 5d transition-metal atom doped Au_6 clusters were systematically investigated by Meng et al. [2]. They found that doping by 3d, 4d and 5d transition-metal atoms could stabilize the Au_6 ring. Li et al. [3] have studied magnetic properties of transition metal doped gold clusters $M@Au_6$ and found that the Au_6 ring in the MAu_6 system serves as a perfect host to store a single transition metal atom. A combined photoelectron spectroscopy (PES) and DFT investigation performed on MAu_{16}^{-} (M=Ag, Zn, In) clusters by Wang et al. [4] show that the electronic properties of the golden buckyball can be systematically tuned through doping. A lot of theoretical and experimental work on gold clusters doped with impurity atoms focuses mainly on transition metal atoms as dopant [5-16]. There are relatively very few systematic investigations done on the study of gold clusters doped with group 14 elements (C, Si, Ge).

Silicon is the most important semi conducting element in microelectronics industry. Si clusters have been investigated both experimentally [17] and theoretically [18] for their potential applications as building blocks to build up well controlled nanostructures. The most intriguing finding is the structure of $SiAu_4$ cluster, which possess T_d geometry, analogous to silane or SiH_4 [19]. Walter et al. [20] conducted theoretical study on Si doped inside neutral Au_{16} cage. They found that Si doped Au_{16} exhibits different reactivities toward oxygen. Another theoretical study by Wang et al. [21] shows that the global minima of anion golden cage Au_{16}^{-} doped with Si, Ge and Sn possess exohedral structures.

Germanium and silicon are isovalent, but their chemical properties are quite different. It will be interesting to see how silicon doped gold clusters are different from germanium doped gold clusters. Spiekermann et al. [22] have reported the synthesis and structural characterization of the first ligand-free anionic germanium–gold cluster and have asserted that the stability of such clusters would lead to their use both as a catalytic seed for the growth of germanium nanowires [23] and the use of the cluster itself as a building block for one-dimensional systems. A joint experimental and theoretical study on the structures of gold clusters doped with a group-14 atom: MAu_x^- (M = Si, Ge, Sn; x = 5-8) have shown that these doped clusters have a strong tendency of forming planar structures [24].

In this chapter, we will study in detail the structural and electronic properties of Au_nSi (n=1-12) clusters and compare them with pure gold clusters and germanium doped gold clusters. We have calculated the equilibrium geometries, bond lengths, ionization potentials, electron affinities and HOMO-LUMO gap of these clusters using density functional theory. We will also present a comparative study of Germanium doped gold clusters at the end.

The organization of the chapter is as follows. The computational details are given in Section 4.2, results and discussions are presented in Section 4.3. The germanium doped gold clusters are discussed in section 4.5

4.2 Computational details

We have used the well known Spanish Initiative for Electronic Simulation with Thousands of Atoms computational code, SIESTA, [25-27] based on Density Functional theory [28]. The electron density functional is treated by the generalized gradient approximation (GGA) with exchange correlation functional parameterized by Perdew, Zunger and Ernzerhof (PBE) scheme [29]. The core electrons are replaced by non-local norm conserving relativistic pseudopotential factorized by Kleimann-Bylander form [30]. Relativistic pseudo potential for gold is generated with atomic valence electron configurations $5d^{10} 6s^1$. The pseudo potentials for silicon and germanium are generated with atomic valence electron $3s^2 3p^2$ and $4s^2 4p^2$ respectively. The core radii (in units of Å) for gold are as follows: s (2.55), p (2.98), d (2.22), f (2.00). For silicon, they are: s (1.77), p (1.96), d (2.11) and f (2.11) and for germanium, they are: s (2.06), p (2.85), d (2.58) and f (2.58). The valence states were described using DZP (double-zeta + polarization) basis sets. The reciprocal space

integrations are carried out at the gamma point. The clusters are optimized inside simulation cell of 15 Å and energy cutoff of 150 Ry. The symmetry unrestricted geometry optimization is carried using conjugate gradient method until all the forces are less than 0.001eV/Å.

We have verified the computational procedure by calculating the ionization potential (IP) for a gold atom and performing test calculations on Au_2 and Si_2 dimer. The IP of the gold atom is found to be 8.90 eV which is in fair agreement with the experimental value of 9.22eV [31]. The structural parameters such as binding energy per atom and bond length for Au_2 are found to be 1.43 eV and 2.55 Å respectively which are in agreement with experimental values, 1.15 eV and 2.47 Å [32].

For Si_2, the Binding energy per atom is 2.40 eV and the bond length is 2.28 Å which agree with the experimental values of 1. 67 eV and 2.25 Å [33]. The ionization potential of Si_2 is 7.97 eV which agrees with the experimental reported values, 7.87eV [34] and 7.97-8.08 eV [35]. The structural parameter such as bond length for Ge_2 and AuGe dimer is 2.42 Å and 2.37 Å respectively which are in fair agreement with the experimental and theoretical reported value [36-38]

In order to obtain the lowest energy structures of Au_nX (X= Si, Ge), we have considered all the possible isomeric structures obtained by placing the X atom at each distinct position of Au_{n+1} clusters .The ground state geometries of Au_nX (X= Si, Ge) along with their isomers reported in the literature were also considered and each structure is relaxed to a desired convergence limit.

The harmonic vibrational frequency analysis was carried out on the ground state structure to verify the structure.

4.3 Results and Discussions

Using the scheme mentioned in section 4.2, we have obtained the lowest energy structures of Au_nX (X= Si). The simulation parameters obtained from Au_{n+1} calculation was used for searching the ground states of Au_nX (X= Si) and calculating their equilibrium properties. The minimum energy structures as well as their isomers for Au_nSi clusters are presented in Figs. 4.2 – 4.6. The Au-Au and Au-Si bond lengths, as well as the point symmetries for all the lowest energy structures are tabulated in Table 4.1.

In order to study the relative stabilities of the clusters, we study binding energy per

atom, the dissociation energy and the second difference in energies. These have been plotted in Figs. 4.7 – 4.9. The electronic properties -- HOMO-LUMO gap, ionization potentials, electron affinities and chemical hardness are plotted in Figs. 4.11 – 4.13.

4.3.1 Au_{n+1} clusters

We have first obtained the ground state (GS) structures for pure Au_{n+1} cluster, which have already been discussed in Chapter 3. It was found that for n=1-12 the ground state configurations adopt planar geometries. For Au_3, Au_4, Au_5 and Au_6 the global minima structures are found to be a triangle with C_{2v} symmetry, a rhombus with D_{2h} symmetry, a trapezoidal 'W-shaped' structure with C_{2v} symmetry and a planar triangular structure with D_{3h} symmetry respectively. These results are in agreement with previously reported results [39-42].

The Au_7 cluster has a capped triangular structure reported by Bonacic - Koutecky and Lee et al. The minimum energy geometries for Au_8, Au_9 and Au_{10} have D_{2h}, C_{2v} and D_{3h} symmetries respectively, all of which are planar, in agreement with other theoretical results [42-44]. Our calculations predict Au_{n+1} with n =11-13 to have two dimensional geometries as well, in agreement with other reported results [42, 45].

4.3.2 $Au_n Si$ clusters

The ground state (GS) structures for Si doped Au clusters for n=1 -12 are presented in Fig. 4.1 along with the pure gold clusters geometries to give a comparison between the two. To obtain the low lying isomers of $Au_n Si$, we start with the pure gold cluster Au_{n+1} and replace one gold atom with a Si atom and optimize the geometry. This is repeated with replacement of Au with Si on another site and so on till all the non-equivalent sites have been tried.

The $Au_1 Si$ dimer bond length is found to be 2.29 Å which is smaller than the Au-Au bond which is 2.55Å. This bond length (2.29 Å) is in good agreement with the theoretically reported value 2.25 Å [46].

$Au_2 Si$, a triangular structure (3a in Fig. 4.1) with C_{2v} symmetry is more stable than its linear isomer (3b) by 1.30 eV. In the triangular structure, the Au-Si bond length 2.29 Å is in agreement with the reported value, 2.28 Å [40]. The Au-Au bond distance is 3.25 Å and has increased significantly compared to that in Au_2 dimer.The angle Au-Si-Au is found to be 89° where as the reported value is 112° [47].

For $Au_3 Si$, three different geometries are considered and are shown in Fig. 4.1 (4a -

4c). If an Au atom is replaced by Si in stabilized Au_4, a planar rhombus, the lowest structure for Au_3Si is obtained – a three dimensional capped triangle with C_{2v} symmetry in agreement with the geometry predicted in other theoretical calculations [46, 47]. The Au-Si bond lengths are found to be in the range 2.39 – 2.46 Å and the maximum angle between Au-Si-Au bonds is found to be 105.8^o. In Au_{n+1} the transition from two dimensional to three dimensional structures occurs for $n > 13$. The preference to planar low energy structures in pure gold clusters is attributed to relativistic effects which enhance the stronger *sd* hybridization and *dd* interaction in gold upto 13 atoms. It is observed that for Au_nSi, the transition from two dimensional to three dimensional configuration starts early, i.e., at $n = 3$. The reason for this early onset has been attributed to directional covalent bonding of Si with Au [47].

The lowest energy geometry of Au_4Si (5a in Fig. 4.1) is a square prism with C_{4v} symmetry. The Au-Si and Au-Au bond lengths are 2.48 Å and 2.79 Å respectively. The angle between Au-Si-Au bonds is found to be 68.48^o.

This lowest energy geometry of the Au_4Si cluster is similar to the results presented by Li et al. [46] but in disagreement with Majumder [47] according to whom tetrahedral configuration similar to CH_4 methane molecule is the lowest energy isomer. In our calculations tetrahedral configuration is only 0.28 eV higher than the square prism.

While the Au_6 prefers a planar triangular structure, the Au_5Si (6a) stabilizes as a 3D structure with C_{4v} symmetry. The structure of Au_4Si cluster may be described as the square prism arrangement capped with a fifth Au atom which is in close competition with low lying isomer (6b) of C_{3V} symmetry .Our result does not agrees with that of Majumder et al. [48]

The lowest lying isomer of Au_6Si is pentacoordinated (7a) with C_1 symmetry and is in agreement with Majumder [47] but different from the low lying isomer for $SiAu_6^-$ proposed by Rhitanker et al. [24]. The Au_7Si (8a) and Au_8Si (9a) lowest energy geometries with C_s symmetry also agree with the result predicted by Majumder [47]. It is observed that in lowest energy clusters of Au_nSi with n= 6-8, the Si atom is tetra- coordinated with Au atoms and all Au atoms prefer planar configuration.
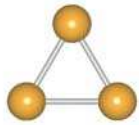
Au₃   Au₂Si (3a)   0.00   (3b) +1.30
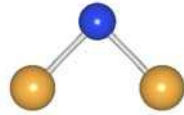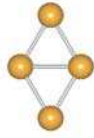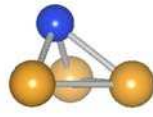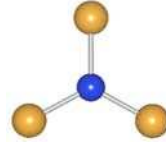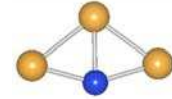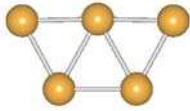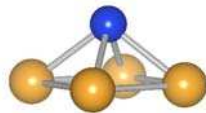
Au₄   Au₃Si (4a) 0.00   +0.35   (4c) +0.41

Au₅   Au₄Si (5a) 0.00   (5b) +0.15   (5c) +0.28

Au₆   Au₅Si (6a) 0.00   (6b) +0.03   (6c) +1.00

Au₇   Au₆Si (7a) 0.00   (7b) +0.06   (7c) +1.03
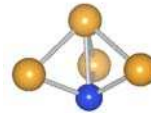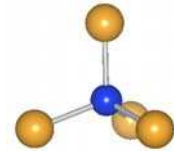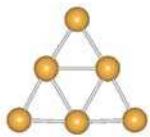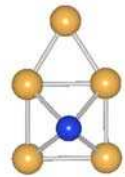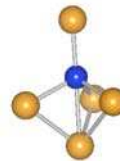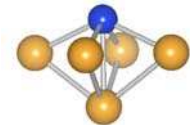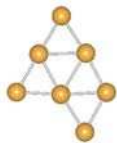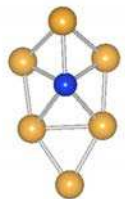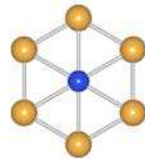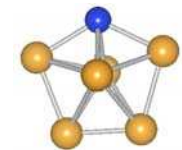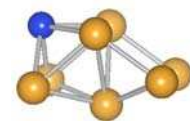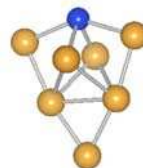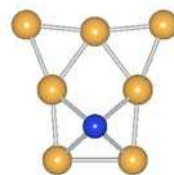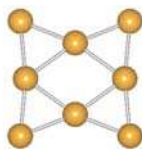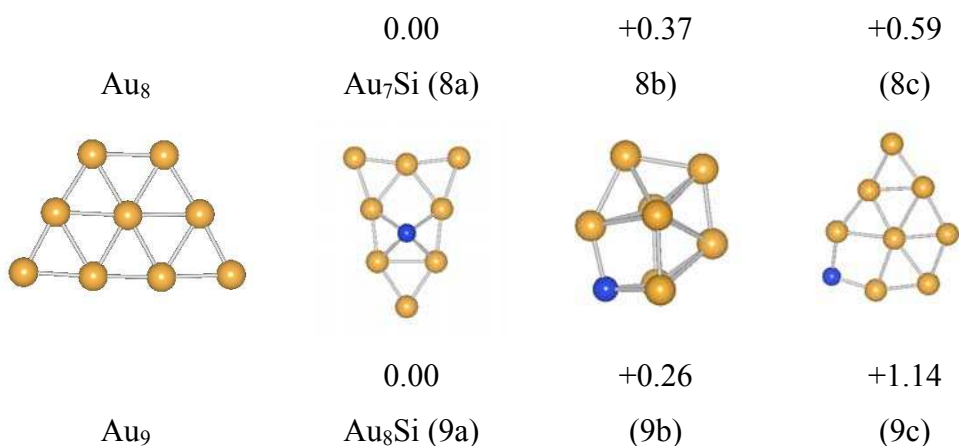
Figure 4.1. The ground state structures of Au_{n+1} and Au_nSi for n = 1-8. The numbers under the structures are relative difference of energy w.r.t the ground state structure. The blue and golden ball represents Si and Au atoms respectively.

In Au_9Si ((a) in Fig. 4.2) it is found that there are two lowest energy geometries with coordination numbers of Si as three and four. These structures are degenerate with a difference of only 0.002 eV in energies. The other close lying isomers are also shown in Fig. 4.2.
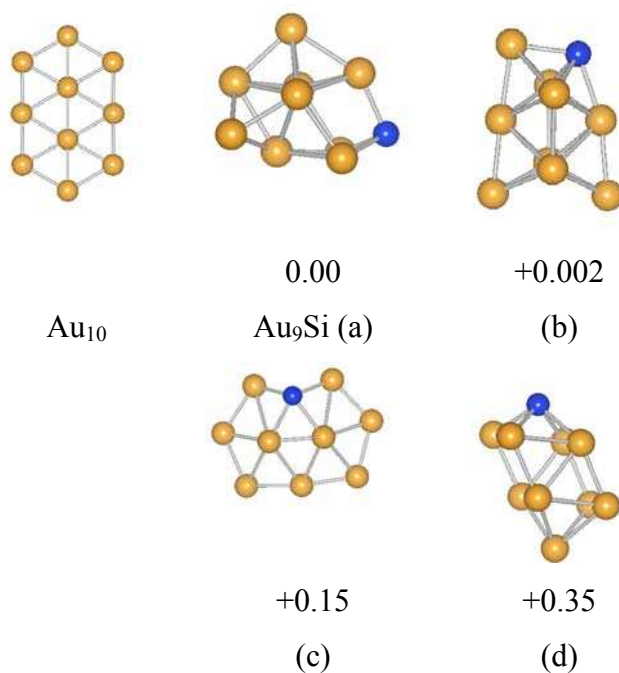
Figure 4.2. The ground state structure of Au_{10} and Au_9Si with other low lying isomers. The numbers under the structures are relative difference of energy w.r.t the ground state structure. The blue and golden ball represents Si and Au atoms respectively.

In $Au_{10}Si$, there are two isomers ((a) and (b) of Fig. 4.3) are nearly isoenergetic with an energy difference of 0.001 eV. Other less favored isomers are also presented in Fig. 4.3. It can be observed that there is clear preference for clusters having Si with a coordination number of four.

| Au_{11} | $Au_{10}Si$ (a) 0.00 | +0.001(b) |

| +0.159 (c) | +0.182 (d) |
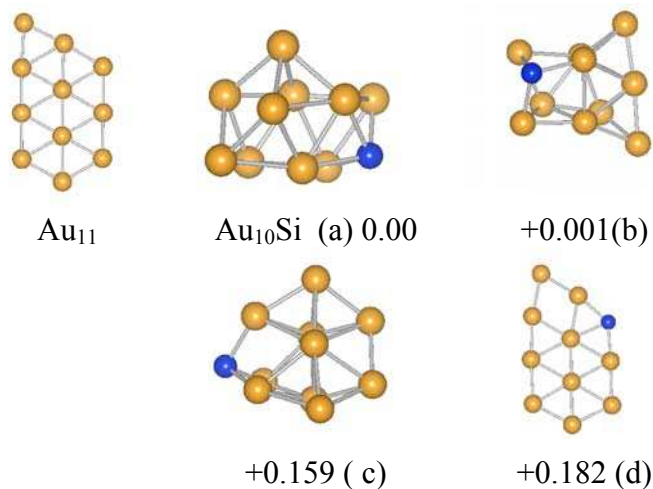
Figure 4.3 The ground state structure of Au_{11} and $Au_{10}Si$ with other low lying isomers. The numbers under the structures are relative difference of energy w.r.t the ground state structure. The blue and golden ball represents Si and Au atoms respectively.

To obtain the lowest energy isomer of $Au_{11}Si$ ((a)-(c), Fig. 4.4), we begin with initial geometries of Au_{12}, such as icosahedron or cuboctahedron; out of which every atom is replaced by a Si atom by turns. The lowest energy structure is (a) with C_1 symmetry.

| Au_{12} | $Au_{11}Si$ (a) 0.00 | +0.43 (b) |

| +0.64 (c) |
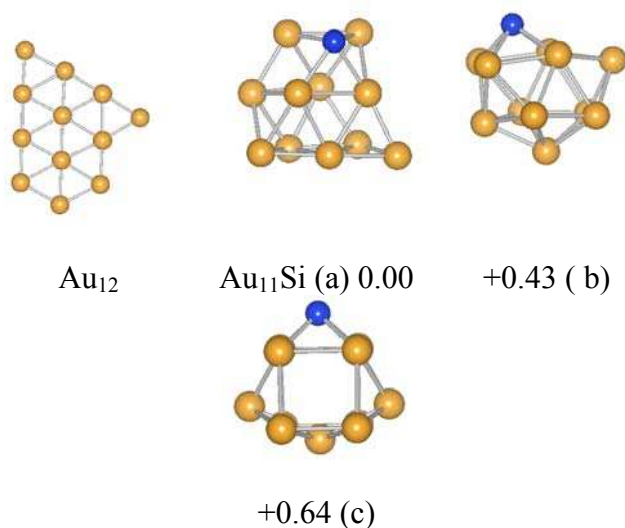
Figure 4.4 The ground state structure of Au_{12} and $Au_{11}Si$ with other low lying isomers. The numbers under the structures are relative difference of energy w.r.t the ground state structure. The blue and golden ball represents Si and Au atoms respectively.

The lowest energy structure of $Au_{12}Si$ (a) is slightly distorted cuboctahedron. It is presented in Fig. 4.5. It was found that the silicon prefers peripheral position than at the centre of cuboctahedron .Other isomers were found to have very high binding energy w.r.t this structure hence are not shown here.
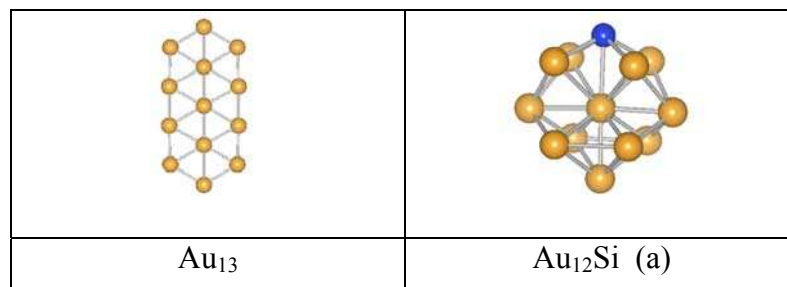
| Au_{13} | $Au_{12}Si$ (a) |

Figure 4.5 The ground state structure of Au_{13} and $Au_{12}Si$. The blue and golden ball represents Si and Au atoms respectively

Structures of clusters from n = 7 -12 (Fig. 4.1- 4.5) show that the lowest energy geometry always has silicon on the surface, with silicon preferring a tetra coordinated geometry, of the type 5a in Fig. 4.1. The cluster with n = 9 is an exception where the lowest energy geometry happens to be one with a coordination number of three for the Si atom; however, the next structure shown, (b in Fig. 4.2) where coordination number is four, is found to be isoenergetic. Another pair of nearly isoenergetic 3 and 4 coordinated structures occurs for n = 10 in Fig. 3((a) and (b)).

In Fig. 4.1, we find that it is possible to have local minima structures which are nearly planar. As mentioned in the above paragraph we observe that Si prefers 4-coordination with Au atoms forming a square.

4.3.3 Energetics

The binding energy per atom is a measure of stability. The average atomic binding energy for these clusters can be defined as

$$E_b(n) = [E_T(Si) + nE_T(Au) - E_T(Au_n Si)]/(n+1) \qquad (4.1)$$

where E_T (Au) and E_T (Si) denote total energies of Au and Si atoms and E_T (Au_n Si) denotes the energy of the Au_nSi cluster in its lowest energy configuration. The comparison between the binding energy per atom of Au_nSi with Au_{n+1} cluster is plotted in Fig. 4.6. Table 4.1 presents the binding energy (E_b) of Au_nSi clusters. The structural parameters presented are the bond lengths -- Au-Si (R_{Au-Si}) and Au-Au (R_{Au-Au}).

Table 4.1 Binding energy per atom (E_b) and bond lengths ($R_{au\text{-}si}$ and $R_{au\text{-}au}$) of Au_nSi clusters

Cluster	Symmetry	B.E.(eV/atom)	Rau-si (A^o)	Rau-au (A^o)
(Au_1Si) 2a	D_{infh}	2.17	2.29	------
(Au_2Si) 3a	C_{2v}	2.80	2.32	3.25
(Au_3Si) 4a	C_{2v}	2.76	2.42	2.82
(Au_4Si) 5a	C_{4v}	2.94	2.48	2.79
(Au_5Si) 6a	C_s	2.81	2.46-2.53	2.71-2.82
(Au_6Si) 7a	C_1	2.90	2.43-2.63	2.66-2.83
(Au_7Si) 8a	C_s	2.86	2.47-2.51	2.63-2.88
(Au_8Si) 9a	C_s	2.91	2.49-2.52	2.65-2.83
(Au_9Si) 10a	C_1	2.88	2.45-2.55	2.70-2.90
$(Au_{10}Si)$ 11a	C_1	2.93	2.47-2.56	2.73-2.92
$(Au_{11}Si)$ 12a	C_1	2.95	2.46-2.52	2.73-2.97
$(Au_{12}Si)$ 13a	C_1	2.89	2.50	2.73-2.81

The binding energy of the gold-silicon clusters Au_nSi is seen to increases with increasing cluster size. The binding energy per atom of Au_1Si is 2.17 eV while that for Au_2 dimer is 1.47 eV which are in fair agreement with the experimental values of 1.58 eV and 1.16eV respectively [49]. The higher binding energy of Au_nSi clusters can be attributed to strong covalent bonding between Au and Si atoms.

For Au_n, atomic binding energy increases upto n=6 with small odd-even oscillations whereas the binding energy of Au_nSi rises sharply upto n=4 after which it falls slightly showing a dip at n=7. The graph indicates high stabilities of Au_6 and Au_4Si clusters.

These trends in binding energy are in close agreement with the results of Majumder [47]. We also observe that as the size of the cluster grows, the average Au- Au bond length approaches the bulk value. Similarly, the Au- Si bond length also approaches a limiting value as in Table 4.1.
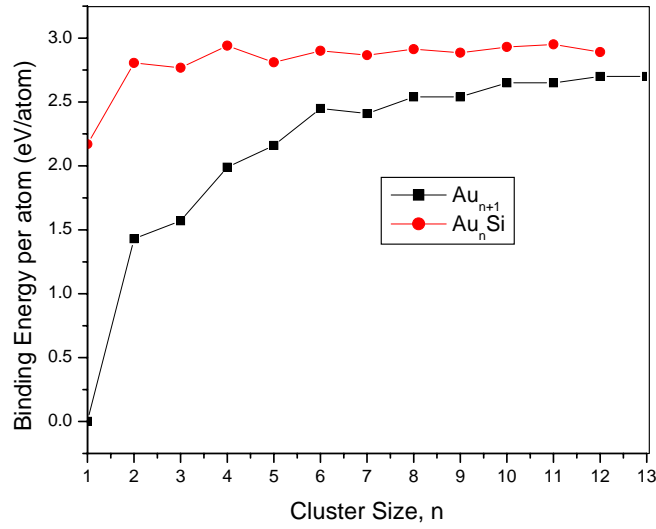
Figure 4. 6 The binding energy per atom curve of Au_nSi and Au_{n+1} cluster for n=1-12

In order to examine the relative stability of clusters of different sizes we calculate their dissociation energy and the second order difference of the total energy. The dissociation energy D_e is defined as

$$D_e = E_T\left(Au_{n-1}Si\right) + E_T\left(Au\right) - E_T\left(Au_nSi\right) \qquad (4.2)$$

where $E_T\left(Au\right)$, $E_T\left(Au_{n-1}Si\right)$, $E_T\left(Au_nSi\right)$ represent energies of Au and the lowest energies of $Au_{n-1}Si$ and Au_nSi clusters respectively. The results are plotted in Fig. 4.7 and presented in Table 4.2.

Table 4.2 Second order differences (eV) and Dissociation Energy (eV) of Au_nSi clusters

Cluster	Second Order differences (eV)	Dissociation Energy(eV)
Au_2Si	1.05	4.127
Au_3Si	-1.03	2.589
Au_4Si	1.42	3.626
Au_5Si	-1.23	2.17
Au_6Si	0.84	3.422

74

Cluster	Second Order differences (eV)	Dissociation Energy(eV)
Au_7Si	-0.70	2.591
Au_8Si	0.65	3.29
Au_9Si	-0.81	2.634
$Au_{10}Si$	-0.33	3.444
$Au_{11}Si$	0.89	3.113

The computed values of dissociation energy given in Table 4.2 and in Fig. 4.7, show that local maxima appear in dissociation energy D_e at n = 2, 4, 6, 8, 10 which correspond to clusters Au_2Si, Au_4Si, Au_6Si ,Au_8Si and $Au_{10}Si$ indicating that these clusters have higher stability. The calculated dissociation energies lie between 2.58eV and 4.12 eV, being highest at n=2.
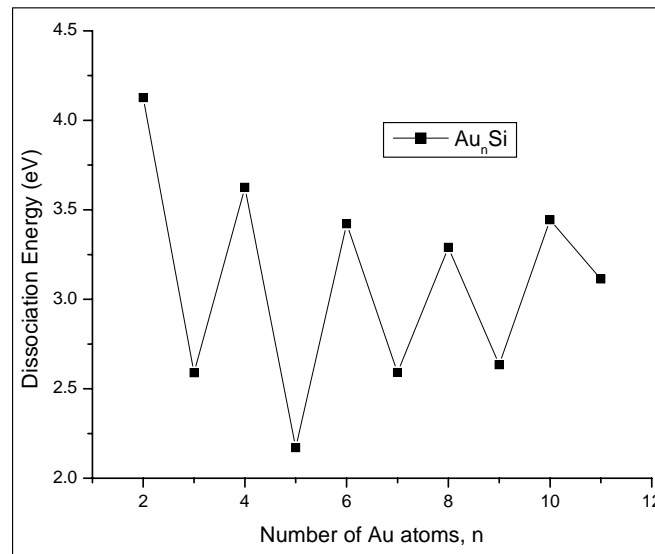
Figure 4.7 The dissociation energy curve of Au_nSi cluster for n=1-12

The second-order difference (Δ_2E) of the total energy is a sensitive quantity that characterizes relative stability of atomic clusters as a function of cluster size for different sized Au_nSi clusters. It is defined as

$$\Delta_2 E(n) = E_T\left(Au_{n+1}Si\right) + E_T\left(Au_{n-1}Si\right) - 2E_T\left(Au_n Si\right) \qquad (4.3)$$

Δ_2E as a function of cluster size is plotted in Fig. 4.8, and the values are given in Table 4.2. It again shows odd-even staggering with peaks at n = 2, 4, 6 and 8, indicating that these clusters are more stable than their neighboring clusters. It can be seen that the Au_{n+1} and Au_nSi clusters follow the same stability pattern. The exceptionally high stability of Au_4Si and Au_6, as evidenced in Fig. 4.6, can be observed from this graph also.
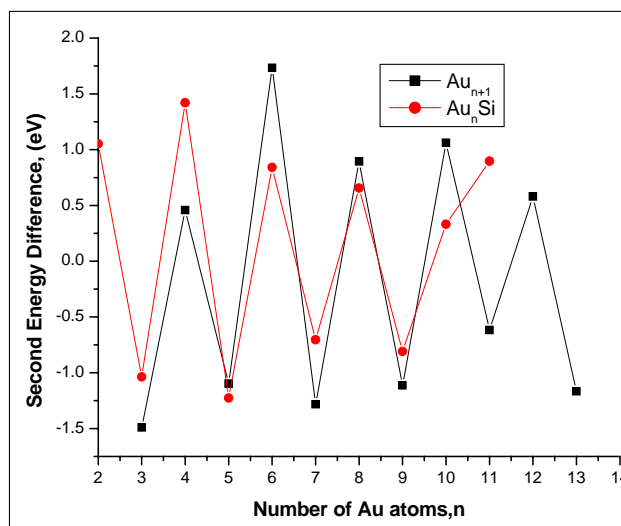
Figure 4.8 The second difference of energy Δ_2E of Au_nSi and Au_{n+1} cluster for
n=1-12

4.4 Electronic Properties

The size dependent electronic properties of Au_nSi are investigated by calculating the HOMO-LUMO gap, adiabatic ionization potentials, chemical hardness and electron affinities. The values are presented in Table 4.3.

4.4.1 HOMO-LUMO gap

The HOMO-LUMO gap reflects the ability of clusters to undergo activated chemical reactions with small molecules.

Table 4.3 and Fig. 4.9 illustrates the HOMO-LUMO gaps of the lowest energy Au_nSi (n=1 -12) clusters. It is found that the gap lies between 0.0 eV and 2.03 eV. For the AuSi dimer, the gap is 0.0 eV and Au_4Si has the largest gap of 2.03 eV indicating its higher stability. Most of the values of HOMO-LUMO gap are in typical magnitude (i.e, less than 2.0 eV) of semiconductors. Therefore it could be expected that the stable Au_nSi clusters might be considered as the novel building blocks in practical applications e.g., cluster- assembled semiconductors or optoelectronic materials.
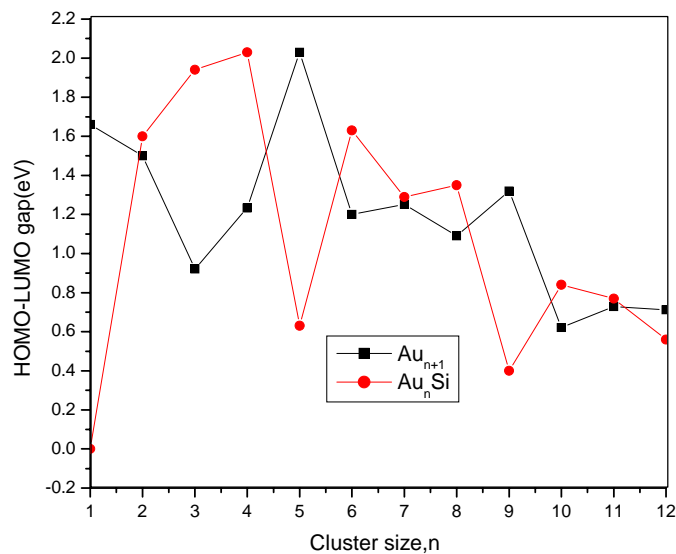
Figure 4.9 HOMO-LUMO gap of Au_nSi and Au_{n+1} cluster (n=1-12)

Table 4.3 HOMO-LUMO gap (E_g), Electron Affinity (AEA), Adiabatic Ionisation Potential (AIP), Chemical Hardness (η), Magnitude of charge ($Q_n(e)$) on Si atom from Au atom Q(e) in Au_nSi clusters. All values are in electron volts (eV).

Cluster	HOMO – LUMO gap (eV)	Ionization Potential (eV)	Electron Affinity (eV)	Chemical Hardness(η)	$Q_n(e)$
Au_1Si	0.0	6.968	0.13	3.419	-0.08
Au_2Si	1.60	5.86	2.434	1.715	-0.12
Au_3Si	1.94	6.769	3.865	1.452	-0.02
Au_4Si	2.03	5.742	2.658	1.542	0.01
Au_5Si	0.63	6.05	1.51	2.27	0.04
Au_6Si	1.63	6.998	1.17	2.914	0.0
Au_7Si	1.29	6.285	2.243	2.021	0.04
Au_8Si	1.35	6.868	1.63	2.619	0.02
Au_9Si	0.40	5.966	2.07	1.948	0.08
$Au_{10}Si$	0.84	5.817	1.95	1.933	0.11
$Au_{11}Si$	0.77	5.93	2.14	1.895	0.12
$Au_{12}Si$	0.56	4.945	2.07	1.437	0.11

4.4.2. Ionization Potential and Electron affinity

The Ionization potential (IP) and electron affinity (EA) are defined using equations (4.4) and (4.5)

$$IP\left(Au_n Si\right) = E\left(Au_n Si^+\right) - E\left(Au_n Si\right) \qquad (4.4)$$

$$EA\left(Au_n Si\right) = E\left(Au_n Si\right) - E\left(Au_n Si^-\right) \qquad (4.5)$$

The variation in adiabatic ionization potential and electron affinity of Au_nSi clusters are plotted in Fig. 4.10 as a function of cluster size and the computed values are given in Table 4.3. It is observed from the graph that IP shows peaks at n=2 and n=4, then after n = 5 it again shows two maxima at n =7 and n=9. The electron affinity exhibit opposite trend to ionization potential except that it is highest at n=4, for Au_3Si cluster indicating its high reactivity.
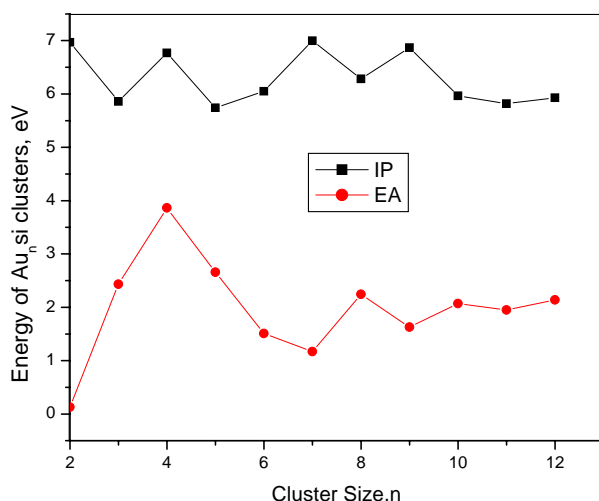
Figure 4.10 The electron affinities (EAs) and ionization potentials (IPs) Au_nSi cluster for n=1-12

4.4.3. Chemical Hardness

Chemical hardness is an electronic property used to characterize the relative stability of molecules. Chemical hardness η is interpreted as the resistance towards change in number of electrons. The chemical hardness (η) is defined as η = (VIP-EA)/2, displayed in Fig. 4.11 and the values are presented in Table 4.3. The graph shows peaks for even number of gold atoms, n=2, 7, 9, indicating high stability of these Au_nSi clusters.

78
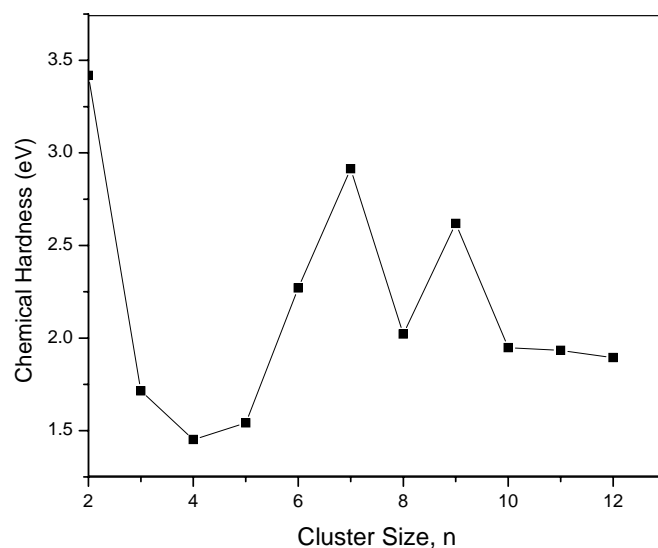
Figure 4.11 Size dependence of the calculated chemical hardness (η) of lowest energy Au_nSi clusters

4.4.4 Mulliken Charge Analysis

We find the charge at each site, which helps to determine the qualitative nature of bonding in Au_nSi clusters. This data is tabulated in Table 4.3.

It is observed that upto n= 5 the charge on Si decreases except at n=4 and for n> 5 charge on silicon increases. Since the amount of charge transfer from Au to Si is very small, it can be concluded that the bonding between Au and Si atom is covalent in nature.

4.5 Germanium doped Gold clusters, Au_nGe (n =1 -10)

Since Germanium belongs to the same group as Silicon and has same number of valence electrons in the outermost shell, it will be interesting to see how the different properties of gold cluster changes when doped with a Germanium atom. The aim of present study is to give a comparison between the structural and electronic properties of Au_nGe with that of silicon doped gold clusters and pure gold clusters.

To study the lowest energy structures of Au_nGe (n = 1 - 10) the simulation parameters obtained from Au_nSi calculation were used. To find the low lying structures of Au_nGe clusters only the minimum energy structures of Au_nSi clusters and their first isomers were considered and the different geometries were obtained by replacing Si with Ge atom. The structures obtained are presented in Fig. 4.12 and different properties such as binding energy etc are presented in Table 4.4.

4.5.1   Structure of Au_nGe

The lowest energy clusters of Au_nGe are presented in Fig. 4.12. The AuGe cluster has a bond length of 2.37 A^o which is smaller than Au-Au bond of bond length 2.55A^o and is larger than the Au-Si bond of bond length 2.29 A^o. The bond length 2.37 A^o of AuGe is in good agreement with the experimental   reported value 2.38A^o [38].

For Au_2Ge, a triangular structure with C_{2v} symmetry is more stable than its linear isomer. It is observed that the Au_2Si also prefers triangular geometry over the linear arrangement.

For Au_3Ge, an Au atom is replaced by Ge in stabilized Au_4, a planar rhombus the lowest structure for Au_3Ge is three dimensional capped triangles with C_{2v} symmetry similar to Au_3Si. It is observed that both Au_nGe and Au_nSi cluster, the transition from two dimensional to three dimensional configuration starts early at n = 3 in comparison with Au_{n+1} clusters which prefers planar geometry upto n =13.

The Au_4Ge is a square prism with C_{4v} symmetry as the lowest energy geometry shown in Fig. 4.12. The Au-Si bond length is 2.48 A^o and Au-Au bond length is 2.79 A^o.

While the Au_6 prefers a planar triangular structure, the lowest energy geometry of Au_5Ge can be viewed as derived by adding an additional Au atom to square pyramidal Au_4Ge similar to the lowest energy structure of Au_5Si.

The lowest lying isomer of Au_6Si is pentacoordinated with C_1 symmetry while Au_6Ge

prefers planar geometry with coordination number two. The Au_7Ge and Au_8Ge lowest energy geometries with C_s symmetry are similar to structures predicted by Rhitaker et al.for Au_7Ge^- and Au_8Ge^- geometries [24]. It is observed in lowest energy clusters of Au_nGe with n= 4-10, that Ge atom is tetra coordinated with Au atoms except at n=6. In Au_9Ge and $Au_{10}Ge$ clusters, Ge atom also prefers coordination number four.

It is observed that the ground state geometries of the clusters show patterns similar to silicon doped gold clusters except for n = 6, 9 and 10. It can be observed that as the size of the cluster increases there is deviation in the lowest energy geometries of Ge doped gold clusters from Silicon doped gold clusters. Germanium atom prefers tetra coordination just like silicon when doped in a gold cluster, for n > 3, except for Au_6Ge cluster which stabilizes with co ordination number two.

Au_2Ge Au_3Ge Au_4Ge

Au_5Ge Au_6Ge Au_7Ge

Au_8Ge Au_9Ge $Au_{10}Ge$
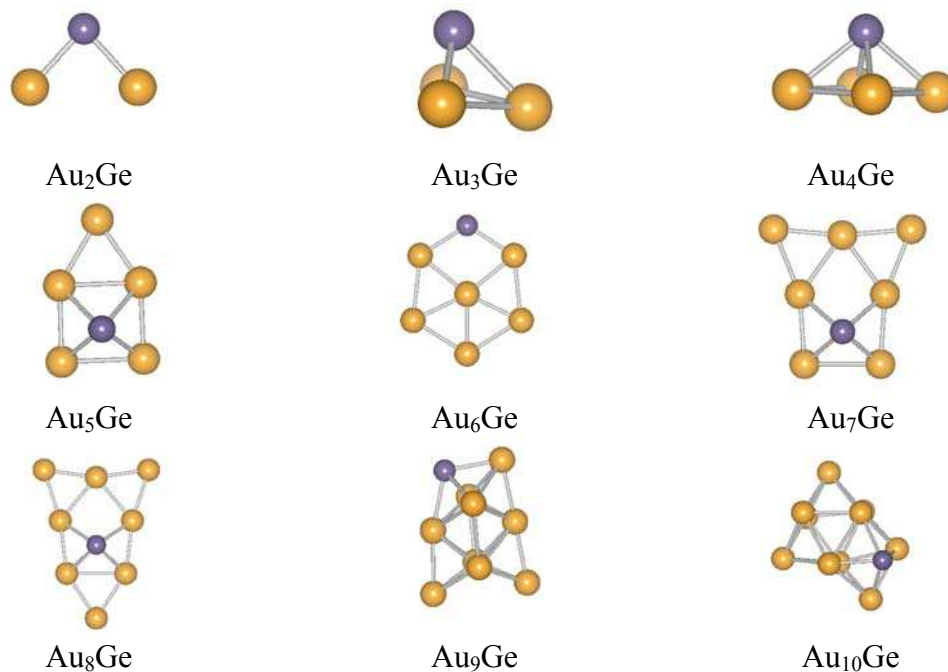
Figure 4.12 The ground state structures of Au_nGe for n = 1-10 .The numbers under the structures are relative difference of energy w.r.t the ground state structure. The grey and black ball represents Ge and Au atoms respectively

4. 5. 2 Energetics

The binding energy per atom is the measure of stability. The average atomic binding energy of Au_nGe (n=1-10) can be defined as

$$E_b(n) = \left[E_T(Ge) + nE_T(Au) - E_T(Au_nGe) \right]/(n+1) \qquad (4.6)$$

where E_T (Au), E_T (Ge), E_T (Au_n Ge) denote total energies of Au, Ge and the lowest energies of Au_nGe The comparison between the binding energy per atom of Au_nGe w.r.t. Au_{n+1} and Au_nSi clusters is plotted in Fig. 4.13
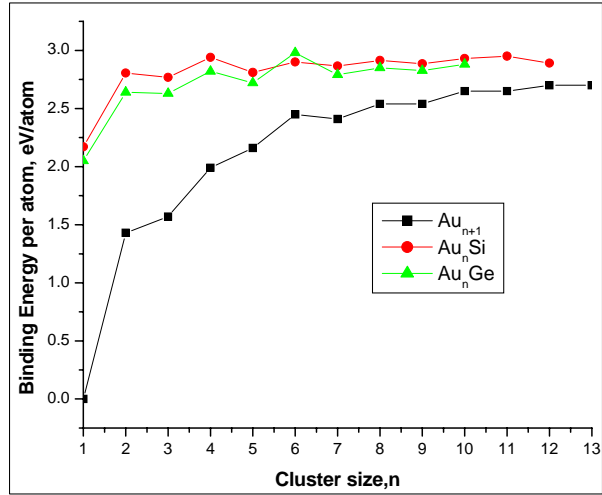
Figure 4.13 Comparison of the binding energy per atom Au_nGe with Au_nSi and Au_{n+1} clusters.

It is observed from the graph that the introduction of germanium atom has increased the binding energy of gold clusters. The binding energy curve of Au_nGe cluster exhibits higher values for even n compared to odd n, with peak at Au_6Ge. It is observed that the binding energy curve for Au_nGe and Au_nSi clusters show similar pattern. The binding energy per atom of germanium doped cluster is smaller than the corresponding silicon doped gold clusters.

The second-order difference (Δ_2E) of the total energy is computed using equation (4.3) and is plotted as function of number of gold atoms in Fig. 4.14 and the values are given in Table 4.4.
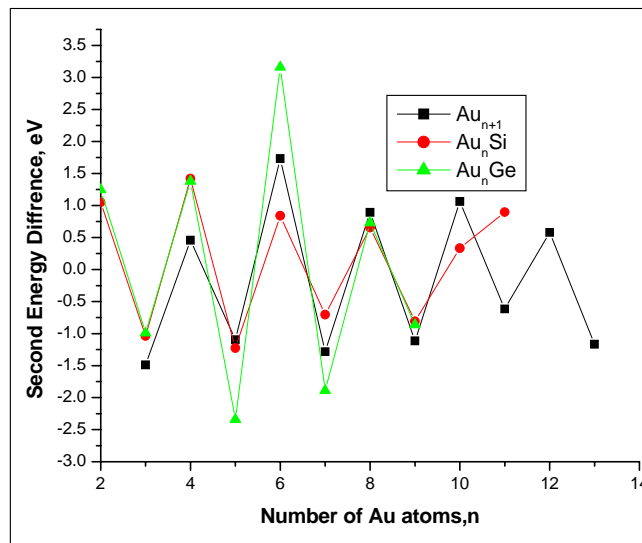
Figure 4.14 Comparision of the second difference of energy Δ_2E of Au_nGe, Au_nSi and Au_{n+1} cluster.

The germanium doped gold clusters are found to exhibit odd-even staggering with peaks at n = 2, 4, 6 and 8, indicating that these clusters are more stable than their neighboring clusters It can be seen that the Au_{n+1} and Au_nSi clusters follow the same stability pattern.

Table 4.4 Binding Energy per atom (eV/atom), Second Energy Difference (eV), HOMO-LUMO gap (E_g), in Au_nGe (n= 1- 10) clusters.

Cluster	B.E.(eV/atom)	Second Energy Difference (eV)	E_g (eV)
(Au_1Ge)	2.05	--	2.09
(Au_2Ge)	2.64	1.246	1.45
(Au_3Ge)	2.63	-0.99	1.89
(Au_4Ge)	2.82	1.38	2.02
(Au_5Ge)	2.72	-2.34	0.72
(Au_6Ge)	2.98	3.16	0.63
(Au_7Ge)	2.79	-1.89	1.32
(Au_8Ge)	2.85	0.73	1.5
(Au_9Ge)	2.826	-0.864	0.46
$(Au_{10}Ge)$	2.88	--	0.86

4.5.3 Electronic properties

The HOMO–LUMO gaps of the lowest energy Au_nGe (n = 1=10) clusters in comparison with the HOMO-LUMO gap of silicon doped and pure gold clusters are plotted in Fig. 4.15.

The HOMO-LUMO gap (E_g) for Au_n Ge clusters is found to vary between 0.46 eV – 2.09 eV. It is seen that E_g for AuGe dimer is maximum while for AuSi is zero. This implies that AuGe dimer is chemically more stable than AuSi dimer. In general, it can be observed that the graphs peaks at Au_6 for pure Au_{n+1} clusters, at Au_5Si for Silicon doped gold clusters and at AuGe for germanium doped gold clusters. Similar to Au_nSi clusters the HOMO–LUMO gap values are in the range of semiconductors.
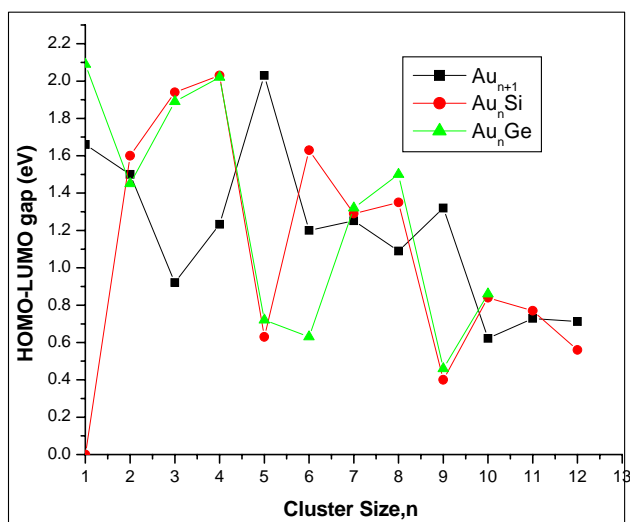
Figure 4.15 Comparison of HOMO-LUMO gap of Au_nGe with Au_nSi and Au_{n+1} clusters

The Mulliken charge analysis indicates that charge of order of 0.1e always transfers from germanium atom to gold atom. Since there is no significant charge transfers take place between Ge atoms and Au atoms, it implies that the bonding is covalent in nature.

4.6 Conclusion

We have presented the results of our DFT based investigations of Au_nSi and Au_nGe clusters in comparison with Au_{n+1} cluster. The structural and electronic properties are investigated systematically and the results can be summarized as follows.

The Au_nSi clusters adopt 3D structures from n=3 onwards, while pure Au_{n+1} clusters prefer planar structures upto n =13. In the stable structures (with n>4), Si is coordinated with 4 Au atoms. These four atoms are arranged in a square rather than the familiar tetrahedron associated with bulk Si. The ground state geometries of the Au_nGe clusters show patterns similar to silicon doped gold clusters except for n = 6 , 9 and 10. Germanium atom prefers tetra coordination like silicon when doped in a gold cluster, for n > 3,

- The binding energy per atom of Au_nSi clusters, compared with Au_{n+1} cluster, show an increase with the introduction of Si. The binding energy per atom of germanium doped clusters is smaller than the corresponding silicon doped gold clusters.

84

- All three curves -- binding energy, second energy difference and dissociation energy, show that even number of gold atoms in a cluster makes it more stable compared to its odd numbered neighbours. In fact Au_4Si and Au_6 are most stable in their respective classes.

- The HOMO–LUMO gap values of both Silicon and Germanium doped gold clusters lies in the range of semiconductors.

- The Mulliken charge analysis of Au_nSi and Au_nGe clusters indicates covalent bonding between Si and Au atoms, Ge and Au atoms.

Bibliography

[1]   P.Pyykko, N. Runeberg, Angew. Chem., Int. Ed. 41, 2174 (2002).

[2]   M. Zhang, X. J. Feng, L. X. Zhao, L. M. H. Li and Y. H. Luo, Chin. Phys. B 19, 4 043103 (2010).

[3]   X Li, B. Kiran, L.F. Cui and L. S. Wang, Phys. Rev. Lett. 95, 253401(2005).

[4]   L. M. Wang, R. Pal, W. Huang, X. C. Zeng, L. S. Wang, J. Chem. Phys. 130 , 051101 (2009).

[5]   H. Häkkinen, S. Abbet, A. Sanchez, U. Heiz , U. Landman, Angew. Chem, Int. Ed., 42, 1297(2003).

[6]   X. D. Zhang, M. L. Guo, D. Wu , P. X. Liu , Y. M. Sun , L. A. Zhang , Y. She, Q. F. Liu, F. Y. Fan, Int. J. Mol. Sci 12, 2972-2981(2011).

[7]   E. Janssens, H. Tanaka, S. Neukermans, R. E. Silverans, P. Lievens, New J. Phys. 5, 46 (2003).

[8]   E. Janssens, H. Tanaka, S. Neukermans, R. E. Silverans, P. Lievens, Phys. Rev. B 69, 085402 (2004).

[9]   H. Tanaka, S. Neukermans, E. Janssens, R. E. Silverans, P. Lievens, J. Am. Chem. Soc. 125, 2862 (2003).

[10]   L.Gagliardi, J. Am. Chem. Soc. 125, 7504 (2003).

[11]   M. Heinebrodt, N. Malinowski, F. Tast, W. Branz, I. M. L. Billas, T. P. Martin, J. Chem. Phys. 110, 9915 (1999).

[12]   D. W. Yuan, Y. Wang, Z. Zeng, J. Chem. Phys. 122, 114310 (2005).

[13]   B. R. Sahu, G. Maofa, L. Kleinman, Phys. Rev. B 67, 115420 (2003).

[14]   H. Tanaka, S. Neukermans, E. Janssens, R. E. Silverans, P. Lievens, J. Chem. Phys. 119, 7115 (2003).

[15]   K. Koyasu, M. Mitsui, A. Nakajima, K. Kaya, Chem. Phys. Lett., 358, 224 (2002).

[16]   M. B. Torres, E. M. Fernández, L. C. Balbás, Phys. Rev. B 71, 155412 (2005).

[17]   J. E. Elkind, J. M. Alford, F. D. Weiss, R. T. Laaksonen , R. E. Smalley, J. Chem. Phys. 87, 2397 (1987); M. F. Jarrold, Science 252, 1085 (1991).

[18]   K. Raghavachari, V. Logovinsky, Phys. Rev. Lett. 55, 2853 (1985) ; K. M. Ho, A. A. Shvartsburg, B. Pan, Z. Y. Lu, C. Z. Wang, J. G. Wacker, J. L. Fye, and M. F. Jarrold, Nature 392, 582 (1998) .

[19]   B. Kiran, L. X, H. J. Zhai, L.F. Cui and L. S. Wang, Angew. Chem. Int. Ed. 43, 2125 (2004).

[20]   M. Walter, H. Hakkinen, Phys. Chem., Chem. Phys. 8, 5407 (2006).

[21]   L. M. Wang, S. Bulusu, W. Huang, R. Pal, L. S. Wang, X. C. Zeng , J. Am. Chem. Soc., 129, 15136-15137 (2007).

[22]   A. Spiekermann, S. D. Hoffmann, F. Kraus,T. F. Fassler, Angew. Chem. Int. Ed. 46, 1638 –1640 (2007).

[23]   J. Hu, T .W. Odom, C . M. Lieber, Acc. Chem. Res. 32,435 (1999).

[24]   R. Pal, L.M. Wang , W. Huang , L. S. Wang , X. C. Zeng , J Am Chem Soc. , 131, 9, 3396-3404 (2009).

[25]   P Ordejon, E. Artacho, J. M. Soler, Phys. Rev. B 53, R10441 (1996).

[26]   D. Sanchez-Portal, P. Ordejon, E. Artacho,   J. M. Soler, Int. J.Quantum Chem 65, 453 (1997).

[27]   J. M. Soler, E. Artacho, J. D. Gale, A. Garcia, J. Junquera, P. Ordejon, D. Sanchez-Portal, J. Phys. Condens. Matter 14, 2745 (2002).

[28]   G. P. Robert, Y. Weitao, Density-Functional Theory of atoms and Molecules, Oxford University Press NewYork (1989).

[29]   Perdew, Burke, Ernzerhof , Phys. Rev. Lett., 77, 3865 (1996).

[30]   L. Kleinman, D. M. Bylander, Phys. Rev. Lett. 48, 1425 (1982).

[31]   C. Kittle, Introduction to Solid State Physics, 7th ed.,Wiley, New York (1996).

[32]   R. C. Weast, CRC Handbook of Chemistry and Physics, 55th ed., CRC press, Cleveland, OH (1974).

[33]   K. Raghavchari, J. Chem. Phys. 84, 5672 (1986).

[34]   D.J. Trevor, D.M Cox, K.C. Reichmann, R. O. Brickmann, A. Kaldor, J. Phys. Chem. 91, 2598 (1987).

[35]   C. B. Winstead, S. J. Pankstis, J. L. Gole, Chem. Phys. Lett. 237, 81-85. (1995).

[36]   I. Shim, M. Sai Baba, K. A. Gingerich, Chem. Phys. 277, 9 (2002).

[37]   V. Pershina, J. Anton, B. Fricke, J. Chem. Phys. 127, 134310(2007).

[38]   J. E. Jr Kingcade, U. V. Choudary, K. A. Gingerich, Inorg. Chem.18, 3094 (1979).

[39]   G. Bravo Perez, I. L.Garzon, O. Novaro, J. Mol. Struct. (Theochem) 493, 225-231(1999).

[40]   J. Wang, G.Wang, J. Zhao, Phys Rev. B. Condens. Matter   66,035418 (2002).

[41]   H. Hakkinen, U. Landman, Phys. Rev. B., Condens Matter 61,287 (2000).

[42]   H.M Lee, M. Ge, B. R. Sahu, P. Tarakeshwar , K. S. Kim, J. Phys. Chem. 107, 9994 (2003).

[43]   V. Bonacic-Koutecky, J. Burda, R. Mitric, M. Ge, G. Zampella, P. Fantucci, J. Chem. Phys. 117,3120 (2002).

[44]   L. Wang, L. Xiao, Chem. Phys. Lett. 392, 452-455 (2004).

[45]   H. Hakkinen, B. Yoon, U. Landman, X. Li, H. J. Zhai, L. S. Wang, J. Phys. Chem. A 107, 6168 (2003).

[46]   S. F. Li, X. Xue, Y. Jia, G. Zhao, M. Zhang, X. G. Gong, Phys. Rev. B 73, 165401 (2006).

[47]   C. Majumder, Phys. Rev. B 75, 235409 (2007).

[48]   C. Majumder, A. K. Kandalam, P. Jena, Phys. Rev. B 74, 205437 (2006).

[49]   R. C. Weast, CRC Handbook of Chemistry and Physics, 49th ed. (1969).

Chapter 5

5. Doped Golden Fullerenes

5.1 Introduction

In previous chapters we have seen that gold clusters exhibit intriguing geometrical structures. They favor two-dimensional planar structures up to $n = 13$, a perfect tetrahedron at Au_{20} followed by tubular structures at Au_{24} and Au_{26}. This size-dependent evolution of geometric structure of gold for cluster size up to several hundred atoms strongly impacts its electronic, optical, and chemical properties. For such applications it is important to have a detailed knowledge of the cluster structures and their identification for the controlled use in future nanotechnology.

Along with the small gold clusters, the medium-sized gold clusters have also been extensively studied [1-3]. Lechtken et al. [4] using a combination of trapped ion electron diffraction (TIED) method, PES, and (time dependent (TD)) density functional theory (DFT) have shown that Au^-_{34} cluster adopts a chiral structure. A highly stable Au_{32} cage cluster with the icosahedral (I_h) symmetry same as C_{60} was predicted by Johansson *et al.*[5] which was later confirmed by Ji et al. [6] using a photoelectron spectroscopy (PES) experiment combined with quantum mechanical calculations. They found that the Au_{32} fullerene is the most stable at zero temperature. This structure has been reported to be synthesized using ligands [7]

As discussed in the last chapter, a suitable impurity can bring structural changes as well as can modulate different properties of the low lying geometries of pure gold clusters. By doping gold clusters with Si and Ge atoms, we can have early onset of 3D geometries in gold clusters. A relativistic density functional theory (DFT) of Au_{32} cluster by Himadri et al. [8] have shown that the bare fullerene Au_{32} cluster (without any stabilizing ligands) can be used for potential catalytic applications. In an another theoretical study, Deng et al. [9] have doped Ag atom in the hollow cage-like and space-filling structures of Au_{32} and found that the $Au_{31}Ag$ cluster with the hollow cage-like configuration is highly stable. It has been recently found that coating of 20 Au atoms on an Al_{13} cluster leads to a highly stable and icosahedrally symmetric endohedral $Al@Al_{12}Au_{20}$ compound fullerene [10].

Similar studies have been performed by Meng et al. [11] using first-principles calculations on the nano golden cages $M_{12}@Au_{20}$ (*M*=Na, Al, Ag, Sc, Y, La, Lu, and Au) clusters to explore their structural and electronic properties. In this chapter we

will perform the DFT study of effect of group 14 elements(C, Si, Ge) on the structural stability and electronic properties of Au_{32} cage. We have calculated the binding energies, bond lengths, HOMO-LUMO gaps and plotted the partial density of states (PDOS) of these clusters.

The organization of the chapter is as follows. The computational details are given in Section 5.2, results and discussions are presented in Section 5.3.

5.2 Computational Details

We have used the SIESTA code, based on Density Functional theory method. The electron density functional is treated by the generalized gradient approximation (GGA) with exchange correlation functional parameterized by Perdew, Zunger and Ernzerhof (PBE) scheme [12-14]. The pseudo potentials for Carbon, Silicon and Germanium atoms are generated with atomic valence electron $2s^2 2p^2$, $3s^2 3p^2$ and $4s^2 4p^2$ respectively. The core radii (in units of Å) for Carbon are s (1.49), p (1.52), d (1.52) and f (1.49): For Silicon, they are: s (1.77), p (1.96), d (2.11) and f (2.11) and for Germanium, they are: s (2.06), p (2.85), d (2.58) and f (2.58). The valence states were described using DZP (double-zeta + polarization) basis sets. The reciprocal space integrations are carried out at the gamma point. The clusters are optimized inside simulation cell of 15 Å and energy cutoff of 200 Ry. The symmetry unrestricted geometry optimization is carried using conjugate gradient and quasi Newtonian methods until all the forces are less than 0.01eV/Å.

We have already given the verification of the computational procedure for Au-Si and Au-Ge dimer in the last chapter. The test calculation results for the bond length of the ground state of AuC molecule is 1.875 A ˚ which is in the good agreement with the reported values (1.88 A ˚) .The calculated value of the binding energy per atom for AuC is 2.47 eV which higher than the other reported values(1.97eV)[15].

5.3 Results and discussions

5.3.1 Structure and Energetics of $M_{12}@Au_{20}$

The structure of the hollow golden fullerene Au_{32} can be regarded as I_h symmetry 12-atom icosahedron combined with I_h symmetry Au_{20} dodecahedron as shown in Fig. 5.1. We have replaced Au atom at the center of each pentagon of Au_{32} with another metal atom to construct $M_{12}@Au_{20}$ clusters (M= C, Si and Ge) similar to Meng et al.[11].The initial structure and the final optimized structures of Au_{32} after doping are given in Fig. 5.1 and various computed values are given in Table 5.1.

Au$_{32}$

(a)

Si$_{12}$@Au$_{20}$

(b)

Ge$_{12}$@Au$_{20}$

(c)

C$_{12}$@Au$_{20}$

(d)
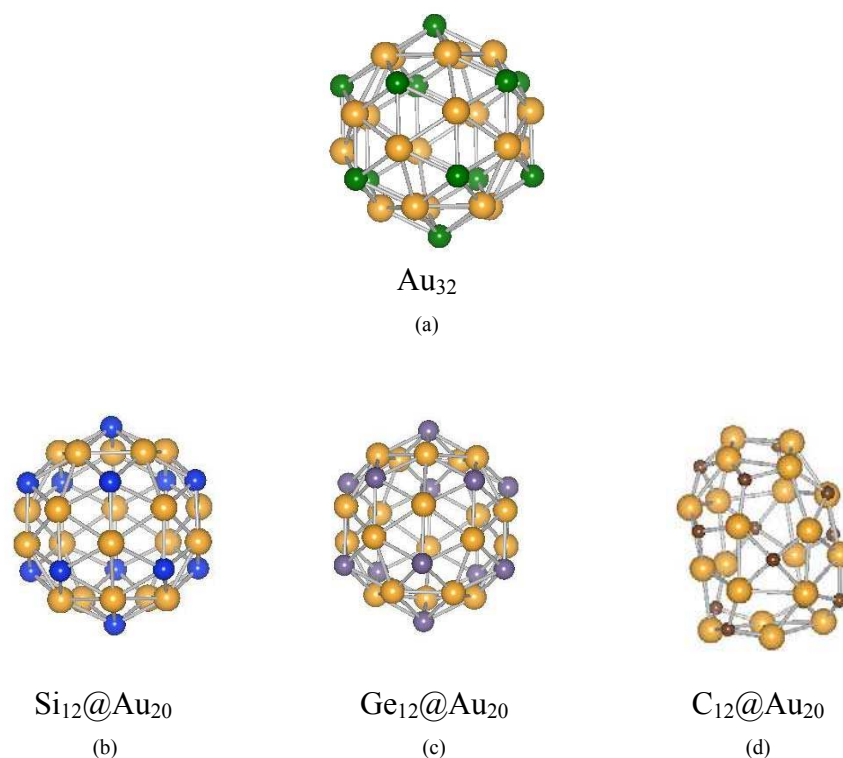
Figure 5.1 The initial geometry of Au$_{32}$ cage with position of dopant (*M*) atoms is shown in (a) by green spheres. The low lying geometries of the M_{12}@Au$_{20}$ clusters (*M*= Si, Ge and C) obtained from symmetry unrestricted optimization using density functional theory. The Si atom is represented by blue spheres (b), Ge atom is represented as purple spheres (c) and C atom is represented as brown spheres (d).

It is found that after optimization the Si and Ge atoms doped M$_{12}$@Au$_{20}$ clusters retains the I_h symmetry of the initial Au$_{32}$ fullerene but the Carbon doping completely destroys it. It is also found the coordination number of Si and Ge atoms is 5 and of C atoms is 3 and 4 in M$_{12}$@Au$_{20}$ cluster.

Table 5.1 Symmetry, Binding Energy per atom (eV/atom), HOMO-LUMO gap (E$_g$)

Cluster	Symmetry	E$_b$ (eV/atom)	Eg (eV)
Au$_{32}$	I$_h$	3.16	1.59
C$_{12}$@Au$_{20}$	C$_1$	4.17	0.51
Si$_{12}$@Au$_{20}$	I$_h$	4.02	0.57
Ge$_{12}$@Au$_{20}$	I$_h$	3.77	0.91

We can conclude by looking at the different optimized geometries of Si doped Au clusters that Si is hyper valent and can have a coordination of 3, 4(in Chapter 3), 5 or even 6(in Chapter 7).

The Binding Energy (E_b) gives the measure of thermodynamic stability of cluster. It is calculated using equation (1) and values are given in Table1.

$$E_b = \left[E_T\left(M_{12}Au_{20}\right) - 12E_T(M) - 20E_T(Au) \right]/(32) \qquad (5.1)$$

The variation in binding energy of Au_{32} cluster with changing dopants is presented in Fig.5.2. The calculated binding energy per atom of Au_{32} is found to be 3.166 eV which is higher than the value predicted by Meng et al. [11].
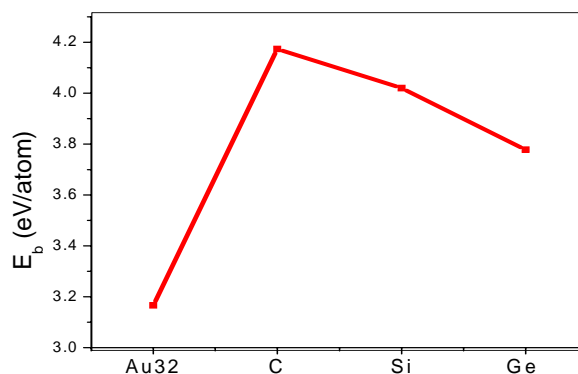
Figure 5.2 The average binding energy (E_b) of the M_{12}@Au_{20} clusters (M=C, Si and Ge)

It can be seen from the graph addition of dopant atom to Au_{32} cage has increased its binding energy. The binding energy C_{12}@Au_{20} is 1.00 eV higher than of Au_{32} cage and is found to be thermodynamically more stable than its neighboring clusters.

5.4 Electronic properties

The HOMO–LUMO energy gap (E_{gap}) of the M_{12}@Au_{20} clusters is given in Table 5.1 Earlier theoretical studies on Au_{32} in I_h symmetry have shown that it has a large HOMO– LUMO gap and is expected to be chemically inert. The energy gap of 1.59 eV of Au_{32} in our computations is in good agreement with the previous results [2, 5, 9].

Table 5.1 shows the E_g of the doped fullerene M_{12}@Au_{20} is smaller than the gap of Au_{32}. Interestingly, C_{12}@Au_{20} has the smallest HOMO–LUMO gap of only about 0.51 eV, suggesting that it should be relatively chemically reactive. The Si_{12}@Au_{20} cluster is found to have the largest HOMO-LUMO gap of 0.91 eV. It can be concluded that while C_{12}@Au_{20} is thermodynamically more stable, the Si_{12}@Au_{20} is chemically more stable.

The decrease in the band gap of pure Au_{32} cage after doping can also be seen in

PDOS plot in Fig. 5.3 ((a)-(g)) .It can be clearly seen that a band gap exists at Fermi level for the Au_{32} cage. After doping the Au_{32} , there is an increased electron density due to overlapping of s and p orbitals of the dopants around Fermi level and thus reducing the HOMO-LUMO gap of cage .

It can also be seen that when the dopant atoms are placed into Au_{32} cage, the PDOS of Au is shifted to the low energy side below Fermi level, causing an increase in the bonding electron numbers at lower energy level. As a result, the structural stability of the Au_{32} cluster increases. As a result, the structural stability of the $M_{12}@Au_{20}$ clusters increase. Therefore we can conclude on doping of C, Si and Ge atom improves the conductivity as well as stability of Au_{32} cage.
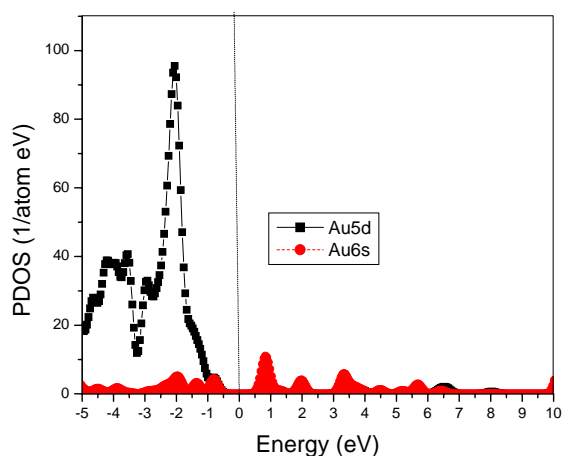
Au_{32} cage(a)
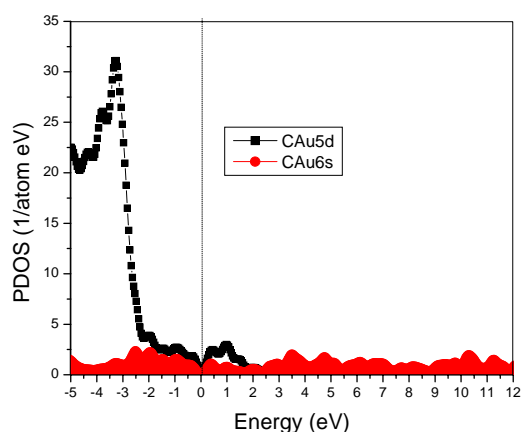
$C_{12}Au_{20}$ (b)
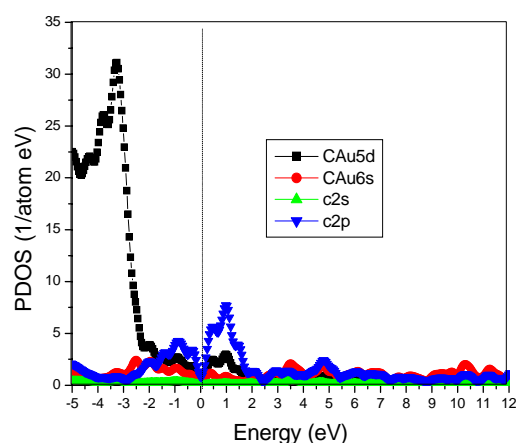
(c)
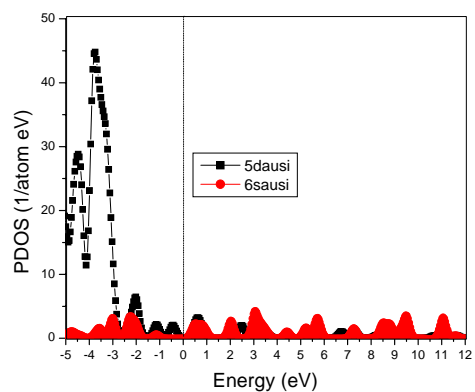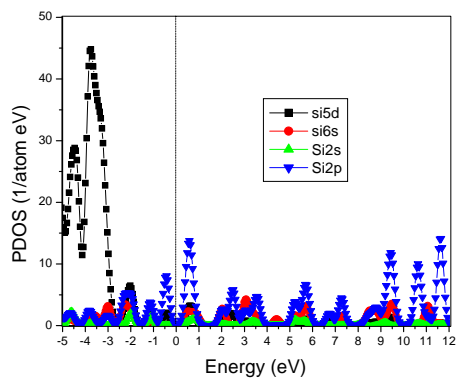
Si$_{12}$Au$_{20}$ (d)   (e)
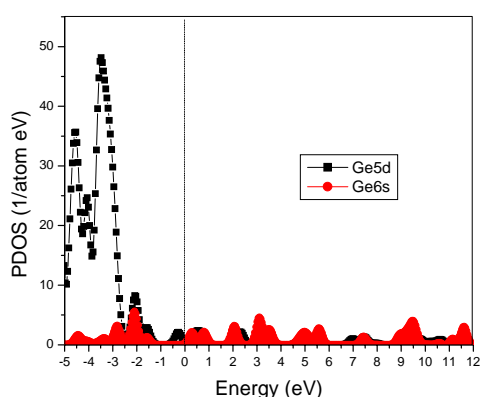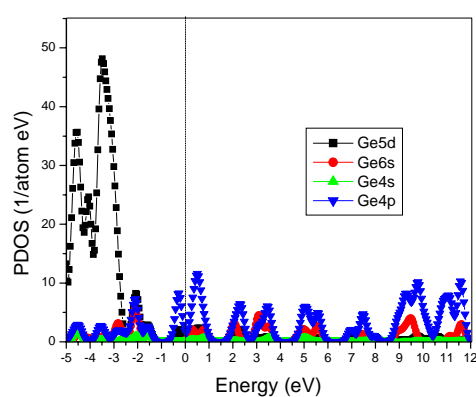
Ge$_{12}$Au$_{20}$ (f)   (g)

Figure 5.3 Partial density of states for (a) Au$_{32}$, C$_{12@}$Au$_{20}$ (b&c), Si$_{12@}$Au$_{20}$ (d&e) and Ge$_{12@}$Au$_{20}$ (f&g) clusters with their lowest-energy configurations. Fermi level is set at zero on the energy axis.

5.5 Conclusion

We have carried out a first-principles investigation with the density functional theory (DFT) to study the M_{12}@Au$_{20}$ (M= C, Si and Ge) clusters.

- The Au$_{32}$ cage retains its I$_h$ symmetry after doping with Si and Ge atoms.
- It is found that the addition of dopant atoms has increased the average binding energy. C$_{12}$@Au$_{20}$ is highly stable with the highest binding energy.
- The HOMO–LUMO gap of M$_{12}$@Au$_{20}$ clsuter is much smaller, compared with that in the Au$_{32}$ cluster, suggesting that they should be relatively chemically reactive. This is also confirmed by looking at the PDOS plots.

We hope these results can inspire the experimentalist for further validation.

Bibliography

[1]   Y. Donga, M. Springborgb Eur. Phys. J. D 43, 15–18 (2007).

[2]   X. Gu, M. Ji, S. H. Wei, X. G. Gong, Phys. Rev. B 70, 205401 (2004).

[3]   Y. Gao, X. C. Zeng, J. Am. Chem. Soc. 127, 3698 (2005); P. Acioli, J. Jellinek, Phys. Rev. Lett. 89, 213402 (2002).

[4]   A. Lechtken, D. Schooss, J. R. Stairs, M. N. Blom, F. Furche, N. Morgner,O. Kostko, B. Von Issendorff, and M. M. Kappes, Angew. Chem. Int. Ed. 46, 2944 − 2948 (2007).

[5]   M. P. Johansson, D. Sundholm and J.Vaara Angew.Chem. Int. Ed. 43, 2678 (2004).

[6]   M. Ji, X. Gu, X. Li , X. G. Gong, J. Li and L. S. Wang , Angew. Chem. Int. Ed. 44, 7119 (2005).

[7]   M. J. Oila, A. M. P. Koskinen, ARKIVOC 15, 76 (2006)

[8]   H. S. De, S. Krishnamurty, S. Pal, Catalysis Today 198, 106− 109(2012).

[9]   Q. M. Deng , L. X. Zhao , X. J. Feng , M. Zhang , W. L. Zhang, B. Fang, Y. H. Luo, Comp. and Th. Chem. 976, 183–187 (2011).

[10]   V. Kumar, Phys. Rev. B 79, 085423 (2009).

[11]   Z. Meng, F. X. Juan, Z. L. Xia, Z. H. Yu, L. Y. Hua, Chin. Phys. B, 21, 5, 056102 (2012).

[12]   J. M.Soler, E. Artacho, J. D. Gale, A. Garcia, J. Junquera, P. Ordejon, D. Sanchez-Portal, J. Phys. Condens. Matter 14, 2745 (2002).

[13]   G. P. Robert, Y. Weitao, Density-Functional Theory of atoms and Molecules, Oxford University Press NewYork (1989).

[14]   Perdew, Burke, Ernzerhof , Phys. Rev. Lett. 77, 3865 (1996).

[15]   F. Naumkin, Phys. Chem. Chem. Phys. 8, 2539–2545, 2539 (2006).

Chapter 6

6. The Structural and Electronic Properties of Doped Tubular Gold Cages

6.1 Introduction

In the last chapter we have studied medium sized gold clusters . Just like small sized gold clusters the medium gold clusters also have size dependent geometries. Recent studies have found that Au_{18}, Au_{32}, Au_{50} and Au_{72} clusters are icosahedron based cages exhibiting high thermodynamic stabilities [1-4]. Although the gold cage is still one of the focuses of attention, gold nanotubes and nanowires [5-9] have also attracted much interest in recent years. A joint theoretical and experimental study conducted by Bulusu et al. [10] of low-lying structures and structural transitions of gold cluster anions Au^-_n in the size range of n= 21-25 suggests that the ground state are the pyramid-based structures for n = 21-23 and at n = 24, the hollow-tubular structures dominate the low-lying isomers while structural transition from hollow tubular to core/shell compact structure is observed at n= 25. Other theoretical studies also suggest the possible existence of highly symmetric hollow-cage structures Au_{32}, Au_{42}, and Au_{50} as well as hollow-tubular structure Au_{26} [1, 2,11-13]. The possibility to form a hollow tubular Au_n cluster by closing ends of a SWGNT has opened the possibilities of new stable structures in competition with other possible structures, such as the amorphous, the bulk fragment, and the cage-like ones. The tubular structure of Au_{24} has been verified both theoretically and experimentally [14,15]. It is obvious that the tubular Au_{24} structure can accommodate guest atoms to form a new kind of endohedral tubular gold cluster.

It is known that coinage metals (Cu, Ag, Au) have many similarities in their bulk behavior and exhibit some differences at the stage of small clusters. In recent years, the transition bimetallic clusters, particularly of Au, Ag, and Cu, have received much attention because of their particular physical and chemical properties and potential technological applications in solid-state chemistry, materials science, nanotechnology, catalysis, biology, and medicine. [16-19]. A density functional study with relativistic effective core potential by Zhao et al. [20] indicate that the stability of copper-gold clusters is higher than that of bare gold clusters and then the bare gold clusters is more stable than the sliver-gold isomers.

Another similar study by Ghanty et al. [21] on the structural and electronic properties of $Au_{19}X$ clusters doped with Li, Na, K, Rb, Cs, Cu, and Ag suggests that the endohedrally doped $Au_{19}X$ clusters (X = Li, Na, and Cu) have higher binding energies comparable to those of the corresponding exohedrally doped clusters and the endohedrally doped cage-like structures of larger atoms (X = K, Rb, Cs, and Ag) are found to be less stable than the corresponding exohedral structures. Kanhere et al.studied the equilibrium geometries of Au^-_n and $Au_{n1-1}Cu^-$ (n=13-19) using Density Functional Theory (DFT). They have found that the introduction of copper atom has enhanced the binding energy per atom of gold cluster anions [22]. Haeck et al. [23] have studied Carbon monoxide adsorption on silver doped gold clusters and observed that inclusion of a single silver atom causes significant changes in the reactivity for a few cluster sizes. The structural and magnetic properties of the tubular Au_{24} doped with different 3d transition-metal atoms M (M = V, Cr, Mn, Fe, Co, and Ni) is studied by Yang et al. [24] using the scalar relativistic DFT calculations. It is found that all of the $M@Au_{24}$ clusters retain their tubular structure even when the dopant atom is located at the center of the Au_{24} cluster.

There are lot of studies on doping of gold clusters with Ag and Cu atoms but they limited to smaller size range. As we have already discussed the importance of Au_{24} tubular cage, we would like to introduce transition metals Cu and Ag as dopant and study their effect on structural and electronic properties of these gold tubular cages in details.

6.2 Computational Details

The computational method is same as explained in previous chapters. The core radii used for pseudopotential generation (in units of Å) for Cu are as follows: s (2.74), p (2.39), d (2.13), f (2.13); for Ag: s (2.46), p (2.65), d (2.46), f (2.46). The core radii for gold are the same as given in the previous chapter. The structures are optimized until the forces on atoms reduce down to 0.01eV/Å or less.

The calculated bond length from DFT for Au-Cu dimer is 2.37Å and for Au-Ag is 2.56Å, which is in good agreement with experimental value [25, 26].

6.3 Results and Discussion

6.3.1   Structure of M@Au$_{24}$ (M = Cu, Ag)

We have studied the effect of doping transition metals such as Cu and Ag in the 24 atom gold cluster. As discussed in the introduction, Au$_{24}$ is found to have an interesting tubular structure and is presently studied for modification of its structural and electronic properties by encapsulation of different dopants [14, 15, and 23].

We will consider two initial structures of Au$_{24}$ tube i.e., Au$_{24}$-I and Au$_{24}$-II, differing only in the relative orientation of their end-caps, with D$_{3d}$ and D$_{3h}$ symmetries respectively. These structures of Au$_{24}$ tubular gold are then optimized using DFT. The ground state structure of both Au$_{24}$-I and Au$_{24}$-II obtained after optimization are then used for doping. For the initial doped structure, we have placed two atoms of each transition-metal M (M = Cu, Ag) at the centre of Au$_{24}$-I and Au$_{24}$-II structures respectively. Then the respective structures are optimized without any geometric or symmetry constraint. The same optimization procedure is repeated by placing three atoms of Cu and Ag at the center of Au$_{24}$-I and Au$_{24}$-II structure respectively .The ground state structures of the Au$_{24}$ and M@Au$_{24}$ (M = Cu, Ag) after optimization are displayed in Fig. 6.1 and the various computed values such as binding energy per atom, HOMO-LUMO gap etc are presented in Table 6.1.

Au$_{24}$-II

Au$_{24}$-I

Ag$_2$Au$_{24}$-I	Cu$_2$Au$_{24}$-I	Ag$_2$Au$_{24}$-II	Cu$_2$Au$_{24}$-II
(a)	(b)	(c)	(d)

Ag₃Au₂₄-I	Cu₃Au₂₄-I	Ag₃Au₂₄-II	Cu₃Au₂₄-II
(e)	(f)	(g)	(h)
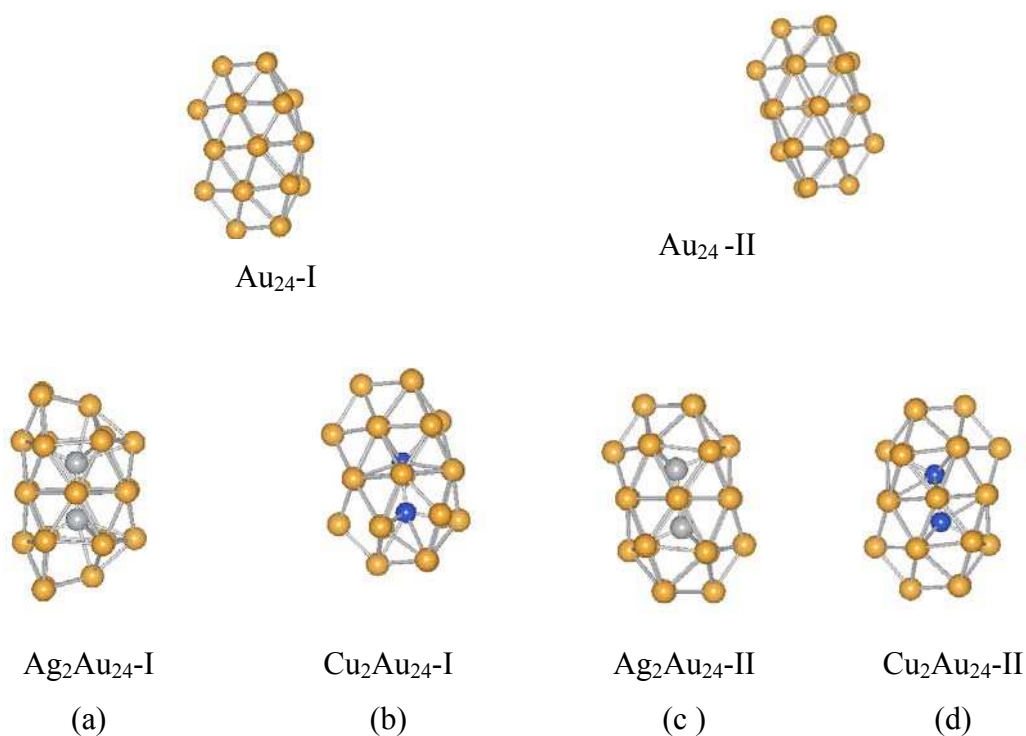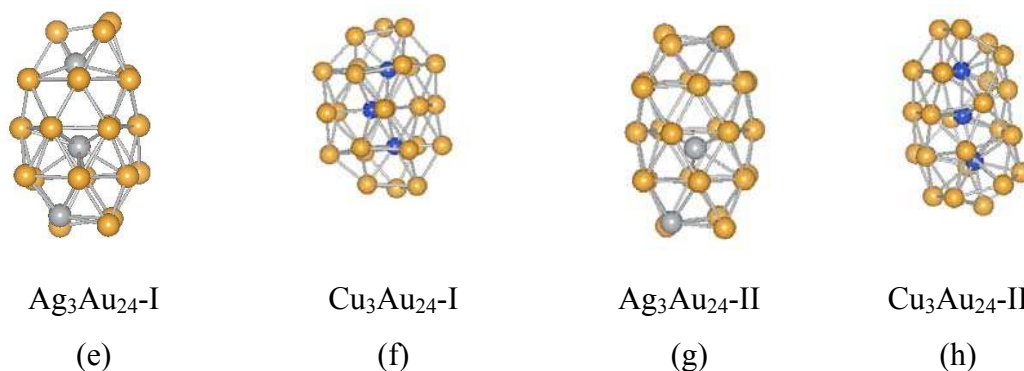
Figure 6.1 Au_{24}-I and Au_{24}-II represents the two different arrangement of Au_{24} cage and other represents the optimized geometries of M@ Au_{24} where M is Cu, Ag. The yellow ball represents Au atom, silver ball is Ag atom and blue ball represents Cu atom.

From the study of the optimized geometries in Fig.6.1 ((a) - (d)), it can be seen that the introduction of two impurity atoms (M = Cu, Ag) has not deformed the structure of Au_{24}-I and Au_{24}-II cage. The same observation can be made from the bond distance values of Au-Au atoms given in Table 6.1. The ranges of bond distances between Au-Au atoms in doped gold cages are almost same as the empty gold cages. It can also be seen that the bond distance of Ag-Ag atom is larger than that of Cu-Cu atom. The distance between the Cu atoms in both M@Au_{24}-I and M@Au_{24}-II structures is comparable with the interlayer distance Au-Au atoms. Hence it can be inferred that Cu atoms are more suitable for endohedral doping in the Au tubular cage.

To confirm this, we put an additional impurity atom (M= Ag, Cu) in our initial two atom impurity structures of M@Au_{24}-I and M@Au_{24}-II cages.

These structures are then optimized and are given in Fig. 6.1 ((e)-1(h)). As expected the bond distances between Ag –Ag atoms (Table 6.1) has become greater than the interlayer distance of Au-Au atoms. In both structures Ag_3Au_{24}-I and Ag_3Au_{24}-II the Ag atom has come out on the surface of the cages.

While in both Cu_3Au_{24}-I and Cu_3Au_{24}-II the copper atoms has stayed well within the cage. In terms of geometry the Cu_3Au_{24}-I has retained its tubular shape while the Cu_3Au_{24}-II cage is distorted. Thus we can conclude that copper atoms are better suited to be substituted as a backbone in gold tubular cage.

Table 6.1 Average Binding Energy per Atom (E_b), Average Distances of Dopants from the bonded Au atoms in the shell (R), HOMO-LUMO gap (E_g)

Cluster	E_b (eV)	R (Å)		Eg (eV)
		Au-Au (inter layer)	X-X (at centre)	
Au$_{24-I}$	**3.031**	**2.75-2.83**	---	**0.64**
Cu$_2$Au$_{24-I}$	3.142	2.75-2.83	2.48	0.38
Cu$_3$Au$_{24-I}$	3.17	2.75-2.83	2.56	0.35
Ag$_2$Au$_{24-I}$	3.048	2.77-2.91	2.77	0.31
Ag$_3$Au$_{24-I}$	3.039	2.77-2.88	3.55-4.03	0.13
Au$_{24-II}$	**3.045**	**2.73-2.84**	---	**0.97**
Cu$_2$Au$_{24-II}$	3.109	2.77-2.88	2.40	0.09
Cu$_3$Au$_{24-II}$	3.156	2.73-2.91	2.59-2.64	0.35
Ag$_2$Au$_{24-II}$	3.044	2.75-2.97	2.81	0.12
Ag$_3$Au$_{24-II}$	3.047	2.75-2.83	3.97-5.49	0.25

6.3.2 Energetics

In order to compare the relative stabilities of the doped tubular M@Au$_{24}$ (M= Cu, Ag) cages, we compare their average binding energies (BEs) with that of the pure Au$_{24}$ cages and present the results in Fig. 6.2. The computed values of Binding energy per atom are given in Table 6.1. The Binding energy is computed using equation (6.1),

$$E_b = (N E_M + 24 E_{Au}) - E_{M@Au_{24}} \qquad (6.1)$$

where E_M and E_{Au} are the energies of single M (M= Cu , Ag) atom and Au atom, respectively, while E $_{(M@Au24)}$ is the energy of the M@Au$_{24}$ cluster. N is the number of impurity atom doped in Au$_{24}$ cage.

From the binding energy values given in the Table 6.1 and the Fig. 6.2, it is seen that the empty Au$_{24}$ -II has higher binding energy than Au$_{24}$-I. After doping the Au$_{24}$-I and Au$_{24}$-II cages with impurities Cu and Ag, it is observed that their binding energy per atom has increased. It can also be seen addition of Ag atoms has not much changed the binding energy of Au$_{24}$-I and Au$_{24}$-II cage. On the other hand the addition of Cu atoms has increased the binding energy of Au$_{24}$-I and Au$_{24}$-II cage substantially.
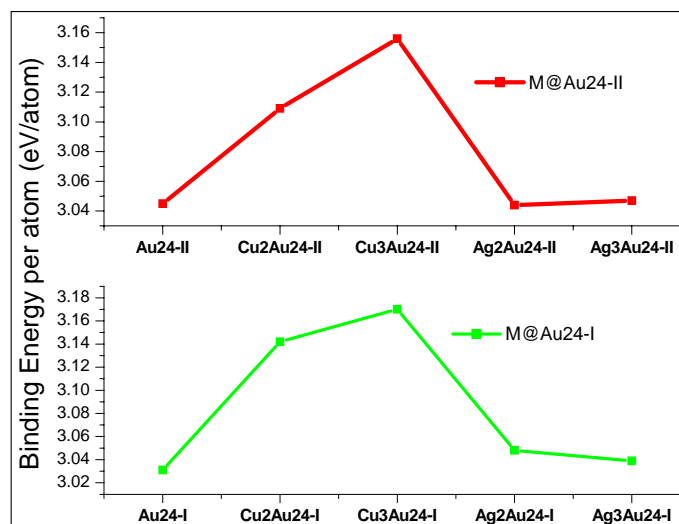
Figure 6.2 The average binding energy of the ground-state of M@Au$_{24}$-I and M@Au$_{24}$-II (M = Cu, Ag)

Thus Cu doped gold cages have higher binding energy than silver doped gold cages. This observation is in agreement with other reported studies [20]. From the graph we can conclude that Cu$_3$Au$_{24-I}$ has the highest binding energy per atom among all the optimized geometries.

6.4 Electronic Properties

6.4.1 HOMO-LUMO gap

A large HOMO-LUMO gap (E_g) corresponds to a high strength required to perturb the electronic structure; namely, a bigger gap indicates a weaker chemical reactivity and higher stability. From Table 6.1 and Fig. 6.3, we observe that Au$_{24}$-II has the large HOMO-LUMO gap of 0.97 eV and also have high binding energy per atom value. It indicates that Au$_{24}$-II has highest stability among all the structures. It is observed that the E_g of all the doped cages M@Au$_{24}$ (M= Cu, Ag) is smaller than the gap of pure Au$_{24}$ cages suggesting that they should be relatively chemically reactive. In general, the Cu doped Au$_{24}$ cages found to have higher energy gap than the Ag doped gold cages except for Cu$_2$Au$_{24-II}$. Thus, Cu doped gold tubular cages have higher stability.

The reduced band gap of M@Au$_{24}$ cages can have interesting possibilities that may serve as a dynamical system in catalysis and nano structured material science
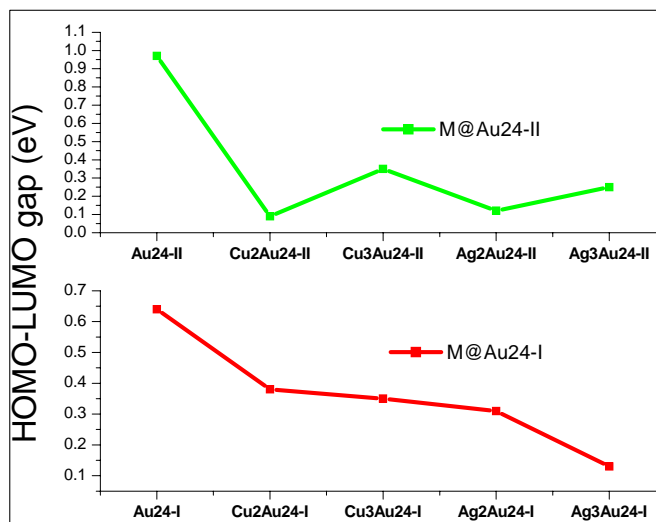
Figure 6.3 The HOMO-LUMO gap of M@Au$_{24}$-I and M@Au$_{24}$-II (M= Cu, Ag)

6.4.2 Mulliken populations (MP)

The MP analysis was performed on the M@Au$_{24}$-I and M@Au$_{24}$-II (M= Cu, Ag) isomers. The MP value of the Cu atoms for all isomers is approximately -0.1 e, which means that the Au atoms act as electron donor in all M@Au$_{24}$-I and M@Au$_{24}$-II (M= Cu) isomers.

The Ag atoms found to act as electron donor in Ag$_2$@Au$_{24}$-I and Ag$_2$@Au$_{24}$-II while in Ag$_3$@Au$_{24}$-I and Ag$_3$@Au$_{24}$-II; it has also become an electron acceptor. The order of magnitude of charge transferred (donor or acceptor) in Ag atoms is about 0.01e - 0.2e. The important factor influencing the charge distribution in the M@Au$_{24}$-I and M@Au$_{24}$-II (M= Cu, Ag) clusters can be the geometric structure of cluster and its symmetry. We also find that 9.93-9.95 electrons in 3d subshell of Cu atoms and 9.73-9.98 electrons occupy the 4d subshell of Ag atoms in M@Au$_{24}$-I and M@Au$_{24}$-II (M= Cu, Ag) isomers. The values reveal that the d obitals of M atoms in M@Au$_{24}$-I and M@Au$_{24}$-II clusters are dominant core orbitals participating in bonding.

6.5 Conclusion

We have studied the effect on the structural stability and electronic properties by doping transition metal such as Cu and Ag in the Au$_{24}$ tubular cage using DFT.

- From the study of binding energy values we find Au$_{24}$-II and Cu$_3$Au$_{24}$-I has the highest binding energy per atom among all the optimized isomers of M@Au$_{24}$-I and M@Au$_{24}$-II (M= Cu, Ag).

- The HOMO-LUMO gap is found to be highest for Au$_{24}$-II cluster. In general,

the Cu doped Au$_{24}$ tubular cages found to have higher energy gap than the Ag doped cages except for Cu$_2$Au$_{24\text{-}II}$.

- On the basis of the calculated Mulliken populations, reveals that the d obitals of M (Cu, Ag) atoms in M@Au$_{24}$-I and M@Au$_{24}$-II clusters are dominant core orbital participating in bonding.

- At the end we can conclude that the Cu doped gold cages are more stable than Ag doped.

Bibliography

[1]   M. P.Johansson, D.Sundholm, J. Vaara, Angew.Chem.Int.Ed. 43, 2678 (2004).

[2]   X. Gu, M. Ji, S. H. Wei, X. G. Gong, Phys. Rev. B 70, 205401 (2004).

[3]   D. Tian, J. Zhao, B. Wang, R. B. King, J. Phys. Chem. A 111, 411 (2007).

[4]   A. J. Karttumen, M. Linnolahti, T. A. Pakkanen, P. Pyykko, Chem.Comm. 465 (2008).

[5]   Y. Kondo, K. Takayanag, Science 289, 606 (2000).

[6]   E. Tosatti, S. Prestipino, Science, 289, 561 (2000).

[7]   Y. Oshima, A. Onga, K.Takayanagi, Phys. Rev. Lett. 91, 205503 (2003).

[8]   R.T.Senger, S. Dag, S. Ciraci, Phys. Rev. Lett. 93, 196807 (2004).

[9]   W. Fa, J. M. Dong, J. Chem. Phys. 124, 114310 (2006).

[10]   S. Bulusu, X. Li, L. S. Wang, X. C. Zeng, J. Phys. Chem. C 111, 4190- 4198. (2007).

[11]   B. Soule de Bas, M. J. Ford, M. B. Cortie, J. Mol. Struct. (TheoChem) 686, 193 (2004).

[12]   J. Wang , J. Jellinek, J. Zhao, Z. Chen, R. B. King, P. V. R. Schleyer, J. Phys. Chem A 109, 9265 (2005).

[13]   E. M. Fernandez, J. M. Soler, L. C. Balbas, Phys. ReV. B. 73, 235433 (2006).

[14]   X. P. Xing, B. Yoon, U. Landman and J. H. Parks, Phys. ReV. B 74, 165423 (2006).

[15]   S. Bulusu, L. Li, L. S.Wang and X. C. Zeng,   J. Phys. Chem. C 111, 190(2007).

[16]   R. Pal, L. M. Wang, W. Huang, X. C. Zeng, J. Am. Chem. Soc. 131, 3396 (2009).

[17]   Y. Zhao, Z. Y. Li, J. L. Yang, Phys. Chem. Chem. Phys. 11, 2329 (2009).

[18]   D. W. Yuan, Y. Wang, Z. Zeng, J. Chem. Phys. 122, 114310 (2005).

[19]   S. Zhao, Y. L. Ren, Y. L. Ren, J. J. Wang, W. P. Yin, J. Phys.Chem. A 114, 4917 (2010).

[20]   Y. R. Zhao, X. Y. Kuang, B. B. Zheng, Y. F. Li and S. J. Wang, J. Phys. Chem. A 115, 569–576 (2011).

[21]   T. K. Ghanty, A. Banerjee, A. Chakrabarti,   J .Phy. Chem. C 114, 20-27 (2010).

[22]   S. Zorriasatein , K. Joshi , D. G. Kanhere , J Chem Phys. 128, 18, 184314 (2008).

[23]   J. De Haeck , N. Veldeman , P. Claes , E. Janssens, M. Andersson , P. Lievens , J. Phys Chem A. 115, 11, 2103-9 (2011).

[24]   A. Yang, W. Fa and J. Dong, J. Phys. Chem. A 114, 4031–4035 (2010).

[25]   G. A. Bishea, J. C. Pinegar, M. D. Morse, J. Chem. Phys. 95, 5630 (1991).

[26]   J. Fabbi , J. D. Langenberg, Q. D. Morse, L. Karlsson, J. Chem. Phys. 115, 7543 (2001).

Chapter 7

7. Tubular Gold Clusters with Spinal Support

7.1 Introduction

In the Chapter 6 we have discussed 24 atom tubular cage like structure of gold with hexagonal cross-section. The existence of the hollow-tubular structures dominating at larger size range in the low-lying isomers for gold has already been pointed out in the last chapter [1-6]. This tubular structure can be extended along z axis to form a single wall gold nanotube (SWGNT). In our group, Veena et al. [7] have studied single wall gold nanotube of various cross sections using Gupta Potential and found that gold nanowires consisting of pentagonal layers are most stable among the structures studied.

The tubular structure of Au_{24} has been verified both theoretically and experimentally as discussed in the Chapter 1. The tubular Au_{24} structure can accommodate guest atoms to form a core–shell structure. Properties of such a core shell system differ from those of its all metal counterparts (empty or filled). A core–shell structure can also be exhibited by a system whose shell is unstable by itself but can be supported by the core. A large number of theoretical and experimental studies have been carried on hollow gold clusters endohedrally doped with various dopants. Some recent examples include a stable icosahedral cluster $W@Au_{12}$ which was confirmed experimentally [8, 9] and gold-encapsulated fullerenes [10]. Such mixed core doping has potential applications as catalyst [11, 12]. For catalytic applications, GNPs are usually first affixed on a support, such as one of various kinds of oxide (e.g., silica, titania, alumina), carbon nanotube, graphene sheet, etc. [13-16]. However, in suspensions GNPs are susceptible to aggregation. To prevent aggregation and increase stability of GNPs in suspension, researchers have utilized different stabilizing ligands such as alkanethiols and alkylamines [17]. The potential use of gold clusters in catalysis , opto-electronic applications etc requires further understanding of the effect of ligands and solvent on the structural and electronic properties and to compliment experimental and theoretical studies[18].

We have discussed in details in Chapter 4 that Si doped gold clusters can form a stable geometry. Hence it is of interest to study the interaction of Si atoms with Au_n clusters of various dimensionalities. In this chapter we place Si atoms as a backbone

in gold nanotube. Silicon has already been incooperated with gold atoms to form nanowires. For example, an Au–Si alloy is used for microchip packing and interconnection in microelectro-mechanical systems (MEMS).The Au–Si eutectic nanowires of diameter 60nm have been generated by Lin et al. successfully. The SEM and TEM images of the nanostructure of Au–Si eutectic nanowires show Si nanoparticles dispersed in the Au matrix [19].

Another element we are going to dope with gold cages is Aluminum. Although Al and Au are metals in their bulk form, the atomic states have large difference in their electro negativity values which are 2.54 and 1.61 for Au and Al respectively [20]. Therefore, it is expected that the interaction between Al and Au would involve significant charge transfer or, in other words, the chemical bonding will have more ionic than covalent character. Walter and Hakkinen show that endohedral doping of the Au_{16} cage by Al or Si yields a geometrically robust, tunable oxidation and reduction agent [21]. A study on the atomic and electronic structures of Au_5M clusters, where M atom represents elements of the second period, revealed that with the exception of S, impurities with p electrons (Al, Si, P) adopt non-planar geometries while those with s electrons (Na, Mg) prefer planar geometries [22, 23].

The possibility to form a hollow tubular Au_N cluster by closing the ends of a SWGNT has opened the possibilities of new stable structures in competition with other possible structures, such as the amorphous, the bulk fragment, and the cage-like ones. Though a lot of theoretical and experimental work has been carried out recently to study the interaction of Al or Si atoms with small gold clusters (n <16), very few studies are available which investigate the interaction Si or Al with gold clusters of larger size.

 In the present study, we have placed Al, Si and Au atoms as backbones to the Au_N tubular cages of different sizes and study their effect on the tubular structure and electronic properties. By this we wish to evaluate some of the important features:

(1) how these impurity atoms with different numbers of 3p valence electrons influence the ground-state properties of gold clusters; (2) how the geometrical structures and electronic properties of 3p atom doped Au_N clusters evolve with increasing cluster size and (3) comparing the changes brought about by Si and Al doping in Au_N clusters with those of all gold clusters (core + shell). The chapter is organized as follows. In Section 7.2 computational method is described. In Section 7.3 , the details of our work are displayed and discussed. Finally, a summary is given.

7.2 Computational Details

All calculations were performed using SIESTA and VASP codes based on the density functional theory (DFT). The details for SIESTA code are same as discussed earlier. The interaction to the (frozen) ion cores was described by scalar-relativistic non-local norm-conserving pseudopotentials using Au ($5d^{10}6s^1$), Al ($3s^23p^1$) and Si ($3s^23p^2$) valence electrons. The valence states were described using DZP (double-zeta + polarization) basis sets and a mesh cut off 250 Ry was used. A tetragonal supercell of size 20 Å X 20 Å X 50 Å has been used and the Brillouin zone integrations were carried out using only the gamma point. The self-consistent equations were solved with an iterative matrix diagonalization scheme. Geometry optimizations were performed with the conjugate gradient algorithm and the geometries were considered to be optimized when the forces were reduced upto 0.006eV/Å. In VASP code, we have used ultrasoft pseudopotentials and plane wave basis set with spin polarized Perdew–Wang generalized gradient approximation to calculate the exchange correlation [24,25]. While optimizing some of the structures using VASP, a quasi-Newtonian algorithm was used to relax the systems to their local minima.

Finally, the vibrational frequency calculation has been performed to validate the stability of $X_M Au_N$ (M= Si, Al and Au) clusters.

Test calculations were done for dimers of Au, AuSi and AuAl in order to verify the accuracy of our computational methodology.

In Table 7.1, we summarize the computed results along with the experimental values which clearly show that the computed values of bond lengths and binding energies (BE) are in fair agreement with experimental values.

Table 7.1 Computed and experimental Binding Energy per atom (BE) and Bond lengths of the dimer

System	Bondlength (Å)		B E per atom (eV/atom)	
	Comp	Exp	Comp	Exp
Au₂	2.53	2.47 [20]	1.22	1.16 [20]
AuSi	2.25	2.25 [26]	--	--
AuAl	2.37	2.34 [27,28]	1.95	1.67 [26,28]

7.3 Results and Discussions

7.3.1 Pure Au_N (N= 24, 42 and 60) cages

We have performed first-principle calculations within the supercell geometry using a tetragonal unit cell. The initial geometries of Au_N tubes (N= 24, 42, 60) are optimized using SIESTA code, and then the relaxed lowest energy geometries are further optimized using VASP code. The optimized   geometries of $X_M Au_N$ (N =24, 42, 60) tubular clusters are shown in Fig. 7.1

24 Au atoms + 3 X atoms	42 Au atoms + 6 X atoms	60 Au atoms + 9 X atoms
Au_{24}	Au_{42}	Au_{60}
$Au_{24}Si_3$	$Au_{42}Si_6$	$Au_{60}Si_9$
$Au_{24}Al_3$	$Au_{42}Al_6$	$Au_{60}Al_9$
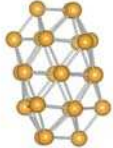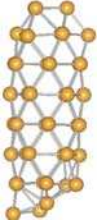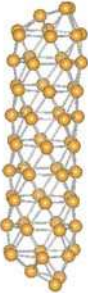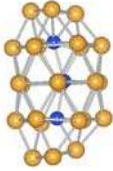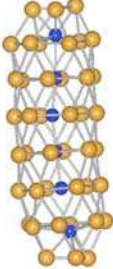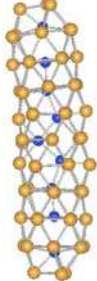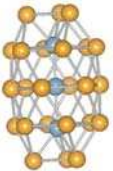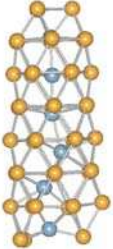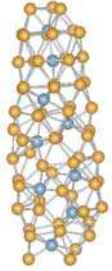
		Au₆₀Au₉
Au₂₄Au₃	Au₄₂Au₆	
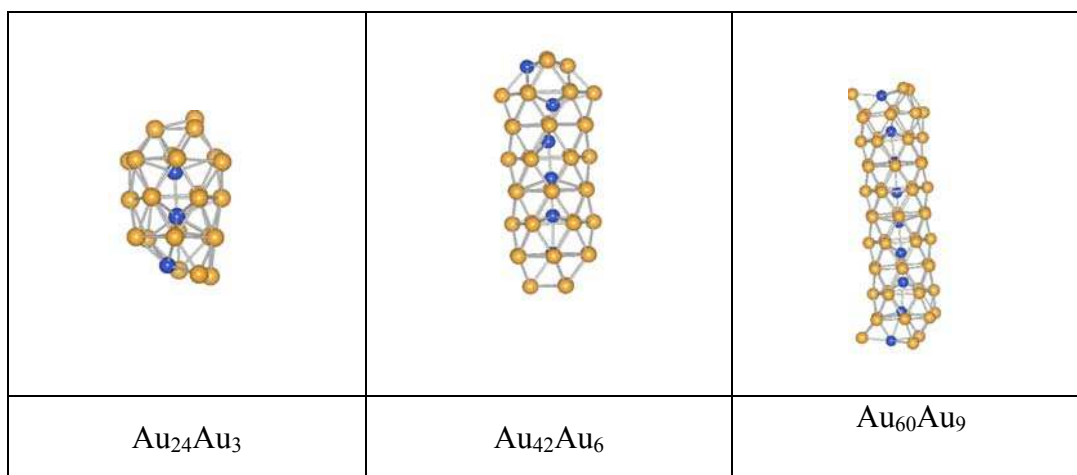
Figure 7.1 Lowest energy geometries of $X_M Au_N$ where X= Si, Al and Au, M=3, 6, 9 and N= 24, 42, 60. The outer tubular framework represents Au atoms and the ball along the central axis of tube represents X, the dopant atoms

The initial structure of Au_N (N=24, 42, 60) is composed of hexagonal rings repeated three, six, nine times respectively with two triangle caps on the two ends . It can be considered as a short segment of the (6, 0) SWGNT (single-wall gold nanotube) capped by two triangle caps at both ends, yielding a highly symmetric tube-like cage with D_{3d} symmetry. It has been found that the end capes remain triangular while the six atom hexagonal layer in contact with the tiangular capes gets distorted and become triangular. The results for Au_{24} agree well with previous studies as far as structure is concerned .The energy differs from that of Zhao et al.by 0.23 eV [29] .

The basic structure of Au_{24} tube can be extended to form larger tubular structures. The structure for Au_{42} and Au_{60} tubular cages are formed by repeating the hexagonal layers present between two triangular caps of Au_{24}. After optimization of initial structures of Au_{42} and Au_{60} tubular cage , it is seen that hexagonal layer in contact with a triangular cap get distorted. This distortion is very pronounced in case of Au_{24} and Au_{42} while in Au_{60} these layers remain hexagonal but somewhat distorted.

7.3.2 Doped Au_N cages ($X_M Au_N$, X = Si, Al and Au)

It has been shown in previous studies that Si and Al form exohedral structures when doped in Au_{16} and Au_{20} cages [30,31]. The endohedral doping of the Au_{16} cage by Al or Si studied by Walter et al.have shown that the ground state consist of the off-center doped clusters [21]. In our case, when we place Si and Al atom at two different positions namely on the surface and at the centre of Au_{24} tube, both Si and Al atom

prefer the exohedral position i.e, on the surface of Au_{24} cluster. The binding energy per atom of $SiAu_{24}$ cluster was found to be 2.549 eV/atom with Si atom on the surface and 2.527 eV/atom with Si atom at the centre; the difference in energy of two low lying configurations is being only 0.022 eV. Similarly for $AlAu_{24}$ cluster the Al atom on surface is the preferred position and the difference in energy of the two low lying configurations is also 0.022 eV. We then place three Si and Al atoms at the center axis of the Au_{24} tube and find that the binding energy per atom has increased.

For Si_3Au_{24} tubular cluster the BE has become 2.679 eV/atom while for Al_3Au_{24} it is 2.645eV/atom, suggesting the possibility of low lying state.

The above results have encouraged us to study the effect of the monatomic chain backbone of Al and Si atoms on the tubular structure of gold. These impurity atoms are from the same row of the periodic table and their principal quantum numbers remain the same while increasing the valence electrons. We have placed an Au, Al or Si atoms at the centre of each hexagonal layer of Au_N (N=24, 42, 60) tubular cluster and tried to see whether a long monatomic chain can be formed inside the Au_N tube. We will also investigate how these $3p$ atoms can influence the ground-state properties of Au_{24} tube.

The dopant atoms X_M (X = Au, Al, Si and M= 3, 6, 9) are placed as the central axis of the tubular Au_N (N= 24, 42, 60) structures respectively and geometry optimizations were performed without any geometric or symmetry constraint. The optimized stable structures of the X_MAu_N cluster are also displayed in Fig. 7.1 and Table 7.2 gives various structural and energetic characteristics of X_MAu_N clusters.

In the Au_{24} cage, the dopants X (X = Si, Al and Au) are placed initially at the center of each of the three hexagonal layers of the tubular Au_{24} structure and the geometry optimizations performed without any geometric or symmetry constraint. It is clearly seen that the ground-state of X_3Au_{24} (X= Si, Al) clusters still maintain the original D_{3d} structural symmetries. In the optimized structures, Si atoms shift sideways while Al atoms stay at the centre of the Au_{24} tube. The low lying geometry of Au_3Au_{24} shows larger distortion after minimization.

It is seen that the bond length between the Au backbone atoms is 2.88 Å which is larger than the interlayer separation in Au_{24} tubular i.e, 2.81 Å .This has caused the two Au atoms to remain inside the cage while the third Au atom has come out of the tubular and converted the triangular cap into a rhombus at one of the ends of the tube. We have optimized the Au_2Au_{24} tubular structure to see whether the two Au atoms

present at the centre remain inside . It is found the two Au atoms present within the Au$_{24}$ cage indeed remain at the center, with negligible distortion to the parent structure.

Table 7. 2 Average Binding Energy per Atom (E_b), Average Distances of Au-Au atoms (inter-layer) and X-X (X=Al, Si, Au) present at the centre(R) and HOMO-LUMO gap (E$_g$), Energy of HOMO level

Cluster	E_b (eV)	R (A^o)		Eg (eV)	Energy of HOMO level
		Au-Au (inter layer)	X-X (at centre)		
Au$_{24}$	2.437	2.77	----	0.97	-4.60
Si$_3$Au$_{24}$	2.679	2.79	Si-Si = 2.58	0.27	-3.86
Al$_3$Au$_{24}$	2.646	2.81	Al-Al = 2.66	0.67	-4.07
Au$_3$Au$_{24}$	2.43	2.80	Au-Au= 2.81	0.07	-4.18
Au$_{42}$	2.529	2.73	----	0.24	-4.74
Si$_6$Au$_{42}$	2.799	2.81-2.90	Si-Si=2.52 -2.92	0.24	-3.84
Al$_6$Au$_{42}$	2.739	2.79-2.86	Al-Al = 2.79 - 2.87	0.26	-4.03
Au$_6$Au$_{42}$	2.529	2.72-2.80	Au-Au = 2.72-2.76	0.19	-4.27
Au$_{60}$	2.579	2.76	----	0.27	-4.45
Si$_9$Au$_{60}$	2.858	2.81-2.85	Si - Si = 2.50-2.60	0.33	-4.11
Al$_9$Au$_{60}$	2.812	2.76-2.86	Al-Al = 3.61-4.71	0.13	-4.14
Au$_9$Au$_{60}$	2.567	2.77-2.83	Au-Au = 2.76-2.89	0.12	-4.29

The doped Au$_{42}$ structure is initiated by placing the dopant atom at the centre of each of the six hexagonal layers. After the geometry optimizations were performed, it was found that the dopant atoms have not distorted the tube like structure of Au$_{42}$ and still form a linear chain at the centre of tube. In the Au doped Au$_{48}$ cluster it is found that similar to the case of Au$_3$Au$_{24}$, one of the gold atoms lying at the central axis has come out to form a rhombus at one end of the tube while rest of the Au atoms form a chain. Interestingly, as Fig. 7.1 shows the Si and Al atoms lying near one end of the Au$_{42}$ tube, has broken off from the rest of the chain. The reason can be assigned to the size mismatch between Si-Si atoms, Al-Al atoms and the interlayer distance between

the Au atoms layers. Since the size mismatch is more pronounced in case of Al –Al atoms, it can be concluded that Si is more compatible as a backbone to Au_N cages.

The doped Au_{60} tube is generated when each dopant atom is placed at the centre of each of the nine hexagonal layers. The resultant geometry is then optimized. The Au_9Au_{60} is found to have similar distortions as Au_3Au_{24} and Au_6Au_{42}. Fig. 7.1 shows that, Au_{60} cage having Si and Au atoms as a backbone has tube like geometry. The Al doped Au_{60} tube is completely deformed due to size mismatch as discussed above and most of the Al-Al bonds are broken. It is also seen that Al atoms are occupying position where they can have maximum coordination number i.e, 7 with Au atoms. However in Si doped Au_{60} cage the size matching between Si-Si atoms and Au layers seems to be more compatible. Therefore the structure is still symmetric with a slightly zigzag backbone.

From these simulations it is apparent that in order to provide a stable backbone, size matching is a requirement. So Si-Si distance which is slightly larger than gold interlayer distance will form a good backbone if it has some breaks instead of being a continuous chain.

With this view we incorporated in our calculations Si_8Au_{60} which has one missing atom compared with presented above. The new structure is shown in Fig. 7.2. It is indeed found true that these chains are absolutely straight and not bent as the backboned Si_9Au_{60} in Fig. 7.1.
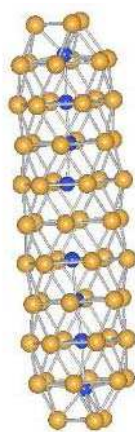
Figure 7.2 The lowest energy geometry of Si_8Au_{60}. The outer tubular framework represents Au atoms and the balls along the central axis of tube represent Si atoms.

7.3.3 Energetics

In order to investigate the stabilities of the doped tubular X_MAu_N clusters, we have compared their average BE with that of the pure Au_N .The obtained results are

presented in Table 7. 2 and Fig. 7.3. The BE is calculated using,

$$E_b = (M E_X + N E_{Au}) - E_{XMAuN} \qquad (7.1)$$

where E_X and E_{Au} are the energies of single X and Au atoms, respectively, while E_{XMAuN} is the energy of the $X_M Au_N$.
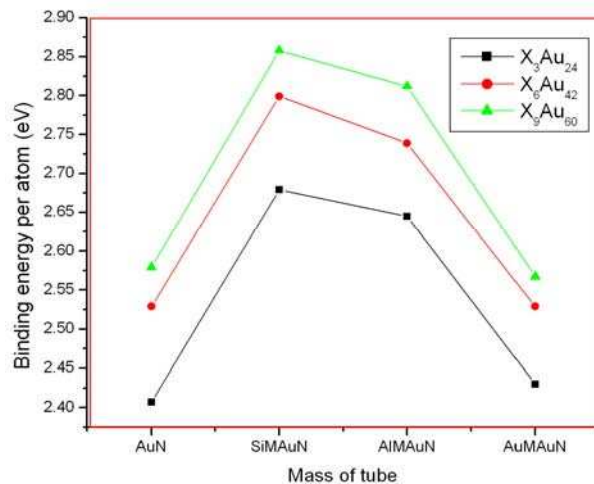
Figure 7.3 The average binding energy ($\overline{E_b}$) of the ground-state $X_M Au_N$ (X= Al, Si and Au, M=3, 6, 9 and N= 24, 42, and 60) tube like structures

It can be seen from Table 7.2 that for all the structures, average binding energy for the doped Au_{24} clusters is larger than that of the ground state pure Au_{24} cluster with D_{3d} symmetry. Therefore, the introduction of dopant atom has enhanced the thermodynamic stability of the tubular Au_{24} cluster. The structure doped with Si and Al atoms have higher binding energy in comparison with Au doped Au_{24} structure. It is found that Au_{24} doped with Si atom is most stable in comparison with Al and Au doped Au_{24} tube.The average binding energy of Au_{42} and Au_{60} is found to be higher than Au_{24} tube by 0.092 eV and 0.142 eV respectively. It indicates that Au_{42} and Au_{60} clusters are thermodynamically more stable than Au_{24} tubular cage.

It is clear from the Fig.7.3, that out of the $Al_6 Au_{42}$ and $Si_6 Au_{42}$, the Si doped Au_{42} cage is the most stable. Similar conclusions can be made about $X_9 Au_{60}$ (X = Si , Al) tubular cage . It is also observed that the presence of Au atoms as backbone has not changed the binding energy of the Au_{42} structure while in case of Au_{60} tube it has lowered the binding energy , making it less stable than pure Au_{60} tube.

From the binding energy graph, it can be concluded that the Si and Al doped Au_N (N= 24, 42, 60) tubes are more stable than Au atom doped Au_N tube for all the structures.

7.4 Electronic Properties

The calculated HOMO-LUMO energy gap (Eg) values of the ground-state geometeries of X_MAu_N clusters are presented in Table 7.2.

7.4.1 HOMO –LUMO Gap

The HOMO-LUMO gap of tubular Au_{24} is found to be 0.97eV, suggests that it is chemically inert and relatively stable. Our result for HOMO-LUMO gap of tubular Au_{24} is in close agreement with Zhao et al.[29]. It can be seen from the PDOS plot in Fig. 7.4 and Table 7. 2 that the dopants have decreased the band gap of pure Au_{24} making it chemically reactive. In Fig. 7.4 (a), it can be clearly seen that a band gap exists at Fermi level for the Au_{24} tube. Similarly the doping of Si inside the Au_{24} tube has increased the electron density around fermi level and reduced the HOMO-LUMO gap of tube to 0.27eV; therefore conductivity of bare tube has been improved.
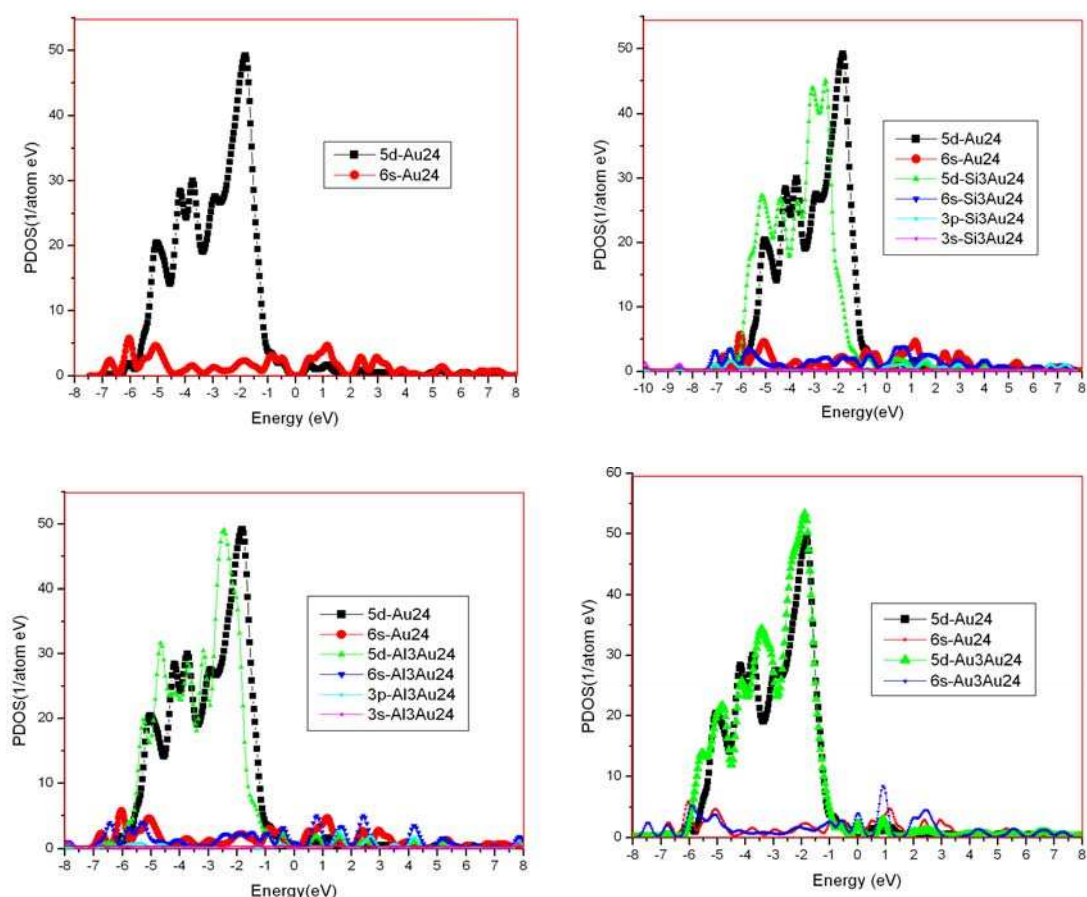
Figure 7. 4 Partial density of states for (a) Au_{24} tube (b) Si_3Au_{24} (c) Al_3Au_{24} and (d) Au_3Au_{24}, clusters with their lowest-energy configurations representing s,d states of Au_{24} tube and comparison of the s, d states of Au_{24} tube after doping with the s and p states of dopant Al and Si. Fermi level is set at zero on the energy axis.

This observation is further strengthened by plot of density of the states. In PDOS plot Fig. 7. 4 (b), there is a clear shift of d-energy levels to deeper energy levels on silicon doping. It can also be seen from Table 7.2, the HOMO level of Au_{24} tube on doping with Si shifts from -4.60eV to -3.86eV. In Fig. 7.4 (d), PDOS of Au_3Au_{24} tube is plotted. The placing of Au atoms within Au_{24} has increased the electron density at Fermi level reducing the band gap to 0.07eV but has not produced any significant shift in the d-orbitals towards lower energy.Thus it can be concluded that Si doping enhances the conductivity and stability of the Au_{24} tube. Similar observations can be made for the Al doped Au_{24} tube. However the effect of Al doping on the shifting of d orbitals of Au_{24} tube and in reducing the HOMO-LUMO gap is less in comparison with Si.

For higher Au_N tubes, the similar trend can be observed. Table 7.2 shows, that the HOMO energy levels of the Al_MAu_N and Si_MAu_N (where M=6, 9 and N= 42, 60) clusters are shifted upwards (less −*ve*) with respect to that of pure Au_N spectrum.

7.4.2 Mulliken Charge Analysis

The Mulliken Charge analysis of silicon doped Au_{24} shows systematic charge transfer from the ends of the tube towards the centre. No such trend is followed by Al atoms doped within Au_N tubular cage. In general the effect of Si doping is more pronounced than Al and Au atoms within Au_N tube.

7.5 Conclusion

In summary, we have made relativistic DFT studies on the stability and electronic properties of the tubular X_MAu_N (X= Si, Al and Au, M=3, 6, 9 and N= 24, 42, 60) clusters. It was found that the encapsulations of Si and Al atoms do not destroy the tubular frameworks of the gold host though they change the energy hierarchy of the pure AuN isomers, showing a high possibility to form a novel binary cluster with gold providing tubular structures.

- The ground states of Al_3Au_{24} and Si_3Au_{24} still possess the D_{3d} structural symmetry of the host tubular Au_{24}, but Au_3Au_{24} have the lower symmetries of C_1 and C_{2V}, respectively, because Au atoms have induced the structural distortions.
- As the size of the Au_N tube increases, the tubular structure of Au_N is retained in presence of Si and Au atoms while it get distorted due to Al atoms.

- The Si and Al atoms can form long chains within Au nanotube if a gap is given after every 4-6 layers of Au atoms to accommodate the size mismatch between Si-Si, Al-Al and Au layers. The Si doping within Au_N tube is more compatible than the Al doping.

- The PDOS of the tubular Au_N tube has been significantly changed by the dopant atoms. The dopant atoms have increased the electron density around fermi level and shifted the d-energy levels to deeper energy levels thus reducing the HOMO-LUMO gap of Au_N tube. The effect is more pronounced in Si doped Au_N than Al and Au atoms doped Au_N tube.

Bibliography

[1]   S. Bulusu, X. Li, L.S.Wang, X. C. Zeng, J. Phys. Chem. C 111, 4190- 4198 (2007).

[2]   X. Gu, M. Ji, S.H. Wei, X.G. Gong Phys. Rev. B 70,   205401 (2004).

[3]   D. Tian, J. Zhao, B. Wang, R.B. King, J. Phys. Chem. A 111, 411(2007).

[4]   B.Soule de Bas, , Ford, M. J., Cortie, M. B. J. Mol. Struct. (THEOCHEM) 686, 193 (2004).

[5]   J. Wang , J. Jellinek, J. Zhao, Z. Chen, R. B. King, P. V. R. Schleyer, J. Phys. Chem A 109, 9265 (2005).

[6]   E. M. Fernandez, J. M. Soler, L.C. Balbas , Phys. Rev. B, 73, 235433(2006).

[7]   V. Verma, K. Dharamvir, J. Nano Research 4, 65- 77 (2008).

[8]   (a) P. Pyykko,N. Runeberg, Angew. Chem. 114, 2278 (2002) (b) P. Pyykko, N. Runeberg, Angew. Chem., Int. Ed., 41,   2174 (2002).

[9]   X. Li, B. Kiran, J. Li, H. J. Zhai, L. S. Wang, Angew. Chem. Int. Ed., 41, 4786 (2002).

[10]   R. J. C. Batista, M. S. C. Mazzoni, L.O. Ladeira, H. Chacham, Phys. Rev. B 72, 085447 (2005).

[11]   M. C. Daniel, D. Astruct, Chem. Rev. 104, 293 (2004).

[12]   Chem. Soc. Rev. 37 , 9 (2008).

[13]   W. H. Fang, J. S. Chen, Q. H. Zhang , Deng, W. P. Y. Wang ,Chem. Eur. J. 17, 1247 (2011).

[14]   Y. C. Chang, Chen , D. H. Hazard, J. Mater. 165, 664 (2009).

[15]   X. Chen, D. Y. Zhao ,Y. L An , Y. Zhang , J. Cheng, B.L. Wang , L.Q. Shi, J. Colloid Interface Sci., 322, 414 (2008).

[16]   H. K. He, C. Gao, Sci. China-Chem., 54 , 397 (2011).

[17]   G. Zaupa, C. Mora , R. Bonomi, L. J. Prins , P. Scrimin, Chem. Eur. J., 17,4879 (2011).

[18]   S. Goel, K. A. Velizhanin, A. Piryatinski, S. A.Ivanov,S. Tretiak, J. Phys. Chem. C 116, 3242−3249 (2012).

[19]   J. S. Lin, C.C. Chen, E. W.G Diau, T. F. Liu, J. Mat. Proc. Tech. 206 , 425– 430 (2008).

[20]   R.C. Weast, CRC Handbook of Chemistry and Physics, CRC,Cleveland 49th ed. (1969).

[21]   M. Walter, H. Hakkinen, Phys. Chem. Chem. Phys. 8, 5407–5411(2006).

[22]   C. Majumder, A. K. Kandalam, P. Jena, P. Phys. Rev. B 74, 20543 (2006).

[23]   C. Majumder, S. K. Kulshreshtha Phys. Rev. B 73, 155427 (2006).

[24]   (a) G. Kresse, J. Hafner, Phys. Rev. B 47, 558 (1993); (b)G. Kresse, Furthmuller, J. Phys. Rev. B 54, 11169 (1996).

[25] P. Perdew, Electronic Structure of Solids '91, edited by P. Ziesche and H. Eschrig Akademie, Berlin (1991).

[26] J. J. Scherer, J. B. Paul, C. P. Collier, A. O'Keeffe, R. J. Saykally, J Chem.Phys. 103, 9187 (1995).

[27] K. P. Huber, G. Herzberg, Constants of Diatomic Molecules, van Nostrand Reinhold , New York (1979).

[28] K. A. Gingerich, G. D. Blue, J. Chem. Phys. 59, 185 (1973).

[29] D. X. Tian, J. J. Zhao, J. Phys. Chem. A 112, 3141 (2008).

[30] Q. Sun, Q. Wang, G. Chen, P. Jena, J. Chem. Phy. 127, 214706 (2007).

[31] R. Chinagandham, C. Majumder, J. Chem. Phy. 130, 234309 (2009).

Chapter-8

8. Gold Monoatomic Chains

8.1 Introduction

Nanoscale materials have peculiar properties different from crystalline structures due to the quantum confinement of electrons. Among the nanostructured materials, nanowires have emerged as one of the important structural components in future nanomaterials, mainly due to their high strength and ductility as compared to bulk materials. Metal nanowires display interesting quantum behavior, quantization of conductance, even at room temperature due to large energy level separation of the transport channels unlike in semiconductors. To simulate these structures a series of wire geometries are studied containing different number of atoms and under varying stretching conditions. The formation of these atomic wires has been supported by many theoretical and experimental calculations [1-4]

Among the metals, Gold nanowires (GNW) exhibit very interesting properties such as quantized conductance and the ability of evolution into linear gold chains which display large Au-Au interatomic distances before breaking as well as great potential in applied fields such as nanoelectronic [5-8].

The evolution, formation, and breaking of atomically thin gold nanowires with diameters of a few atoms, is another important aspect of theoretical and experimental studies. In the case of gold nanowires large interatomic distances for one atom thick nanowires have been reported by various experimental groups. Ohnishi et al. [9] using transmission electron microscopy (TEM) technique reported results of Au−Au distances in the range of 3.5 to 4.0Å for gold chain. Yanson et al. using a mechanically controllable break junction (MCBJ) on a scanning tunneling microscope (STM), reported distances for Au −Au of 3.6Å inferred from histograms of chain lengths and have recently re-analyzed those results and argued that a precise calibration gives Au−Au distances of 2.6 ± 0.2Å [6, 10].

The simulation methods, ranging from effective potentials to tight binding based, up to ab initio electronic structure, have helped to aid the understanding of experiments as well as stimulate new experiments, since these techniques have the predictive power.

The tight-binding molecular dynamics method are much faster than first principles methods but this gain in speed comes with the cost of loosing some of the flexibility of fully ab initio methods.

Novaes et al. [11] have used a density functional theory (DFT)-based tight binding molecular dynamics method (TBMD), to study the formation and breaking of Au nanowires under tension. Their calculations have shown how defects induce the formation of one-atom chains. They have obtained five atoms long chains, before breaking. Similar method had been used by Silva et al. [12] to simulate the formation, evolution and breaking of very thin Au nanowires and the effect of impurities on its properties.

The mechanical response of nanoscale structures is known to be different than that of their macroscopic analogs and surface effects in these high-surface-to-volume devices are important [13]. Young's modulus has a direct relevance to the function of nanoscale devices as it forms the basis of variety of mechanical properties. Diao et al. [14], investigated elastic properties of gold nanowires aligned in the ‹1 0 0› and ‹1 1 1› crystallographic directions using atomistic simulations and have shown the Young's modulus increases with a decrease of cross-sectional area in the nanowires. In an experimental study using an atomic force microscope by Wu et al. it is shown that in Au nanowires, Young's modulus is independent of its diameter [15].

In this Chapter, we will study finite monoatomic gold chains. It has been demonstrated by De Maria and Springborg [16] that finite chains were very similar to infinite chains and the general picture does not change. We will investigate the tensile strength of short monatomic (finite) gold chains of five and seven atoms using DFT and will compare the results of similar calculations done with Gupta potential [17]. The organization of the chapter is as follows. The computational details are given in Section 8.2, results and discussions are presented in Section 8.3 and conclusion in Section 8.4.

8.2 Computational Details

The details of the computational method have already been discussed in previous chapters. In brief, we have used the SIESTA code, based on Density Functional theory method. The electron density functional is treated by the generalized gradient approximation (GGA) .We have used relativistic pseudo potential for gold. The

reciprocal space integrations are carried out at the gamma point. The clusters are optimized inside simulation cell of 15 Å and energy cutoff of 200 Ry.

The results of the test calculations on Gold dimer have already been discussed in the earlier chapters.

8.3   Results and Discussions

In our preliminary work on gold monoatomic chains, we have considered two linear finite chains of gold with different number of atoms i.e., five and seven and studied their structures, energy variations, force and modulus. After the relaxation of linear chain of gold atoms, the minimum energy configuration is found to be a zig-zag chain. The relative stability of zigzag chain has been explained by giving the comparison between the band structure of the linear chain and zigzag chain. In the linear chain, the overlap between the filled d states broadens the d bands until they reach the Fermi level, destabilizing the wire with their associated high density of states. For a given wire length, the zigzag configuration allows a larger bond distance bringing back the d bands below the Fermi level [18]. The zigzag structure is confirmed in the work of Ref. [19]

These zig - zag monatomic chains of gold containing 5 and 7 atoms are then stretched between two fixed end atoms. We displace all the atoms according to a uniform strain along x direction, by fixing the atoms at ends of the nanowires, and then relax the nanowires to obtain the equilibrium configurations of nanowires at the given strain. It is found as the longitudinal strain on the chains is increased the zig-zag chain straightens at a particular length and ultimately disintegrates via an interesting dimer or trimer phase on further increase in strain.

The optimized geometries at various stages of stretching of 5 and 7 atoms gold chains are shown in Fig. 8.1

Five atom gold chain	Seven atom gold chain
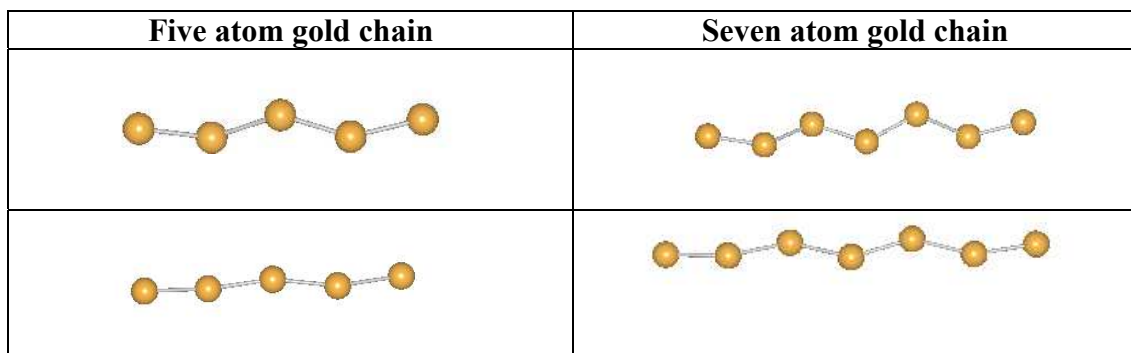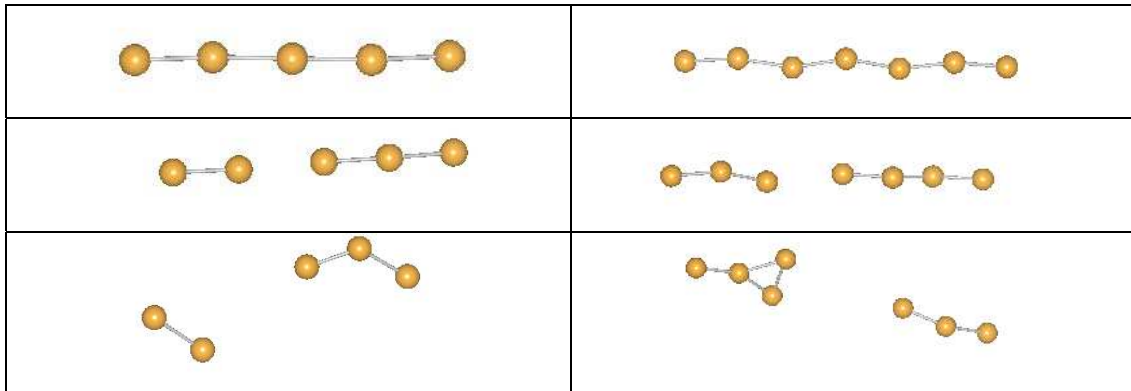
Figure 8.1 Various stages of stretching for pure monatomic Au chain containing 5 and 7 atoms.

8.3.1 Energy vs Length of chain

The variation in total energy (U) of the chain with the increase in total length of the chain for five and seven gold atoms is plotted in Fig. 8.2. The plot shows the comparison of results with the similar calculations done through Gupta Potential (GP) [17].

It can be seen in Fig. 8.2, the total energy is a monotonic function of chain length. From the DFT calculations, the potential energy curve shows the expected minimum while in GP results a plateau is seen where crossover from zig-zag to straight character takes place. In DFT calculations, the minimum in the energy is quite evident for five atoms gold chain than in seven atoms chain. At minimum (or at the plateau in case of GP) the energies are at variance in the two methods, but the chain lengths agree very well.
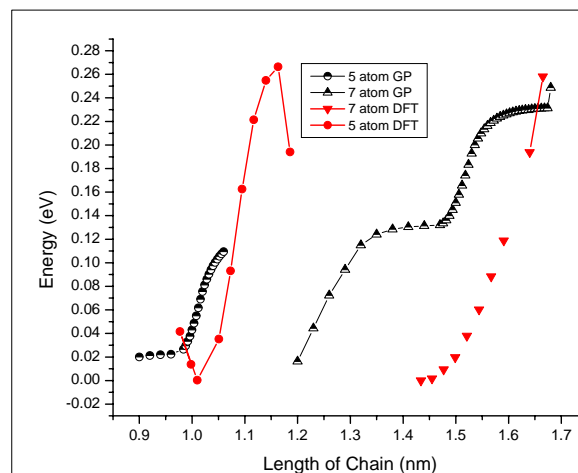
Figure 8.2 Comparison of variation in total energy with the total length of gold chain from different approaches DFT and GP.

This energy vs length of the chain curve is used to find the relation between force and total length of the wire using equation (8.1)

$$F = - \frac{\partial U}{\partial L}$$

(8.1)

8.3.2 Force vs Length of chain

Force as a function of length (or the stress-strain curve) for two different approaches - DFT and GP is shown in Fig. 8. 3. The usual elastic region is where the curve rises with increase in length. However it reaches a maximum and then turns down depicting the onset of plasticity.

Thus the peak represents the maximum permissible force, or the breaking force. The breaking forces calculated by DFT are somewhat larger -- 2.94nN for the 5- atom chain and 2.5nN for the 7-atom chain which are higher than predicted experimental value 1.56 ± 0.3 nN. Though the breaking forces of the chains calculated using Gupta potential of order of 1.6nN, are in better agreement with the experimental value, the overall energy vs. length curve using DFT matches the experimental findings [20].
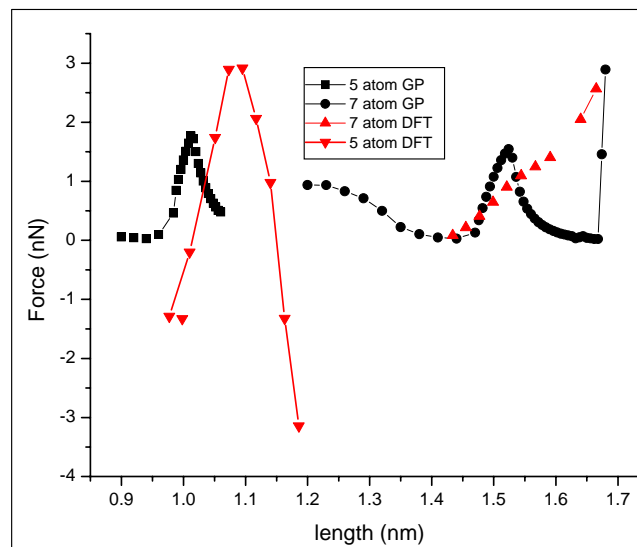
Figure 8.3 Comparison of variation of force with the total length of gold chain of 5 and 7 atoms for DFT and GP

8.3.3 Modulus vs Length of chain

In Fig. 8.4 we have plotted variation in modulus with the total length of the wire. Since for a nano cross-sectioned zig-zag chain, it is difficult to define the area of cross section, the modulus thus defined is taken as proportional to Young's modulus. It is defined using equation (8.2)

$$Modulus \quad = \frac{\partial F}{\partial l} \tag{8.2}$$

The 'unphysical' regions in Fig. 8. 4, where the stress-strain curves have negative slopes moduli are negative, cannot exist as stable states of the wire. However in a dynamic situation (e.g., when the wire is being pulled continuously) they may well exist. These plastic regions are more clearly seen in GP calculations than in DFT.
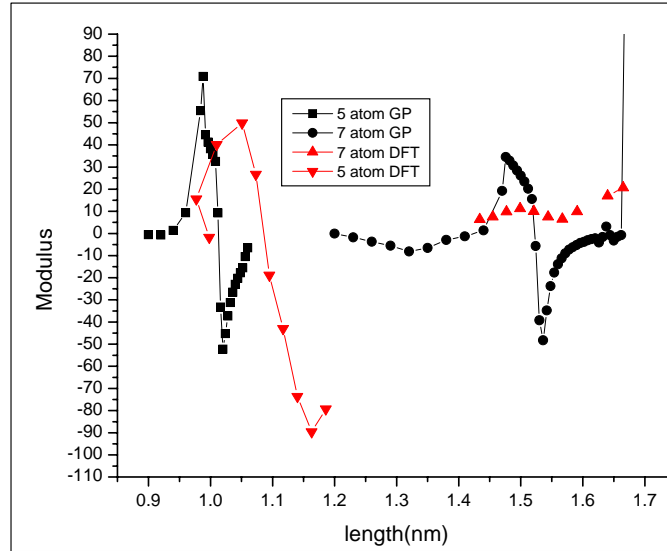
Figure 8.4 Comparison of variation of modulus with total length of gold chain of 5 and 7 atoms for DFT and GP

8.4 Conclusion

We have studied the structures, energy variations, force and modulus of two linear finite chains of gold with five and seven atoms and compared the results with similar calculations done through Gupta Potential.

- It is seen that a given monatomic gold wire which has a zig-zag shape can assume structures containing qualitatively different regions for different strains. Interestingly, such regions of strain are separated by plastic regions which can be accessed by applying the strain dynamically. These plastic regions are more clearly seen in GP calculations than in DFT results.

- The breaking force more or less agrees with experimentally observed values.

Bibliography

[1]   J. A. Torres, E. Tosatti, A. D. Corso, F. Ercolessi, J. J. Kohanoff, F. D. D. Tolla, J. M. Soler, Surface Science 426, L441–L446 (1999).

[2]   H. Hakkinen, R. N. Barnett, A. G. Scherbakov, and U. Landman, J. Phys.Chem. B 104, 9063–9066(2000).

[3]   L. D. Maria and M. Springborg, Chem. Phys. Lett., vol. 323, 293–299 (2000).

[4]   T. Kizuka, Phy. Rev. B 77, 155401 (2008).

[5]   E. Z. da Silva, A. J. R. da Silva, A. Fazzio, Phys. Rev. Lett. 87, 256102 (2001).

[6]   A. I. Yanson, G. R. Bollinger, H. E. van den Brom, N. Agrait, J. M. van. Ruitenbeek, Nature(London) 395, 783 (1998).

[7]   Y. Kondo, K. Takayanagi, Science 289, 606 (2000).

[8]   E. Tosatti, S. Prestipino, S. Kostlmeier, A. Dal Corso, F. D. Di Tolla, Science 291, 288 (2001).

[9]   H. Ohnishi, Y. Kondo, K. Takayanagi, Nature (London) 395, 780 (1998).

[10]   N. Agrait, C. Untiedt, G. R. Bollinger,S. Vieira, Phys. Rev. B 66, 085, 418 (2002).

[11]   F. D. Novaes, A. J. R. Da Silva, A. Fazzio1, Edison Z. Da Silva, Appl. Phys. A 81, 1551–1558 (2005).

[12]   E. Z. da Silva, F. D. Novaes, A. J. R. da Silva, A. Fazzio, Nanoscale Res. Lett. 1:91–98 (2006).

[13]   J. W. Cahn, Acta Metall. 28, 1333 (1980).

[14]   J. Diao, K. Gall, M. L.Dunn, J. Mech. Phys. of Solids 52, 1935 – 1962(2004).

[15]   B. Wu, A. Heidelberg, J. J. Boland, Lett. Nature Mat. 4 (2005).

[16]   L. De Maria,M. Springborg, Chem. Phys. Lett. 323, 293-299 (2000).

[17]   Sumali, Priyanka , V. Verma , K. Dharamvir, AIP Conf. Proc. 1447, 335-336 (2012).

[18]   D. Sanchez-Portal, E. Artacho, J. Junquera, P. Ordejon, A. Garcia, J. M. Soler, Phys. Rev. Lett. 83, 3884 (1998).

[19]   L. De Maria, M. Springborg, Chem. Phys. Lett. 323, 293-299 (2000).

[20]   G. Rubio-Bollinger, S. R. Bahn, N. Agrait, K.W. Jacobsen, S. Vieira, Phys. Rev. Lett. 87, 026101 (2001).

Chapter 9

9. Phonon Dispersion Of Gold Nanotube

9.1 Introduction

The developments of nanoscale devices require the understanding of nanoscale phenomena. At such scale, properties like electrical, optical, vibrational and mechanical become distinctly different from bulk behavior. For example, nanostructures have been observed to exhibit sharper density of states, reduced electron-phonon coupling [1-6]. Nanowires and nanotubes have been widely studied because of their importance in the fundamental physics and the potential applications in the future nanodevices e.g. gold and carbon nanowires and nanotubes [7, 8]. However, the gold nanotubes and nanowires in comparison with the carbon nanotubes CNTs, had been found much later and relatively less studied. A finest gold nanowires of about 0.6 nm in diameter and 6 nm in length were synthesized by Kondo et al.in an ultrahigh-vacuum (UHV) transmission electron microscope with the electron-beam thinning technique. They found using high-resolution electron microscopy that the gold nanowires had a coaxial helical multishell structure, which was similar to that of the multiwalled carbon nanotube [7]. Recently, Oshima *et al.* have experimentally found a single-walled (5, 3) gold nanotube (SWGT) which composed of five atomic rows coiling around the tube axis [8]. The formation of experimentally observed (5, 3) gold tube was explained by Senger et al. [9]. Theoretically, the gold nanowires were studied by Bilalbegović using the molecular-dynamics simulations and the embedded-atom potential. They found that the gold atoms could form the concentric cylindrical sheets and even have a double-walled gold nanotube like structure. In the vibrational density of states (VDOS) study of two cylindrical gold nanowires they found that maximal vibration frequency is about 6 THz (200 cm^{-1}), higher than that of the bulk gold, being 4.7 THz (157 cm^{-1}) [10, 11].

Most of the studies focus on the electronic structures and transport properties of the gold nanowires and nanotubes [12-15] but there are relatively very few studies are available on the vibrational properties of SWGTs and gold nanowires. Most of the vibrational analysis studies focus on finding VDOS; a few studies involve the calculation of vibrational modes of nanowires. The behavior of a material depends on phonon dynamics, and these dynamics are change substantially as nanostructure dimensions approach the phonon mean-free path length. A phonon is a quantized

mode of vibration occurring in a rigid crystal lattice, such as the atomic lattice of the solid. The study of phonons is an important in solid state physics as they play a major role in determining the physical properties of solids such as thermal and electrical conductivities. In a lattice dynamics calculations of gold using phenomenological model Thapa has computed the phonon frequencies, Lattice specific heats, compressibility and Poission's ratio. They have evaluated force constants and phonon dispersion relations of bulk gold along symmetry directions [100], [110] and [111] [16]. The phonon dispersions calculations have been made using both empirical methods and the accuracy *ab initio* calculations [17-21].

Phonons are a quantum mechanical version of type of vibrational motion, known as normal modes in classical mechanics. The normal modes are the elementary vibrations of the lattice and any arbitrary vibrational motion of the lattice can be represented as a superposition of normal modes with various frequencies. Although normal modes are wave like phenomenon in classical mechanics, they acquire particle like character in quantum mechanics. They are then known as phonons. There are two types of phonons: Acoustic and Optical phonons.The Lattice dynamics (LD) deals with problem of finding the normal modes of vibration of a crystal i.e, calculating the energies (or frequencies ω) of the phonons as a function of their wave vector's k . The relationship between ω and k is called phonon dispersion.

Optical phonons are found in crystal with more than one atom in the unit cell and have non zero frequency of vibration, even when the wavelength is large. They are called optical because in ionic crystal they are easily excited by light (infrared light) and therefore are called infrared active. The Longitudinal and Transverse optical phonons phonons are abbreviated as LO and TO respectively.

Acoustic phonons have frequencies that become small at long wavelengths and correspond to sound waves in the lattice. Longitudinal and Transverse acoustic phonons are abbreviated as LA and TA respectively. For system with one atom per unit cell the phonon dispersion curves are represented only by acoustical branches and if the numbers of atoms in a unit cell are more than one, the optical branches will also appear. In acoustic modes the atoms moves in phase with each other while in optical modes the atoms moves out of phase. In general for a system containing N atoms per unit cell there will be 3 acoustical branches (1 longitudinal and 2 transverse) and 3N-3 optical branches (N-1 longitudinal and 2N-2 transverse).

9.2 Methodology

We have discussed in Chapter 3 that GP calculations give good results as far as 3 D geometries of gold clusters is concerned. It is observed that GP predicts 3 D structures as low lying geometries while DFT calculations results in planar geometries for gold clusters upto n =13 . As already pointed the difference in lowest energy structures predicted by GP and DFT has been attributed to relativistic effects in gold clusters. It has been discussed that as size of gold clusters grows the GP results become reasonably better and the calculations with GP are also computationally less demanding in comparision with DFT. Hence it may be suggested that for the larger gold clusters we can use GP.

Keeping in mind the above discussion, we have tried to calculate the vibrational properties of gold nanotube using GP. The GP calculations can give a reasonably good idea about the vibrational properties of gold nanotube in much less computational time than the DFT calculations. We have considered the 120 atoms gold nanotube. It consists of alternate hexagonal rings similar to Au_{60} nanotube already discussed in Chapter 7. The free standing Au_{120} nanotube was optimized using GP.

Since GP has a tendency to form 3 D geometries in case of gold, it was found that the tube gets twisted and distorted. Therefore then the tube was optimized by holding the end layers at fixed heights, the final optimized geometry consisting of 108 atoms of gold nanotube is shown in Fig. 9.1
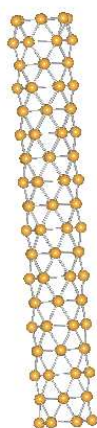
Figure 9.1 The optimized Au_{108} nanotube using GP (without the top and bottom layer)

In general, to find the vibrational properties of any system, we first need to build a dynamical matrix containing the quantities $D_{\alpha i}^{\beta j}\left(\vec{q}\right)$ by calculating the force constants corresponding to the system. For a 2D system [23] containing r number of atoms per unit cell, we have 2r different solutions. For non trivial solutions, we should have

$$Det\left\{D_{\alpha i}^{\beta j}\left(\vec{q}\right)-\omega^2\delta_{\alpha\beta}\delta_{ij}\right\}=0$$

(9.1)

where $D_{\alpha i}^{\beta j}\left(\vec{q}\right)=\frac{1}{\sqrt{M_\alpha M_\beta}}\sum_m \Phi_{0\alpha i}^{m\beta j}\exp\left(i\vec{q}.\vec{r}_m\right)$ and $\Phi_{0\alpha i}^{m\beta j}$ are the force constants which

are calculated, in this work, using Gupta potential. Here r_m are position vector of the mth cell and M are the masses of the atoms. The force constants $\Phi_{0\alpha i}^{m\beta j}$ are defined as the second derivative of energy w.r.t. atomic displacements.

These force constants can generally be determined by numerically displacing the atoms from their equilibrium positions and calculating energies. However, the tube optimized above is not uniform at the atomistic scales and force constants are derived for different atoms gave different results.

Therefore we take recourse to the sheet which, when folded into a cylinder would yield a perfect gold nanotubes. The sheet is then optimized by holding its end layers. The optimized sheet is shown in Fig.9.2
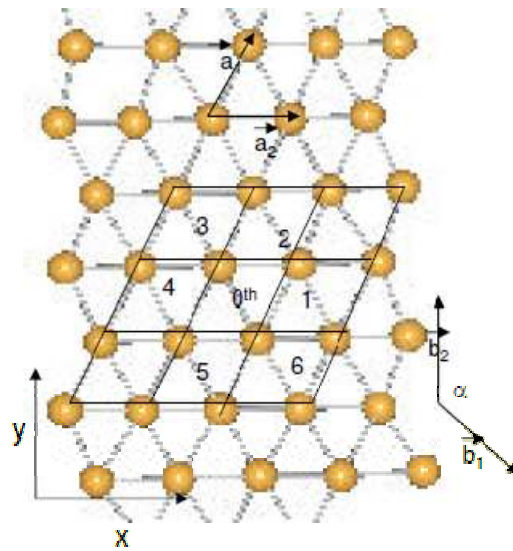
Figure 9.2 The unit cell of sheet of gold atoms having a rhombus crosssection

130

9.2.1 Dynamics of a sheet of Au atoms

From the above diagram we can identify the unit vectors and reciprocal lattice. The basis vectors are shown in Fig. 9.2(a). Each unit cell is a 60° rhombus with side a (a = bondlength) conatins one lattice point.

The basis vectors of the reciprocal lattice are also shown in Fig 9.2 (b). They are

$$\vec{b_2} = \frac{2\pi}{a}\hat{z} \; ; \; \vec{b_1} = \frac{2\pi}{a}\hat{\alpha} \tag{9.2}$$

where $\hat{\alpha} = \frac{\sqrt{3}}{2}\hat{x} + \frac{1}{2}\hat{y}$. We have to study the waves propagating in the z direction (parallel to the axis of tube). According to the geometry of the sheet, the propagation vector in this direction is restricted as follows:

$$0 \le k_y \le \pi/a \tag{9.3}$$

The sheet corresponding to our sheet AuNT is of limited dimensions along x axis- it is only 6 a wide as the propagation vectors are restricted in this direction can have only following values:

$$0, \pm\frac{\pi}{3a}\hat{x}, \pm\frac{2\pi}{3a}\hat{x} \text{ and } \frac{\pi}{a}\hat{x} \tag{9.4}$$

We need to solve for all k_y values in equation (9.3) along with equation (9.4), which can be called the circumferential wave vectors.

9.2.2 Cell at origin and neighboring cells

We shall use the method of dynamical matrix incorporating only forces between nearest neighbours. Therefore we need lattice vectors only for nearest neighbors' cells (nearest to the origin, at the 0th cell). These are denoted by 1, 2 …..6 in the Fig. 9.2 and the corresponding lattice vectors are,

$$\vec{r_1} = a\hat{x} \tag{9.5a}$$

$$\vec{r_2} = \vec{a_1} = \frac{a}{2}\hat{x} + \frac{\sqrt{3}}{2}\hat{y} \tag{9.5b}$$

$$\vec{r_3} = -\frac{a}{2}\hat{x} + \frac{\sqrt{3}}{2}\hat{y} \tag{9.5c}$$

$$\vec{r_4} = -a\hat{x} \tag{9.5d}$$

$$\vec{r_5} = -\vec{a_1} = -\frac{a}{2}\hat{x} - \frac{\sqrt{3}}{2}\hat{y} \tag{9.5e}$$

$$\vec{r}_6 = \frac{a}{2}\hat{x} - \frac{\sqrt{3}}{2}\hat{y} \tag{9.5f}$$

9.2.3 Evaluation of the force constants

We now numerically evaluate the second derivative of energy with respect to any two coordinates of the neighbouring atoms, are of the atoms being the central (0th) one. The symbols used for the force constants is

$$\Phi_{0i}^{nj} = \frac{\partial^2 \Phi}{\partial s_{0i} \partial s_{nj}} \tag{9.6}$$

Where Φ_{0i}^{nj} is the energy of the system; s_{oi} is the ith (i= 1, 2, 3 $\Leftrightarrow$ x, y, z) coordinate of the atom at origin and s_{nj} is the jth coordinate of the atom in the nth cell . We shall need only the following force constants. The self terms i.e.,

$$\Phi_{02}^{03}, \quad \Phi_{02}^{02}, \quad \Phi_{03}^{03}, \quad \Phi_{01}^{02}, \quad \Phi_{01}^{03}, \quad \Phi_{02}^{03}$$

And the interatomic terms,

$$\Phi_{01}^{n1}, n = 1,2,..... 6$$

$$\Phi_{01}^{n3}, n = 1,2,..... 6$$

$$\Phi_{01}^{n2}, n = 1,2,..... 6$$

$$\Phi_{03}^{n3}, n = 1,2,..... 6$$

For numerical calculations, we use the following expressions

$$\Phi_{01}^{01} = \frac{1}{\Delta^2}\left[\left(\Phi\left(x_0 = \Delta\right) + \Phi\left(x_0 = -\Delta\right)\right) - 2\Phi\left(x_0\right)\right] \tag{9.7}$$

$$\Phi_{02}^{02} = \frac{1}{\Delta^2}\left[\left(\Phi\left(y_0 = \Delta\right) + \Phi\left(y_0 = -\Delta\right)\right) - 2\Phi\left(y_0\right)\right] \tag{9.8}$$

$$\Phi_{03}^{03} = \frac{1}{\Delta^2}\left[\left(\Phi\left(z_0 = \Delta\right) + \Phi\left(z_0 = -\Delta\right)\right) - 2\Phi\left(z_0\right)\right] \tag{9.9}$$

$$\Phi_{01}^{02} = \frac{1}{4\Delta^2}\left[\begin{pmatrix} \Phi\left(x_0 = \Delta, y_0 = \Delta\right) - \Phi\left(x_0 = \Delta, y_0 = -\Delta\right) - \Phi\left(x_0 = -\Delta, y_0 = \Delta\right) \\ + \Phi\left(x_0 = -\Delta, y_0 = -\Delta\right) \end{pmatrix}\right] \tag{9.10}$$

And similarly for $\Phi_{02}^{03}, \Phi_{01}^{03}$, where Δ is step size. In our calculations the values of Δ=0.02A^o.The interactive terms are

$$\Phi_{01}^{11} = \frac{1}{4\Delta^2}\left[\left(\begin{array}{l}\Phi\left(x_0 = \Delta, x_1 = \Delta\right) - \Phi\left(x_0 = \Delta, x_1 = -\Delta\right) - \Phi\left(x_0 = -\Delta, x_1 = \Delta\right)\\ + \Phi\left(x_0 = -\Delta, x_1 = -\Delta\right)\end{array}\right)\right] = \frac{\partial^2 \Phi}{\partial s_{01}\partial s_{11}}$$

$$\text{(9.11)}$$

$$= \frac{1}{4\Delta^2}\left[\left(2\Phi\left(x_0 = \Delta, x_1 = \Delta\right) - \Phi\left(x_0 = \Delta, x_1 = -\Delta\right) - \Phi\left(x_0 = -\Delta, x_1 = \Delta\right)\right)\right] \quad \text{(9.12)}$$

$$\Phi_{01}^{12} = \frac{1}{4\Delta^2}\left[\left(\begin{array}{l}\underline{\Phi\left(x_0 = \Delta, y_1 = \Delta\right)} - \underline{\underline{\Phi\left(x_0 = \Delta, y_1 = -\Delta\right)}} - \underline{\underline{\Phi\left(x_0 = -\Delta, y_1 = \Delta\right)}}\\ + \underline{\Phi\left(x_0 = -\Delta, y_1 = -\Delta\right)}\end{array}\right)\right] \quad \text{(9.13)}$$

Here the underlined pairs are equal in magnitude considering the geometry of the lattice, therefore

$$\Phi_{01}^{12} = 0 \qquad \text{(9.14)}$$

Similarly, $$\Phi_{02}^{11} = 0 \qquad \text{(9.15)}$$

The other interactive terms are

$$\Phi_{02}^{12} = \frac{1}{4\Delta^2}\left[\left(2\Phi\left(y_0 = \Delta, y_1 = \Delta\right) - \Phi\left(y_0 = \Delta, y_1 = -\Delta\right) - \Phi\left(y_0 = -\Delta, y_1 = \Delta\right)\right)\right] \quad \text{(9.16)}$$

$$\Phi_{03}^{13} = \frac{1}{2\Delta^2}\left[\left(\Phi\left(z_0 = \Delta, z_1 = \Delta\right) - \Phi\left(z_0 = -\Delta, z_1 = \Delta\right)\right)\right] = \Phi_{03}^{23} = \Phi_{03}^{33} \cdots\cdots = \Phi_{03}^{63} \quad \text{(9.17)}$$

Thus , between atom 0 and 1, we have $\Phi_{0i}^{1i} \neq 0$ and $\Phi_{0i}^{1j} = 0, i \neq j$. The other elements are

$$\Phi_{01}^{22} = \frac{1}{4\Delta^2}\left[\left(\begin{array}{l}\Phi\left(x_0 = \Delta, y_2 = \Delta\right) - \Phi\left(x_0 = \Delta, y_2 = -\Delta\right) - \Phi\left(x_0 = -\Delta, y_2 = \Delta\right)\\ + \Phi\left(x_0 = -\Delta, y_2 = -\Delta\right)\end{array}\right)\right] \quad \text{(9.18)}$$

$$\Phi_{02}^{22} = \frac{1}{2\Delta^2}\left[\left(\Phi\left(y_0 = \Delta, y_2 = \Delta\right) - \Phi\left(y_0 = \Delta, y_2 = -\Delta\right)\right)\right] \quad \text{(9.19)}$$

$$\Phi_{02}^{21} = \frac{1}{4\Delta^2}\left[\left(\begin{array}{l}\Phi\left(y_0 = \Delta, x_2 = \Delta\right) - \Phi\left(y_0 = \Delta, x_2 = -\Delta\right) - \Phi\left(y_0 = -\Delta, x_2 = \Delta\right)\\ + \Phi\left(y_0 = -\Delta, x_2 = -\Delta\right)\end{array}\right)\right] \quad \text{(9.20)}$$

$$\Phi_{01}^{21} = \frac{1}{4\Delta^2}\left[\left(\begin{array}{l}\Phi\left(x_0 = \Delta, x_2 = \Delta\right) - \Phi\left(x_0 = \Delta, x_2 = -\Delta\right) - \Phi\left(x_0 = -\Delta, x_2 = \Delta\right)\\ + \Phi\left(x_0 = -\Delta, x_2 = -\Delta\right)\end{array}\right)\right]$$

$$= \frac{1}{4\Delta^2}\left[\left(2\Phi\left(x_0 = \Delta, x_2 = \Delta\right) - \Phi\left(x_0 = \Delta, x_2 = -\Delta\right) - \Phi\left(x_0 = -\Delta, x_2 = \Delta\right)\right)\right] \quad \text{(9.21)}$$

And by the symmetry of the lattice,

$$\Phi^{31}_{01} = \Phi^{21}_{01}$$

$$\Phi^{31}_{02} = -\Phi^{21}_{02}$$

$$\Phi^{32}_{02} = \Phi^{22}_{02}$$

$$\Phi^{32}_{01} = -\Phi^{22}_{01}$$

The force constant between 0 and 2,3,.....6 can be found by rotation symmetry of the matrix . (Φ^{n3}_{03} are all equal as already shown).

Choose a primed coordinate system x',y' such that x' connects atoms 0 and 2 and y' is normal to it. Then in the rotated coordinate system the new coordinates are

$$\begin{bmatrix} x' \\ y' \end{bmatrix} = \begin{bmatrix} \cos\ 60° & -\sin\ 60° \\ \sin\ 60° & \cos\ 60° \end{bmatrix} \begin{bmatrix} x \\ y \end{bmatrix} \tag{9.22}$$

where

$$x' = \frac{1}{2}x + \frac{\sqrt{3}}{2}y \tag{9.23}$$

$$y' = -\frac{\sqrt{3}}{2}x + \frac{1}{2}y \tag{9.24}$$

The relation between 0 and 1 in original coordinate system is same as that between 0 and 2 in new coordinate sysytem.Therefore

$$\frac{\partial^2 \Phi}{\partial s_{01} \partial s_{11}} = \frac{\partial^2 \Phi}{\partial s_{01}' \partial s_{21}'} \tag{9.25}$$

$$\frac{\partial \Phi}{\partial s_{21}} = \frac{\partial \Phi}{\partial s_{21}'} \frac{\partial s_{21}'}{\partial s_{21}} + \frac{\partial \Phi}{\partial s_{22}'} \frac{\partial s_{22}'}{\partial s_{21}}$$

$$= \frac{1}{2}\frac{\partial \Phi}{\partial s_{21}'} - \frac{\sqrt{3}}{2}\frac{\partial \Phi}{\partial s_{22}'} \tag{9.26}$$

where $s_{21}' = x_2'$, $s_{22}' = y_2'$, $s_{21} = x_2$. Similary we can also write

$$\frac{\partial^2 \Phi}{\partial s_{01} \partial s_{21}} = \frac{1}{4}\frac{\partial^2 \Phi}{\partial s_{01}' \partial s_{21}'} - \frac{\sqrt{3}}{4}\frac{\partial^2 \Phi}{\partial s_{02}' \partial s_{21}'} - \frac{\sqrt{3}}{4}\frac{\partial^2 \Phi}{\partial s_{01}' \partial s_{22}'} + \frac{3}{4}\frac{\partial^2 \Phi}{\partial s_{02}' \partial s_{22}'}$$

$$= \frac{1}{4}\Phi^{11}_{01} - \frac{\sqrt{3}}{4}\Phi^{11}_{02} - -\frac{\sqrt{3}}{4}\Phi^{12}_{01} + \frac{3}{4}\Phi^{12}_{02} \tag{9.27}$$

In equation (9.27), the underlined term will vanish . In general we can write

$$\frac{\partial^2 \Phi}{\partial s_{0i} \partial s_{2j}} = \frac{\partial}{\partial s_{oi}} \frac{\partial \Phi}{\partial s_{2j}} = \frac{\partial}{\partial s_{01}'} \frac{\partial \Phi}{\partial s_{2j}} \cdot \frac{\partial s_{01}'}{\partial s_{0i}} + \frac{\partial}{\partial s_{02}'} \frac{\partial \Phi}{\partial s_{2j}} \cdot \frac{\partial s_{02}'}{\partial s_{0i}}$$

(9.28)

Expanding the equation (9.28) and using

$$\frac{\partial^2 \Phi}{\partial s_{0i}' \partial s_{2j}'} = \frac{\partial^2 \Phi}{\partial s_{0i} \partial s_{1j}}$$

$$\Phi_{01}^{12} = 0 = \Phi_{02}^{21}$$

We can rewrite the equation (9.28)

$$\frac{\partial^2 \Phi}{\partial s_{0i} \partial s_{2j}} = \frac{\partial s_{01}'}{\partial s_{oi}} \cdot \frac{\partial s_{21}'}{\partial s_{2j}} \frac{\partial^2 \Phi}{\partial s_{01} \partial s_{11}} + \frac{\partial s_{02}'}{\partial s_{oi}} \cdot \frac{\partial s_{22}'}{\partial s_{2j}} \frac{\partial^2 \Phi}{\partial s_{02} \partial s_{12}}$$

(9.29)

or

$$\Phi_{oi}^{2j} = \frac{\partial s_{01}'}{\partial s_{oi}} \cdot \frac{\partial s_{21}'}{\partial s_{2j}} \Phi_{o1}^{11} + \frac{\partial s_{02}'}{\partial s_{oi}} \cdot \frac{\partial s_{22}'}{\partial s_{2j}} \Phi_{o2}^{12}$$

(9.30)

Applying the above formulation , we get the following terms

$$\Phi_{o1}^{21} = \left(\frac{1}{2}\right)^2 \Phi_{o1}^{11} + \left(-\frac{\sqrt{3}}{2}\right)^2 \Phi_{o2}^{12} = \frac{1}{4} \Phi_{o1}^{11} + \frac{3}{4} \Phi_{o2}^{12}$$

(9.31)

$$\Phi_{o1}^{22} = \frac{1}{2} \cdot \frac{\sqrt{3}}{2} \Phi_{o1}^{11} + \left(-\frac{\sqrt{3}}{2}\right)\left(\frac{1}{2}\right) \Phi_{o2}^{12} = \frac{\sqrt{3}}{4} \Phi_{o1}^{11} - \frac{\sqrt{3}}{4} \Phi_{o2}^{12} = \Phi_{o2}^{22}$$

(9.32)

$$\Phi_{o2}^{22} = \left(\frac{\sqrt{3}}{2}\right)^2 \Phi_{o1}^{11} + \left(\frac{1}{2}\right)^2 \Phi_{o2}^{12} = \frac{3}{4} \Phi_{o1}^{11} + \frac{1}{4} \Phi_{o2}^{12}$$

(9.33)

Again using the symmetry of lattice we can write the force constants between 0 and 3

$$\Phi_{01}^{31} = \Phi_{01}^{21}$$

$$\Phi_{02}^{31} = - \Phi_{02}^{21}$$

$$\Phi_{02}^{32} = \Phi_{02}^{22}$$

$$\Phi_{01}^{32} = - \Phi_{01}^{22}$$

By the translational symmetry of the lattice (atom # 0→1 and atom # 4→0 everything remain same) . Hence we can write

$$\Phi \, {}^{1j}_{0i} = \Phi \, {}^{0j}_{4i} = \Phi \, {}^{4i}_{0j}$$

$$\Phi \, {}^{41}_{01} = - \, \Phi \, {}^{11}_{01} \ and$$

$$\Phi \, {}^{42}_{02} = \Phi \, {}^{12}_{02}$$

And the rest are zero. Similary writing the force constants for between atom# 0 and 5,

$$\Phi \, {}^{51}_{01} = \Phi \, {}^{21}_{01} \, ; \Phi \, {}^{52}_{01} = \Phi \, {}^{22}_{01} \, ; \Phi \, {}^{51}_{02} = \Phi \, {}^{21}_{02}$$

$$\Phi \, {}^{52}_{02} = \Phi \, {}^{22}_{02}$$

For atom # 0 and 6 (atom 6 is opposite to atom 3)

$$\Phi \, {}^{6j}_{0i} = \Phi \, {}^{3j}_{0i}$$

The calculated values of the required force constants of the optimized two dimensional gold sheet for the nearest neighbours are

$$\Phi \, {}^{01}_{01} = \Phi \, {}^{02}_{02} = 4.1025 \ eV \ / \ A^{\circ -2}$$
$$\Phi \, {}^{03}_{03} = -1.25 \times 10^{-3} eV \ / \ A^{\circ -2} \tag{9.34}$$

The other force constants are

$$\Phi \, {}^{21}_{01} = \Phi \, {}^{31}_{01} = \Phi \, {}^{51}_{01} = \Phi \, {}^{61}_{01} = 0.216695 \tag{9.35a}$$
$$\Phi \, {}^{11}_{01} = \Phi \, {}^{41}_{01} = 1.3123 \tag{9.35b}$$
$$\Phi \, {}^{11}_{02} = \Phi \, {}^{41}_{02} = \Phi \, {}^{42}_{01} = \Phi \, {}^{12}_{01} = 0 \tag{9.35c}$$
$$\Phi \, {}^{21}_{02} = \Phi \, {}^{51}_{02} = \Phi \, {}^{22}_{01} = \Phi \, {}^{52}_{01} = 0.632526 \tag{9.35d}$$
$$\Phi \, {}^{31}_{02} = \Phi \, {}^{61}_{02} = \Phi \, {}^{32}_{02} = \Phi \, {}^{62}_{02} - 0.632526 \tag{9.35e}$$
$$\Phi \, {}^{12}_{02} = \Phi \, {}^{42}_{02} = -0.1485 \tag{9.35f}$$

$$\Phi \, {}^{22}_{02} = \Phi \, {}^{32}_{02} = \Phi \, {}^{52}_{02} = \Phi \, {}^{62}_{02} = 0.9471 \tag{9.35g}$$

9.2.4 Evalution of Dynamical Matrix

The secular determinent of the dynamical matrix to be solved as

$$\left[\begin{matrix} \left(D_1^1 - \omega^2\right)\left(D_1^2\right) \\ \left(D_1^2\right)\left(D_2^2 - \omega^2\right) \end{matrix} \right] = 0 \tag{9.36}$$

On solving the above 2 X 2 matrix we get the frequency as,

$$\omega^2 = \frac{D_1^1 + D_2^2}{2} \pm \frac{1}{2}\sqrt{\left(D_1^1 - D_2^2\right)^2 + \left(D_1^2\right)^2} \qquad (9.37)$$

where the dynamical matrix elements can be solved as

$$D_1^1 = \frac{1}{M}\left[\Phi_{01}^{01} + \sum_n \Phi_{01}^{n1} e^{i\vec{q}\cdot\vec{r_n}}\right] \qquad (9.38)$$

$$D_1^2 = \frac{1}{M}\left[\Phi_{01}^{02} + \sum_n \Phi_{01}^{n2} e^{i\vec{q}\cdot\vec{r_n}}\right] = D_2^{1*} \qquad (9.39)$$

$$D_2^2 = \frac{1}{M}\left[\Phi_{02}^{02} + \sum_n \Phi_{02}^{n2} e^{i\vec{q}\cdot\vec{r_n}}\right] \qquad (9.40)$$

For expanding equations (9.38 – 9.40) , we have used the r_n values from equations 9.5 (a-f) and we take $\vec{q} = q\hat{n}$. Then the on simplification above equations become

$$D_1^1 = \frac{1}{M}\left[\Phi_{01}^{01} + 2\Phi_{01}^{11}\cos\left(q_x a\right) + 4\Phi_{01}^{21}\cos\left(\frac{q_x a}{2}\right)\cos\left(\frac{q_y a}{2}\sqrt{3}\right)\right] \qquad (9.41)$$

$$D_1^2 = \frac{1}{M}\left[\Phi_{01}^{02} - 4\Phi_{01}^{22}\sin\left(\frac{q_x a}{2}\right)\sin\left(\frac{q_y a}{2}\sqrt{3}\right)\right] = D_2^{1*} \qquad (9.42)$$

$$D_2^2 = \frac{1}{M}\left[\Phi_{02}^{02} + 2\Phi_{02}^{12}\cos\left(q_x a\right) + 4\Phi_{02}^{22}\cos\left(\frac{q_x a}{2}\right)\cos\left(\frac{q_y a}{2}\sqrt{3}\right)\right] \qquad (9.43)$$

These elements of the dynamical matrix are solved for the different values of q_x and q_y. The allowed values of q_x are 0, $\pm\frac{2\pi}{6a}, \pm\frac{4\pi}{6a}, \frac{\pi}{a}$ and for each value of q_x , we have taken the values of q_y lying between $0 < q_y < \frac{\pi}{a}$. After finding the value of elements of the dynamical matrix, we diagonalise it using equation 9.36 and frequencies are calculated using equation 9.37. The calculated dispersion curve is plotted in Fig. 9.3. The dispersion curve shows six branches corresponding to each atom in hexagonal layer of Au_{60} nanotube.
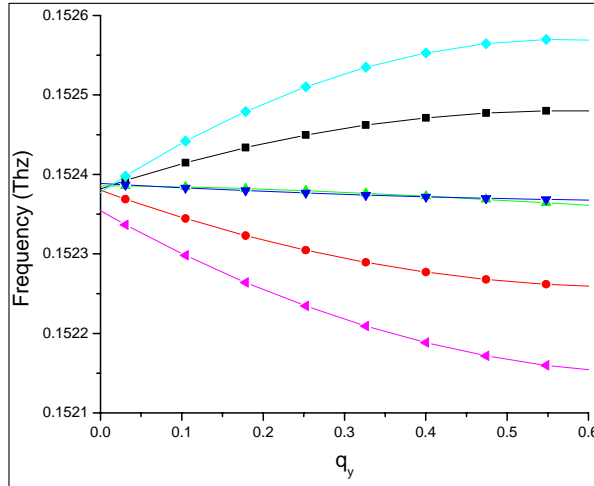
Figure 9.3 Dispersion curve for 2D gold sheet

9.3 Conclusion

We have developed algebra for computing a phonon -dispersion curves for gold nanotube using Gupta potential and explained it by taking an example of small 2D gold sheet. As far as our knowledge very few theoretical works literature are available on calculating the vibrational modes using Gupta potential (GP) of gold nanotubes. In case of first principle study of the phonon frequencies and vibrational modes, the dynamical matrix is diagonalized but in order to get an accurate dynamical matrix, one needs to take a very large supercell including more number of atoms .In such cases the GP can give reasonable results in less computational time with more careful optimization of the initial geometry.We will further improve upon this work by plotting the dispersion curve for gold sheet with larger number of atoms using both Gupta potential and DFT.

Bibliography

[1]   D. A. B. Miller, D. S. Chemla, S. Schmitt-Rink, Appl. Phys. Lett. 52, 2154, (1988).

[2]   H. Sakaki, Jpn. J. Appl. Phys. Part 2, 28, L314 (1989).

[3]   U. Bockelmann, G. Bastard, Phys. Rev. B 42, 8947 (1990).

[4]   J. Diao, K. Gall, M. L. Dunn, J. Mech. Phys. Solids 52, 1935 (2004).

[5]   J. Diao, K. Gall, M. L. Dunn, Nat. Mater. 2, 656 (2003).

[6]   J. Zou , A. Balandin, J. Appl. Phys. 89, 2932 (2001); A. Khitun, A. Balandin, K. L. Wang, G. Chen , Physica E (Amsterdam) 8, 13 (2000); B. Yang , G. Chen, Phys. Low-Dimens. Semicond. Struct. 5–6, 37 (2000).

[7]   Y. Kondo, K. Takayanagi, Science 289, 606(2000).

[8]   Y. Oshima, A. Onga, K. Takayanagi, Phys. Rev. Lett. 91, 205503 (2003).

[9]   R. T. Senger, S. Dag, S. Ciraci, Phys. Rev. Lett. 93, 196807 (2004).

[10]   G. Bilalbegović, Phys. Rev. B 58, 15412 (1998).

[11]   G. Bilalbegović, Vacuum 71, 165 (2003).

[12]   T. Ono, K. Hirose, Phys. Rev. Lett. 94, 206806 (2005); M. Zhuang, M.Ernzerhof, J. Chem. Phys. 120, 4921 (2004).

[13]   Y. Mokrousov, G. Bihlmayer, S. Blügel, Phys. Rev. B 72, 045402 (2005).

[14]   M. Okamoto, T. Uda, K. Takayanagi Phys. Rev. B 64, 033303 (2001).

[15]   C. K. Yang, Appl. Phys. Lett. 85, 2923 (2004).

[16]   S.R.B.Thapa, The Himalayan Physics 1, 1 (2010).

[17]   D. Sánchez-Portal, E. Artacho, J. M. Soler, A. Rubio ,P. Ordejón, Physical Review B 59, 19 (1999).

[18]   L. H. Ye, B. G. Liu, D. S. Wang, R. Han, Physical Review B 69,23 (2004)

[19]   D. Kumar, V. Verma, K. Dharamvir, H.S.Bhatti, Pramana, 81, 6, 1021-1035 (2013).

[20]   A. D. Corso, J. Phys.: Condens. Matter 25, 145401(2013).

[21]   Li Yang, M Y Chou, Nano Letters 11, 7, 2618-21(2011).

[22]   R. Ma, Y. Bando, T Sato, Adv. Mater. 14, 366(2002).

Chapter 10

Summary and Conclusions

This thesis focuses on different geometries of gold nanostructures of various sizes such as gold clusters, gold nanotubes and nanowires over different size ranges. Keeping in view the vast amount of literature available theoretical as well as experimental on the intriguing nature of the lowest energy geometries of gold clusters we have employed two different approaches i.e., a semi empirical potential and first principle method - density functional theory .The changes in the structural and electronic properties of gold nanostructures with the introduction of different foreign elements as a substitutional or at the endohedral sites of the nanostructures were also studied using DFT.

We have presented a detailed discussion on the different geometries of small gold clusters using Gupta Potential and DFT. The two approaches predict different lowest geometries for gold clusters for n ≤ 13 .While the use of Gupta Potential has predicted the early onset of 3D geometries, the DFT predicts planar structures for n up to 13. The results of our calculations are in fair agreement with available theoretical and experimental data. It can be remarked that GP are gives reasonably good results as far as 3D geometries of gold clusters are concerned. It is recommended that GP can be used to study higher atom gold clusters as it gives reasonably good results with the increasing size (n) and is computationally less demanding than DFT.

There is lot of research on the effect of doping on gold nanostructures due to the observation of interesting changes in its geometry and different properties with the introduction of impurity. The focus of the research is mainly on doping of gold clusters with transition metals. In our work we have presented a systematic study of the effect of doping Si and Ge on the ground state structures of pure gold clusters. It is found that on doping of silicon and germanium atoms in Au_n clusters, they adopt 3D structures from n=3 onward. The introduction of Si and Ge atoms in Au_{n+1} cluster increase their binding energy per atom. Silicon doped gold clusters have higher binding energy than germanium doped clusters. The HOMO–LUMO gap values of both Silicon and Germanium doped gold clusters lies in the range of semiconductors. The Au_{32} is a highly stable cage with the icosahedral (I_h) symmetry which has been verified both theoretically and experimentally. We have carried out a DFT study of the $M_{12}@Au_{20}$ (M= C, Si and Ge) clusters. The addition of dopant atoms has increased the average binding energy of Au_{32} cage. Pure Au_{32} cage is chemically

inert with HOMO-LUMO gap of 1.59eV, the substitutional doping of impurity atoms have found to decrease this gap making them relatively chemically reactive. Hence these materials can be used as novel materials in nanostructured devices.

Cu, Ag and Au are known as 'coinage elements' and forms an isoelectronic series .The study of interaction of these elements with each other forms a part of research for long time. We have studied the effect of encapsulation of small chain of Cu and Ag atoms within a short segment of gold nanotube i.e., Au_{24} tubular cage using DFT. In general, the Cu doped Au_{24} tubular cages found to have higher energy gap than the Ag doped cages except for Cu_2Au_{24-II}. The Mulliken population analysis, reveals that the d obitals of M (Cu, Ag) atoms in M@Au_{24}-I and M@Au_{24}-II clusters are dominant core orbital participating in bonding.

We have further extended our work of studying the interaction of group 14 elements with gold by studying the structural and electronic properties of of the tubular X_MAu_N (X= Si, Al and Au, M=3, 6, 9 and N= 24, 42, 60) clusters. It is known from previous studies that silicon when doped in gold clusters , forms an exohedral geomerty. In our work , we have shown that the Silicon can be doped inside the gold cluster, though we recommend futher theoretical and experimental research on this . We have found that the encapsulations of Si and Al atoms within the tubular frameworks of the gold host do not destroy its geometry though they change the energy hierarchy of the pure Au_N isomers. It was concluded that the Si and Al atoms can form long chains within Au nanotube if a gap is given after every 4-6 layers of Au atoms to accommodate the size mismatch between Si-Si, Al-Al and Au layers. The Si doping within Au_N tube is more compatible than the Al doping. This research shows a high possibility of a novel binary clusters with gold providing tubular framework.

Lastly we have studied the structures, energy variations, force and modulus of two linear finite chains of gold with five and seven atoms . The calculated value of breaking force for two monoatomic chains using DFT is more or less in agreement with the experimental value. The Chapter IX gives brief review of literature and the results of some prelimilnary work on the phonons study of hollow gold (6,0) nanotube using GP.

In brief, this work provides an insight to the systematic theoretical understanding of the geometric optimization, relative stability, electronic properties of gold clusters and gold nanotubes of different sizes. The present study can be useful for the analysis of the theoretical and experimental data related to gold clusters and their applications in nanodevices.

List of Publications

Papers in Journals

1. The structural and electronic properties of tubular gold clusters with a spinal support, Priyanka and Keya Dharamvir, Phys. Chem. Chem. Phys., 15, 12340 (2013).

2. Structure of Small Gold Clusters with Si Doping Using DFT (Au_nSi, n=1- 10, 19), Priyanka, Sumali Bansal and Keya Dharamvir, Journal of Nano Research Vol. 24, 203-212 (2013).

3. Structure, electronic and optical properties of doped Golden Fullerenes, Priyanka, Keya Dharamvir (Communicated)

Papers in Conference Proceedings

1. A study of various geometries of gold nanowires and effect of doping, Priyanka, Sumali Bansal, Rajiv Bhandari, and Keya Dharamvir, AIP Conf. Proc. 1591, 417 (2014).

2. A comparative study of transition metal doped tubular gold cages: M@Au24 (M = Au, Cu, Ag), Sumali, Priyanka, and Keya Dharamvir, AIP Conf. Proc. 1512, 282-283 (2013).

3. Stretching of short monatomic gold chains-some model calculations, Sumali, Priyanka, Veena Verma, and Keya Dharamvir, AIP Conf. Proc. 1447, 335 (2012).

4. Comparison of Cluster Calculation with Different Software-The Case of Small Clusters, Neetu Goel, Seema Gautam, Priyanka and Keya Dharmavir, AIP Conf. Proc. 1393, 289-290 (2011).

5. Structure and Stability of $GeAu_n$, n=1-10 clusters: A Density Functional Study, Priyanka, Hitesh Sharma and Keya Dharamvir, AIP Conf. Proc., 1393, 189(2011).

Papers presented and Conferences attended

1. International Seminar on Current Trends in Quantum Gases, BEC and Solitions, Department of Physics, Panjab University, Chandigarh, 3-6 Mar 2014.

2. A study of various geometries of gold nanowires and effect of doping, Priyanka, Sumali Bansal, Rajiv Bhandari, and Keya Dharamvir 58th DAE-Symposium, at Thapar University from 17- 21 Dec 2013.

3. Structure of Small Gold Clusters with Si Doping Using DFT (AunSi, n=1-10, 19), Priyanka, Sumali Bansal, and Keya Dharamvir, International Conference on Nanotechnolgy "Nanocon 2012", Bharti Vidyapeeth University, Pune, 18, 19 Oct 2012.

4. Structure and Stability of $GeAu_n$, n=1-10 clusters: A Density Functional Study, Priyanka, Hitesh Sharma and Keya Dharamvir, International Conference on advances in condensed and nano materials, Department of Physics, Panjab University, Chandigarh, 23- 26 Feb 2011.

5. Ionisation potential and electron affinity of silicon doped gold clusters, Priyanka, Keya Dharamvir, 3rd International Symposium on Material Chemistry BARC, Mumbai, 7-11 Dec 2010.

6. Density Functional Calculation for the structural and stability of silicon doped gold clusters, Priyanka, Keya Dharamvir, National Conference on Advance trends in Engg. and Technology (ATET-09), GGSCMT, Kharar, 6-7th Nov 2009

7. National Seminar on 'Advances in Physics , Department of Physics, Panjab University, Chandigarh, 28 Feb –Mar 2008.

8. National Seminar on 'Theoretical and Experimental Techniques in Nanoscience and Nanotechnology', Department of Physics, Panjab University, Chandigarh, 29-30 Mar, 2007